



Generalized quasi-Keplerian solution for eccentric, non-spinning compact binaries at 4PN order and the associated IMR waveform

Gihyuk Cho ^{1,*}, Sashwat Tanay ^{2,†}, Achamveedu Gopakumar,³ and Hyung Mok Lee⁴

¹*Deutsches Elektronen-Synchrotron DESY, Notkestr. 85, 22607 Hamburg, Germany*

²*Department of Physics and Astronomy, The University of Mississippi, University, MS 38677, USA*

³*Department of Astronomy and Astrophysics, Tata Institute of Fundamental Research, Mumbai 400005, India*

⁴*Department of Physics and Astronomy, Seoul National University, Seoul 151-742, Korea*

(Dated: March 11, 2022)

We derive fourth post-Newtonian (4PN) contributions to the Keplerian-type parametric solution associated with the conservative dynamics of eccentric, non-spinning compact binaries. The solution has been computed while ignoring certain zero-average, oscillatory terms arising due to 4PN tail effects. We provide explicit expressions for the parametric solution and various orbital elements in terms of the conserved energy, angular momentum and symmetric mass ratio. Canonical perturbation theory (along with the technique of Padé approximant) is used to incorporate the 4PN nonlocal-in-time tail effects within the action-angles framework. We then employ the resulting solution to obtain an updated inspiral-merger-ringdown (IMR) waveform that models the coalescence of non-spinning, moderately eccentric black hole binaries, influenced by Ref. [I. Hinder *et al.*, Phys. Rev. D 98, 044015 (2018)]. Our updated waveform is expected to be valid over similar parameter range as the above reference. We also present a related waveform which makes use of only the post-Newtonian equations and thus is valid only for the inspiral stage. This waveform is expected to work for a much larger range of eccentricity ($e_t \lesssim 0.85$) than our full IMR waveform (which assumes circularization of the binaries close to merger). We finally pursue preliminary data analysis studies to probe the importance of including the 4PN contributions to the binary dynamics while constructing gravitational waveform templates for eccentric mergers.

I. INTRODUCTION

The routine detection of transient gravitational waves (GWs) from merging binary black holes (BHs) and the observations of both GWs and multi-wavelength electromagnetic radiation from the coalescence of a neutron star binary, GW170817/EM170817, are establishing the era of GW astronomy [1–5]. More importantly, these events allow us to do astrophysics, cosmology and test general relativity with GWs [6–8]. Further, the upcoming observational campaigns of LIGO [9], Virgo [10] and KAGRA [11] should provide astrophysical evidences for the dominant formation channel for the ubiquitous binary BH (BBH) events [12]. This is because the so far observed BBH events are thought to have originated from two distinct formation channels [13]. The first scenario involves BH binaries which are formed in galactic fields via isolated binary stellar evolution and therefore are expected to have tiny orbital eccentricities of around 10^{-4} when their GWs enter aLIGO frequency window [14–16]. The second possibility involves dynamical formation of BH binaries in dense stellar environments and this is possible in globular clusters, young star clusters, and galactic nuclei [17–20]. Interestingly, these two BBH formation scenarios lead to distinct distributions for the masses and spins of binary constituents [21–23]. Additionally, accurate measurements of orbital eccentricities when BBHs enter terrestrial GW observatory frequency

windows should allow us to constrain their likely formation channel as dynamical formation scenarios tend to support non-zero orbital eccentricities [18, 24, 25].

Ready-to-use templates that model GWs from BH binaries merging along general relativistic eccentric orbits are crucial to detect such events and to extract crucial astrophysical information they carry [26, 27]. Indeed, there are many ongoing efforts to construct eccentric Inspiral-Merger-Ringdown (IMR) waveform families, both in the frequency and time domains [28–41]. It is customary to employ post-Newtonian (PN) approximation for describing the near-zone BBH inspiral dynamics and their far-zone inspiral GWs. This approximation provides general relativistic description for the orbital dynamics of comparable mass compact binaries in terms of $(v/c)^2$ corrections to their Newtonian dynamics with v and c being the orbital speed and the speed of light in vacuum, respectively. In this terminology, the 4PN order investigation presented in this paper deals with the derivation of general relativistic corrections up to the order $(v/c)^8$ to the Newtonian Keplerian parametric solution. Further, it is customary to employ the GW phasing approach of Refs. [42, 43] to describe temporally evolving PN-accurate GW polarization states $h_{\times,+}(t)$ associated with compact binaries inspiralling along general relativistic eccentric orbits. This approach is required as it provides an accurate and efficient way to incorporate the orbital, periastron advance and gravitational radiation reaction time scale variations, inherent in the dynamics of such binaries, on to $h_{\times,+}(t)$ in a PN-accurate manner.

It turns out that PN-accurate Keplerian type parametric solution is a key ingredient to implement GW phasing

* gihyuk.cho@desy.de

† stanay@go.olemiss.edu

for eccentric inspirals. Such solutions were presented in Refs. [44] and [45] at 2PN and 3PN orders, respectively. The solution of Ref. [45] that solves 3PN-accurate conservative orbital dynamics, detailed in Refs. [46, 47], is crucial to model the inspiral part of two IMR families, available in Refs. [28, 29]. Further, the Keplerian type parametric solution is also important to compute GW emission induced secular evolution of the orbital elements [48–51]. This paper computes 4PN order corrections to the 3PN-accurate generalized quasi-Keplerian parametric solution of Ref. [45] in the Arnowitt, Deser, and Misner (ADM) coordinates. We have dropped certain zero-average oscillatory terms from our solution arising due to 4PN tail effects due to them being relatively unimportant in GW data analysis. It was demonstrated that the total 4PN-accurate conservative Hamiltonian is the sum of instantaneous (local-in-time) near-zone Hamiltonian [52] and time-symmetric but nonlocal-in-time tail Hamiltonian [53]. These instantaneous contributions in the center-of-mass frame are similar in structure to 3PN-accurate Hamiltonian, as is evident from Eqs. (8.40) and (8.41) of Ref. [52]. Therefore, it is reasonable to expect that this part should admit Keplerian type parametric solution. Unfortunately, 4PN contributions to the time-symmetric but nonlocal-in-time tail Hamiltonian, given by Eq. (8.32) of Ref. [52], do not support any closed-form exact-in- e_t (e_t stands for the eccentricity) expression. Instead, we compute the approximate-in- e_t (valid up to $e_t \lesssim 0.9$), secular dynamics (ignoring the oscillatory ones) of the tail effect by employing canonical perturbation theory. This is reflected in corrections to the mean motion and the periastron advance, using Padé-like approximants. We perform detailed consistency checks to ensure the correctness of our lengthy solution. Further, we have verified that our local and non-local 4PN order expressions for the rate of periastron advance is consistent with similar expressions that are present in Refs. [54, 55].

We employ our 4PN order results to obtain an improved version of a restricted class of time-domain eccentric IMR family, detailed in Ref. [28]. This IMR family invokes PN approximation and employs temporally evolving quadrupolar order $h_{\times,+}$ associated with compact binaries inspiralling along 3PN-accurate eccentric orbits while being under the effects of 4.5PN-accurate (or relative 2PN order) GW damping. As for the merger-ringdown part, we implement the approach of Ref. [28] exactly (as a blackbox), explained in some detail in Sec. IIIB. This approach rests on identifying certain epochs during the inspiral-merger of the binary such as $t_{\text{blend}} < t_{\text{circ}} < t_{\text{peak}}$. For $t < t_{\text{blend}}$, PN equations of motion are used and for $t > t_{\text{circ}}$ we use the circular merger model (CMM) which is based on the assumption that the binary is essentially circular for $t > t_{\text{circ}}$. The CMM model is got via interpolation between circular numerical relativity (NR) waveforms for different q (mass ratio) values. To build the waveform between t_{blend} and t_{circ} , a certain ‘blending’ procedure is employed which just like

the CMM model, rests on the ideas of interpolation although of a different nature than the one employed to construct the CMM model. Ref. [28] used 23 NR simulations (with various mass ratios and initial eccentricities) as a basis for these interpolations which finally give the CMM and the blended waveforms.

We adapt the publicly available MATHEMATICA package [56] of Ref. [28] to obtain an updated eccentric IMR family using our 4PN-order parametric solution which can be found at Ref. [57, 58]. Moreover, we improve their inspiral description in a number of ways which results in a computationally more efficient (and higher PN order accurate) implementation of the eccentric inspiral dynamics of the binary. This includes the use of closed-form expressions to model orbital time scale variations and an improved way to tackle the PN-accurate Kepler equation (Mikkola method in conjunction with an ‘auxiliary eccentric anomaly’). We also pursue preliminary data analysis implications of our approximant to assess the importance of the 4PN order contributions to the inspiral part.

We expect our IMR waveform to be valid across a slightly larger parameter range than that for the waveform of Ref. [28], although we have not checked it; see the end of Sec. III for more details. Apart from our main IMR MATHEMATICA package, we also present a derived package which makes use of only the PN equations of motion to produce the waveforms and hence can be trusted only for the inspiral part. Because this PN package has nothing to do with the CMM, it should be valid for a much higher range of e_t ($e_t \lesssim 0.85$) than our main IMR package.

The plan of the paper is as follows. In Sec. II, we detail the derivation of 4PN order generalized quasi-Keplerian parametric solution after giving a brief introduction to the approach. We then discuss how to incorporate the tail effect into it. In Sec. III, we describe how we employed our parametric solution to develop an accurate and efficient eccentric inspiral waveform and obtain its IMR version, influenced by Ref. [28]. Some preliminary data analysis explorations are also discussed. Some of the computational details and lengthy expressions are provided in the appendices.

Convention: From Sec. III onwards, t denotes the ADM coordinate time, whereas in Sec. II, it denotes the ADM coordinate time scaled down by a factor of GM , with G and M standing for the gravitational constant and the total mass of the binary; more details below.

II. KEPLERIAN TYPE SOLUTION AT 4PN ORDER

We begin by summarizing Keplerian type parametric solution that describes efficiently the Newtonian dynamics of point mass binaries in eccentric orbits and its PN-accurate extensions. These extensions, detailed in Refs. [44, 45, 59, 60], may be referred to as the ‘general-

ized quasi-Keplerian' parametric solution for describing PN-accurate orbital dynamics of compact binaries in eccentric orbits. How we derive Keplerian type parametric solution associated with the 4PN-accurate near-zone local-in-time Hamiltonian $\mathcal{H}_{4\text{PN}}^{\text{local}}$, given by Eq. (8.41) of Ref. [52], is detailed in Sec. IIB.

A. Keplerian type solution and its 3PN extensions

The classical Keplerian parametric solution provides a semi-analytic description for the temporal evolution of a point mass binary in non-circular orbits under the influence of Newtonian dynamics [61]. In other words, it provides a parametric description for the relative separation vector $\mathbf{R} \equiv R(\cos \phi, \sin \phi, 0)$ in the usual center-of-mass reference frame of the binary. These angular and radial variables describe the position of the reduced mass $\mu = m_1 m_2 / M$ around the total mass $M = m_1 + m_2$ (m_1 and m_2 being the individual masses). We parametrize R and ϕ by

$$r = a(1 - e \cos u), \quad (1a)$$

$$\phi - \phi_0 = v \equiv 2 \arctan \left[\left(\frac{1+e}{1-e} \right)^{1/2} \tan \frac{u}{2} \right], \quad (1b)$$

where $r = R/(GM)$ and the auxiliary angles u and v are called eccentric and true anomalies, respectively. Further, a and e denote the semi-major axis and orbital eccentricity of the Newtonian closed orbit of μ around M . The explicit temporal evolution for \mathbf{R} is specified by the classical Kepler equation, namely

$$l \equiv n(t - t_0) = u - e \sin u, \quad (2)$$

where l and n are usually referred to as the mean anomaly and the mean motion, respectively. Further, $n = 2\pi/P$ with P being the orbital period and t_0 and ϕ_0 stand for some initial coordinate time and initial orbital phase, respectively. We reserve the symbol t for the re-scaled coordinate time $t = t'/(GM)$, where t' represents the ADM time coordinate whose unit is seconds. The explicit expressions for these orbital elements a, e and n are given by

$$a = \frac{1}{(-2E)}, \quad (3a)$$

$$e^2 = 1 + 2Eh^2, \quad (3b)$$

$$n = (-2E)^{3/2}, \quad (3c)$$

where E is the orbital energy per unit reduced mass while the reduced angular momentum h is given by $h = J/(GM)$ with J being the orbital angular momentum per unit reduced mass. It is customary to employ $J_s(se)$, the Bessel functions of the first kind, to express u in terms l as [62]

$$u = l + \sum_{s=1}^{\infty} \frac{2}{s} J_s(se) \sin(sl). \quad (4)$$

Remarkably, it is also possible to find Keplerian type parametric solution to the conservative orbital dynamics of compact binaries moving in relativistic orbits in the PN approximation. It was Damour and Deruelle who first proposed certain quasi-Keplerian parametrization to tackle 1PN accurate orbital dynamics of non-spinning compact binaries [59]. Thereafter, Schäfer and his collaborators developed the generalized quasi-Keplerian parametric solution to tackle both the 2PN and 3PN-accurate orbital dynamics of compact binaries [44, 45, 60]. The fully 3PN-accurate generalized quasi-Keplerian parametrization for a compact binary in an eccentric orbit may be written as

$$r = a_r (1 - e_r \cos u), \quad (5a)$$

$$l = n(t' - t'_0) = u - e_t \sin u + \left(\frac{g_{4t}}{c^4} + \frac{g_{6t}}{c^6} \right) (v - u) + \left(\frac{f_{4t}}{c^4} + \frac{f_{6t}}{c^6} \right) \sin v + \frac{i_{6t}}{c^6} \sin 2v + \frac{h_{6t}}{c^6} \sin 3v, \quad (5b)$$

$$\frac{2\pi}{\Phi} (\phi - \phi_0) = v + \left(\frac{f_{4\phi}}{c^4} + \frac{f_{6\phi}}{c^6} \right) \sin 2v + \left(\frac{g_{4\phi}}{c^4} + \frac{g_{6\phi}}{c^6} \right) \sin 3v + \frac{i_{6\phi}}{c^6} \sin 4v + \frac{h_{6\phi}}{c^6} \sin 5v, \quad (5c)$$

where $v = 2 \arctan[\sqrt{(1+e_\phi)/(1-e_\phi)} \tan(u/2)]$ (see Ref. [45]). A casual comparison of Eqs. (5) with Eqs. (1a) and (2) reveals that at PN orders there are three different eccentricities which are denoted by e_r, e_t and e_ϕ . These radial, time and angular eccentricity parameters are introduced to ensure that the resulting PN-accurate parametric solution looks Keplerian at the first post-Newtonian order (at higher PN orders it gains additional terms as can be seen in Eqs. (5)). The orbital elements a_r and n provide certain PN-accurate semi-major axis and mean motion while the factor $2\pi/\Phi$ gives the angle of advance of the pericenter per orbital revolution. Further, we have many orbital functions that appear at 2PN and 3PN orders and these are denoted by $g_{4t}, g_{6t}, f_{4t}, f_{6t}, i_{6t}, h_{6t}, f_{4\phi}, f_{6\phi}, g_{4\phi}, g_{6\phi}, i_{6\phi}$, and $h_{6\phi}$. The explicit 3PN-accurate expressions for these orbital elements and functions in terms of 3PN accurate orbital energy E , angular momentum h and the symmetric mass ratio $\eta = \mu/M$ are provided in Ref. [45]. Additionally, Ref. [63] derived 3PN-accurate extension of Eq. (4) thereby providing a closed-form solution of the 3PN Kepler equation, namely Eq. (5b). Further, Ref. [64] provided hyperbolic extension of Eq. (5a) to model PN-accurate GWs from compact binaries in hyperbolic passages. We note in passing that the 1PN-accurate parametric solution is usually referred to as the quasi-Keplerian parameterization as it looks functionally similar to its Newtonian counterpart. However, the parametric solutions at higher PN orders are termed the generalized quasi-Keplerian parameterizations and this is mainly due to the appearances of PN-accurate orbital functions in the expressions for $(\phi - \phi_0)$ and the Kepler equation.

These PN-accurate parametric solutions are of definite interest from observational points of view. For ex-

ample, the 1PN-accurate Keplerian type parametric solution is crucial to operationalize the widely employed Damour-Deruelle timing formula to time relativistic binary pulsars [65, 66]. Moreover, the above parametrization is also employed to construct accurate and efficient GW templates for compact binaries inspiralling along PN-accurate eccentric orbits [42, 43]. Very recently, the above solution was also invoked to model pulsar timing array residuals induced by nano-Hz GWs from massive BH binaries in relativistic eccentric orbits [67]. In what follows, we extend the computations of Ref. [45] to obtain 4PN order Keplerian type parametric solution for eccentric compact binaries.

B. Incorporating local-in-time 4PN Hamiltonian: generalized quasi-Keplerian solution

We employ the local-in-time part of the 4PN accurate ADM Hamiltonian for non-spinning compact binaries, given by Eq. (8.41) of Ref. [52], for computing 4PN order Keplerian parametric solution¹. This Hamiltonian

was crucial to complete the program to derive the 4PN accurate compact binary dynamics that incorporates all the general relativity based $(v/c)^8$ corrections as detailed in Ref. [53, 68]. The above Hamiltonian included certain time-symmetric nonlocal-in-time interactions, which are connected to the dominant order tail effects in the gravitational radiation reaction [69]. The resulting compact binary dynamics extends the 3PN-accurate conservative orbital dynamics, presented in Ref. [70], with the help of lengthy 4PN order computations that employ dimensional regularization and detailed far-zone matching [52, 53, 71, 72]. Very recently, Ref. [55] provided an independent check for the 4PN-accurate Hamiltonian of Schäfer and his collaborators by recomputing it within an effective field theory (EFT) approach in harmonic coordinates. We note that there are independent efforts to obtain 4PN accurate orbital dynamics using the EFT approach [73, 74] and Fokker action computations [75]. We give below the local-in-time near-zone 4PN-accurate reduced Hamiltonian in ADM-type coordinates and in the center-of-mass frame, given by Eq. (8.41) of Ref. [52], as (see footnote 2)

$$\mathcal{H}_{4\text{PN}}^{\text{local}}(\mathbf{r}, \hat{\mathbf{p}}) = \frac{\hat{\mathbf{p}}^2}{2} - \frac{1}{r} + \frac{1}{c^2} \mathcal{H}_1(\mathbf{r}, \hat{\mathbf{p}}) + \frac{1}{c^4} \mathcal{H}_2(\mathbf{r}, \hat{\mathbf{p}}) + \frac{1}{c^6} \mathcal{H}_3(\mathbf{r}, \hat{\mathbf{p}}) + \frac{1}{c^8} \mathcal{H}_4(\mathbf{r}, \hat{\mathbf{p}}), \quad (6)$$

where the explicit expressions for the 1PN, 2PN and 3PN contributions are given in Eq. (7) of Ref. [45]. This reduced Hamiltonian is connected to the Hamiltonian by $\mathcal{H}_{4\text{PN}}^{\text{local}}(\mathbf{r}, \hat{\mathbf{p}}) = H_{4\text{PN}}^{\text{local}}(\mathbf{r}, \hat{\mathbf{p}})/\mu$. The 4PN order contributions, extracted from Eq. (8.41) of Ref. [52], read

$$\begin{aligned} \mathcal{H}_4(\mathbf{r}, \hat{\mathbf{p}}) = & \left(\frac{7}{256} - \frac{63}{256} \eta + \frac{189}{256} \eta^2 - \frac{105}{128} \eta^3 + \frac{63}{256} \eta^4 \right) (\hat{\mathbf{p}}^2)^5 \\ & + \left\{ \frac{45}{128} (\hat{\mathbf{p}}^2)^4 - \frac{45}{16} (\hat{\mathbf{p}}^2)^4 \eta + \left(\frac{423}{64} (\hat{\mathbf{p}}^2)^4 - \frac{3}{32} (\mathbf{n} \cdot \hat{\mathbf{p}})^2 (\hat{\mathbf{p}}^2)^3 - \frac{9}{64} (\mathbf{n} \cdot \hat{\mathbf{p}})^4 (\hat{\mathbf{p}}^2)^2 \right) \eta^2 \right. \\ & + \left(-\frac{1013}{256} (\hat{\mathbf{p}}^2)^4 + \frac{23}{64} (\mathbf{n} \cdot \hat{\mathbf{p}})^2 (\hat{\mathbf{p}}^2)^3 + \frac{69}{128} (\mathbf{n} \cdot \hat{\mathbf{p}})^4 (\hat{\mathbf{p}}^2)^2 - \frac{5}{64} (\mathbf{n} \cdot \hat{\mathbf{p}})^6 (\hat{\mathbf{p}}^2) + \frac{35}{256} (\mathbf{n} \cdot \hat{\mathbf{p}})^8 \right) \eta^3 \\ & + \left(-\frac{35}{128} (\hat{\mathbf{p}}^2)^4 - \frac{5}{32} (\mathbf{n} \cdot \hat{\mathbf{p}})^2 (\hat{\mathbf{p}}^2)^3 - \frac{9}{64} (\mathbf{n} \cdot \hat{\mathbf{p}})^4 (\hat{\mathbf{p}}^2)^2 - \frac{5}{32} (\mathbf{n} \cdot \hat{\mathbf{p}})^6 \hat{\mathbf{p}}^2 - \frac{35}{128} (\mathbf{n} \cdot \hat{\mathbf{p}})^8 \right) \eta^4 \left. \right\} \frac{1}{r} \\ & + \left\{ \frac{13}{8} (\hat{\mathbf{p}}^2)^3 + \left(-\frac{791}{64} (\hat{\mathbf{p}}^2)^3 + \frac{49}{16} (\mathbf{n} \cdot \hat{\mathbf{p}})^2 (\hat{\mathbf{p}}^2)^2 - \frac{889}{192} (\mathbf{n} \cdot \hat{\mathbf{p}})^4 \hat{\mathbf{p}}^2 + \frac{369}{160} (\mathbf{n} \cdot \hat{\mathbf{p}})^6 \right) \eta \right. \\ & + \left(\frac{4857}{256} (\hat{\mathbf{p}}^2)^3 - \frac{545}{64} (\mathbf{n} \cdot \hat{\mathbf{p}})^2 (\hat{\mathbf{p}}^2)^2 + \frac{9475}{768} (\mathbf{n} \cdot \hat{\mathbf{p}})^4 \hat{\mathbf{p}}^2 - \frac{1151}{128} (\mathbf{n} \cdot \hat{\mathbf{p}})^6 \right) \eta^2 \\ & + \left(\frac{2335}{256} (\hat{\mathbf{p}}^2)^3 + \frac{1135}{256} (\mathbf{n} \cdot \hat{\mathbf{p}})^2 (\hat{\mathbf{p}}^2)^2 - \frac{1649}{768} (\mathbf{n} \cdot \hat{\mathbf{p}})^4 \hat{\mathbf{p}}^2 + \frac{10353}{1280} (\mathbf{n} \cdot \hat{\mathbf{p}})^6 \right) \eta^3 \left. \right\} \frac{1}{r^2} \end{aligned}$$

¹ A masterly treatise on the PN computations for compact binary dynamics in the Hamiltonian approach to general relativity is

available in Ref. [46]

$$\begin{aligned}
& + \left\{ \frac{105}{32} (\hat{\mathbf{p}}^2)^2 + \left(\left(\frac{2749\pi^2}{8192} - \frac{589189}{19200} \right) (\hat{\mathbf{p}}^2)^2 + \left(\frac{63347}{1600} - \frac{1059\pi^2}{1024} \right) (\mathbf{n} \cdot \hat{\mathbf{p}})^2 \hat{\mathbf{p}}^2 + \left(\frac{375\pi^2}{8192} - \frac{23533}{1280} \right) (\mathbf{n} \cdot \hat{\mathbf{p}})^4 \right) \eta \right. \\
& + \left(\left(\frac{18491\pi^2}{16384} - \frac{1189789}{28800} \right) (\hat{\mathbf{p}}^2)^2 + \left(-\frac{127}{3} - \frac{4035\pi^2}{2048} \right) (\mathbf{n} \cdot \hat{\mathbf{p}})^2 \hat{\mathbf{p}}^2 + \left(\frac{57563}{1920} - \frac{38655\pi^2}{16384} \right) (\mathbf{n} \cdot \hat{\mathbf{p}})^4 \right) \eta^2 \\
& + \left. \left(-\frac{553}{128} (\hat{\mathbf{p}}^2)^2 - \frac{225}{64} (\mathbf{n} \cdot \hat{\mathbf{p}})^2 \hat{\mathbf{p}}^2 - \frac{381}{128} (\mathbf{n} \cdot \hat{\mathbf{p}})^4 \right) \eta^3 \right\} \frac{1}{r^3} \\
& + \left\{ \frac{105}{32} \hat{\mathbf{p}}^2 + \left(\left(\frac{185761}{19200} - \frac{21837\pi^2}{8192} \right) \hat{\mathbf{p}}^2 + \left(\frac{3401779}{57600} - \frac{28691\pi^2}{24576} \right) (\mathbf{n} \cdot \hat{\mathbf{p}})^2 \right) \eta \right. \\
& + \left. \left(\left(\frac{672811}{19200} - \frac{158177\pi^2}{49152} \right) \hat{\mathbf{p}}^2 + \left(\frac{110099\pi^2}{49152} - \frac{21827}{3840} \right) (\mathbf{n} \cdot \hat{\mathbf{p}})^2 \right) \eta^2 \right\} \frac{1}{r^4} \\
& + \left\{ -\frac{1}{16} + \left(\frac{6237\pi^2}{1024} - \frac{169199}{2400} \right) \eta + \left(\frac{7403\pi^2}{3072} - \frac{1256}{45} \right) \eta^2 \right\} \frac{1}{r^5}. \tag{7}
\end{aligned}$$

where $\mathbf{r} = \mathbf{R}/(GM)$, $r = |\mathbf{r}|$, $\mathbf{n} = \mathbf{r}/r$ and $\hat{\mathbf{p}} = \mathbf{P}/\mu$; \mathbf{R} and \mathbf{P} are the relative separation vector and its conjugate momentum vector respectively. It is easy to show that the above $\mathcal{H}(\mathbf{r}, \hat{\mathbf{p}})$ admits two conserved quantities, namely the 4PN order reduced energy $E = \mathcal{H}_{4\text{PN}}^{\text{local}}$ and the reduced angular momentum $\hat{\mathbf{J}} = \mathbf{r} \times \hat{\mathbf{p}}$ of the binary in the center-of-mass frame due to its invariance under time translations and spatial rotations. These considerations allow us to restrict the motion of our non-spinning compact binary to a plane and employ polar coordinates such that $\mathbf{r} = r(\cos \phi, \sin \phi)$. Naturally, the relative motion follows the following differential equations arising from the Hamiltonian equations

$$\dot{\mathbf{r}} = \mathbf{n} \cdot \frac{\partial \mathcal{H}}{\partial \hat{\mathbf{p}}}, \tag{8a}$$

$$r^2 \dot{\phi} = \left| \mathbf{r} \times \frac{\partial \mathcal{H}}{\partial \hat{\mathbf{p}}} \right|, \tag{8b}$$

where $\dot{r} = dr/dt$, $\dot{\phi} = d\phi/dt$. It is convenient to introduce a variable $s = 1/r$ such that the \dot{r}^2 expression at the Newtonian order becomes a quadratic polynomial in s . In terms of s , we have $\dot{r}^2 = (ds/dt)^2/s^4 = \dot{s}^2/s^4$ which leads to a 4PN order expression for \dot{s}^2 in terms of $(-2E)$, $h = |\hat{\mathbf{J}}|$, η and s . This allows us to obtain PN-accurate expressions for the two turning points of an eccentric orbit, defined by Eqs. (8). Further, we also

compute 4PN order differential equation for $d\phi/ds = \dot{\phi}/\dot{s}$ using Eqs. (8) to tackle the angular part of our 4PN order Keplerian type parametric solution.

We first focus on the 4PN order expression for \dot{r}^2 and it turns out to be a 9th degree polynomial in s . This expression may be written symbolically as

$$\begin{aligned}
\dot{r}^2 = \frac{1}{s^4} \left(\frac{ds}{dt} \right)^2 = & a_0 + a_1 s + a_2 s^2 + a_3 s^3 + a_4 s^4 + a_5 s^5 \\
& + a_6 s^6 + a_7 s^7 + a_8 s^8 + a_9 s^9. \tag{9}
\end{aligned}$$

The explicit 4PN order contributions to these coefficients are provided in the accompanying MATHEMATICA file `Lengthy_Expressions.nb` [57, 58], while their 3PN-accurate contributions are available as Eqs. (A1) in Ref. [45]. Further, the coefficients a_8 and a_9 contain only 4PN order contributions. To obtain parametric solution to Eq. (9), we need to follow a couple of steps. First, we compute the two positive roots of the RHS of Eq. (9) having finite limits as $1/c \rightarrow 0$ by demanding $\dot{r}^2 = 0$ (other roots are pushed to $\pm\infty$ in this limit). We label these 4PN order roots as s_- (pericenter) and s_+ (apocenter). They correspond to the turning points of our PN-accurate eccentric orbits and are functions of E , h and η . For illustration, we display below their 1PN accurate expressions

$$s_{\pm} = \frac{1 \pm \sqrt{1 + 2h^2 E}}{h^2} \mp \frac{1}{c^2} \frac{(1 \pm \sqrt{1 + 2h^2 E})^2 [-\eta - 9 \pm 2(\eta - 7)\sqrt{1 + 2h^2 E} + (3\eta - 1)(1 + 2h^2 E)]}{8h^4 \sqrt{1 + 2h^2 E}}. \tag{10}$$

The explicit 4PN order expressions for these two roots are

available in the accompanying MATHEMATICA notebook

`Lengthy_Expressions.nb` [57, 58]. We now parametrize the 4PN order radial motion with the help of the following ansatz:

$$r = a_r (1 - e_r \cos u), \quad (11)$$

where a_r and e_r are some 4PN order semi-major axis and radial eccentricity, respectively. This ansatz allows us to express both a_r and e_r in terms of s_- and s_+ as

$$a_r = \frac{1}{2} \frac{s_- + s_+}{s_- s_+}, \quad e_r = \frac{s_- - s_+}{s_- + s_+}. \quad (12)$$

This leads in a straightforward manner to the 4PN order expressions for a_r and e_r^2 in terms of E, h and η .

We now move on to obtain an integral connecting t and s after factorizing the above $(ds/dt)^2/s^4$ expression using 4PN order s_- and s_+ expressions. The resulting 4PN order integral may be written as

$$t - t_0 = \int_s^{s_-} \frac{A_0 + A_1 \bar{s} + A_2 \bar{s}^2 + A_3 \bar{s}^3 + A_4 \bar{s}^4 + A_5 \bar{s}^5 + A_6 \bar{s}^6 + A_7 \bar{s}^7}{\sqrt{(s_- - \bar{s})(\bar{s} - s_+)} \bar{s}^2} d\bar{s}, \quad (13)$$

and how we obtain the above integral from our PN-accurate expression for ds/dt is explained in Appendix A. Additionally, we gather from the structure of the expressions of $(ds/dt)^2$, s_- and s_+ that the coefficients A_i (with $i = 1, \dots, 7$) should be some PN-accurate functions of E, h

and η . We now compute the radial orbital period as the value of the above integral between s_- and s_+ , multiplied by two. In other words, 4PN order expression for the radial period reads

$$P = 2 \int_{s_+}^{s_-} \frac{A_0 + A_1 \bar{s} + A_2 \bar{s}^2 + A_3 \bar{s}^3 + A_4 \bar{s}^4 + A_5 \bar{s}^5 + A_6 \bar{s}^6 + A_7 \bar{s}^7}{\sqrt{(s_- - \bar{s})(\bar{s} - s_+)} \bar{s}^2} d\bar{s}. \quad (14)$$

The explicit expression for P will be displayed when we present 4PN order Keplerian type solution. Note that PN-accurate mean motion $n = 2\pi/P$.

We now have all the necessary ingredients to obtain the 4PN order Kepler equation. This requires us to express the mean anomaly $l \equiv n(t - t_0)$ as a function of eccentric anomaly u with the help of our Eqs. (13) and (14) while employing our parametric equation for $r = a_r(1 - e_r \cos u)$. It is convenient to introduce an auxiliary variable $\tilde{v} = 2 \arctan[\sqrt{(1 + e_r)/(1 - e_r)} \tan(u/2)]$ and with the help of a few trigonometric relations involving \tilde{v} , we obtain the following provisional parametrization for l as

$$l \equiv n(t - t_0) = u + \kappa_0 \sin u + \frac{\kappa_1}{c^4} (\tilde{v} - u) + \frac{\kappa_2}{c^4} \sin \tilde{v} + \frac{\kappa_3}{c^6} \sin 2\tilde{v} + \frac{\kappa_4}{c^6} \sin 3\tilde{v} + \frac{\kappa_5}{c^8} \sin 4\tilde{v} + \frac{\kappa_6}{c^8} \sin 5\tilde{v}. \quad (15)$$

The steps required to obtain the above expression from Eq. (13) are sketched in the Appendix B of Ref. [45]. Note that these κ_i coefficients are some PN accurate functions of E, h and η and they can be had from the accompanying

MATHEMATICA notebook `Lengthy_Expressions.nb` [57, 58] and some details of the underlying computations are provided in Appendices A and B. We treat the above expression as a provisional one as it contains 1PN order corrections to the classical Kepler equation due to the presence of PN accurate κ_0 expression that multiplies $\sin u$. Recall that there exists 1PN-accurate Kepler equation that is structurally similar (by “structurally similar” we mean having no explicit 1PN additive correction terms) to the classical Kepler equation, obtained by invoking certain conchoidal transformation [59]. It will be desirable to keep such a structure while computing 4PN order Kepler equation and this will be taken up later.

We move on to tackle the angular part by first computing our 4PN order expression for $d\phi/ds$ with the help of $d\phi/ds = \dot{\phi}/\dot{s}$, where $\dot{\phi}$ expression arises from the usual Hamiltonian equations of motion. Influenced by our approach to tackle the radial motion, we obtain an expression for $d\phi/ds$ which involves a similar factorization based on s_+ and s_- as in Eqs. (13) and (14). The resulting expression may be written as

$$\frac{d\phi}{ds} = \frac{B_0 + B_1 s + B_2 s^2 + B_3 s^3 + B_4 s^4 + B_5 s^5 + B_6 s^6 + B_7 s^7}{\sqrt{(s_- - s)(s - s_+)}} \quad (16)$$

where the coefficients B_i ($i = 1, \dots, 7$), as expected, are some 4PN order functions of E, h and η (the explicit expressions for these coefficients are listed in the accompanying MATHEMATICA notebook). Additionally, we sketch how to obtain 1PN-accurate $d\phi/ds$ expression from $\dot{\phi}$

and dt/ds in Appendix A. The above equation also allows us to compute the amount by which periastron (or pericenter) advances during the above computed 4PN order radial period P . This is obtained by integrating the above equation between our 4PN order roots s_+ and s_- and multiplying the result by two. In other words, the amount of periastron advance during one radial period is

$$\Phi = 2 \int_{s_+}^{s_-} \frac{B_0 + B_1 \bar{s} + B_2 \bar{s}^2 + B_3 \bar{s}^3 + B_4 \bar{s}^4 + B_5 \bar{s}^5 + B_6 \bar{s}^6 + B_7 \bar{s}^7}{\sqrt{(s_- - \bar{s})(\bar{s} - s_+)}} d\bar{s}. \quad (17)$$

It should be obvious that the resulting 4PN order Φ expression depends on E, h and η and we have verified that our expression is consistent with Eq. (20-k) in Ref. [45]. We now invoke 4PN order expressions for Φ (got by evaluating the integral in Eq. (17)) and $d\phi/ds$ to obtain $(\phi - \phi_0) \times (2\pi/\Phi)$ which we symbolically write as

$$\frac{2\pi}{\Phi} \times (\phi - \phi_0) = \int_s^{s_-} \frac{B'_0 + B'_1 \bar{s} + B'_2 \bar{s}^2 + B'_3 \bar{s}^3 + B'_4 \bar{s}^4 + B'_5 \bar{s}^5 + B'_6 \bar{s}^6 + B'_7 \bar{s}^7}{\sqrt{(s_- - \bar{s})(\bar{s} - s_+)}} d\bar{s}, \quad (18)$$

where the primed B'_i coefficients are got from the unprimed B_i 's. It is possible to evaluate the above integral with the help of certain trigonometric relations and steps as detailed in Appendix B. This results in the following provisional parametric expression for the 4PN order angular motion

$$\begin{aligned} \frac{2\pi}{\Phi} (\phi - \phi_0) &= \tilde{v} + \frac{\lambda_1}{c^2} \sin \tilde{v} + \frac{\lambda_2}{c^4} \sin 2\tilde{v} + \frac{\lambda_3}{c^4} \sin 3\tilde{v} \\ &+ \frac{\lambda_4}{c^6} \sin 4\tilde{v} + \frac{\lambda_5}{c^6} \sin 5\tilde{v} + \frac{\lambda_6}{c^8} \sin 6\tilde{v} + \frac{\lambda_7}{c^8} \sin 7\tilde{v}, \end{aligned} \quad (19)$$

where λ_i are some PN accurate functions, expressible in terms of E, h and η .

Following Ref. [45], we obtain our final parametrization for l and ϕ equations with the help of some true anomaly variable $v = 2 \arctan[\sqrt{(1+e_\phi)/(1-e_\phi)} \tan(u/2)]$ that involves a new angular eccentricity parameter e_ϕ . The plan is to write Eq. (19) in terms of v rather than \tilde{v} so that there are no explicit, additive $1/c^2$ corrections, while allowing e_ϕ to differ from e_r by some yet to be determined PN corrections. It is possible to write our \tilde{v} in terms of v

$$\tilde{v} = v + \frac{y}{c^2} \sin v + \frac{y^2}{4c^4} (-2 \sin v + \sin 2v)$$

$$\begin{aligned} &+ \frac{y^3}{12c^6} (3 \sin v - 3 \sin 2v + \sin 3v) \\ &+ \frac{y^4}{32c^8} (-4 \sin v + 6 \sin 2v - 4 \sin 3v + \sin 4v) \end{aligned} \quad (20)$$

where y connects e_ϕ and e_r to 4PN order and it is natural to introduce y such that

$$y = \frac{\sqrt{(1+e_r)/(1-e_r)}}{\sqrt{(1+e_\phi)/(1-e_\phi)}} - 1. \quad (21)$$

We now express $2\pi(\phi - \phi_0)/\Phi$, given by Eq. (19), in terms of v and demand that there are no $\sin v$ terms up to 4PN order. This requirement uniquely determines y as a PN series which connects e_ϕ to e_r . For example, the dominant 1PN contribution of y may be written as

$$y = -\frac{\eta \sqrt{1+2E} h^2}{2c^2 h^2} + \mathcal{O}\left(\frac{1}{c^4}\right). \quad (22)$$

It should be noted that we imposed such a restriction because 1PN-accurate parametric solution, derived in Ref. [59], supported a *Keplerian* like parametrization for the angular part with the help of v . This leads to the following parametric solution for the angular motion while incorporating 4PN order contributions:

$$\begin{aligned} \frac{2\pi}{\Phi} (\phi - \phi_0) &= v + \left(\frac{f_{4\phi}}{c^4} + \frac{f_{6\phi}}{c^6} + \frac{f_{8\phi}}{c^8} \right) \sin 2v + \left(\frac{g_{4\phi}}{c^4} + \frac{g_{6\phi}}{c^6} + \frac{g_{8\phi}}{c^8} \right) \sin 3v \\ &+ \left(\frac{i_{6\phi}}{c^6} + \frac{i_{8\phi}}{c^8} \right) \sin 4v + \left(\frac{h_{6\phi}}{c^6} + \frac{h_{8\phi}}{c^8} \right) \sin 5v + \frac{k_{8\phi}}{c^8} \sin 6v + \frac{j_{8\phi}}{c^8} \sin 7v, \end{aligned} \quad (23)$$

where $v = 2 \arctan[\sqrt{(1+e_\phi)/(1-e_\phi)} \tan(u/2)]$. Inter-

estingly, the contributions at 2PN, 3PN and 4PN orders

are supplemented by other trigonometric functions of v and this is why we term the resulting solution as the generalized quasi-Keplerian parametric solution. We will display shortly the explicit 4PN order expressions for these orbital elements and functions.

We now move to finalize the provisional expression for

our 4PN order Kepler equation, given by Eq. (15). The idea is to express \tilde{v} in terms of v with the help of the above listed PN-accurate relation of Eq. (20). This leads to the following Kepler equation that includes 4PN order contributions in terms of $u, e_t, v(u)$ and its trigonometric functions as

$$l = n(t - t_0) = u - e_t \sin u + \left(\frac{g_{4t}}{c^4} + \frac{g_{6t}}{c^6} + \frac{g_{8t}}{c^8} \right) (v - u) + \left(\frac{f_{4t}}{c^4} + \frac{f_{6t}}{c^6} + \frac{f_{8t}}{c^8} \right) \sin v + \left(\frac{i_{6t}}{c^6} + \frac{i_{8t}}{c^8} \right) \sin 2v + \left(\frac{h_{6t}}{c^6} + \frac{h_{8t}}{c^8} \right) \sin 3v + \frac{k_{8t}}{c^8} \sin 4v + \frac{j_{8t}}{c^8} \sin 5v. \quad (24)$$

The PN accurate expressions for n, e_t and the orbital functions appearing in the above PN-accurate Kepler equation will be listed below.

We now have all the parts to display, in its entirety, the fourth post-Newtonian order generalized quasi-Keplerian parametrization for an eccentric compact binary in ADM-type coordinates as

$$r = a_r (1 - e_r \cos u), \quad (25)$$

$$l = n(t - t_0) = u - e_t \sin u + \left(\frac{g_{4t}}{c^4} + \frac{g_{6t}}{c^6} + \frac{g_{8t}}{c^8} \right) (v - u) + \left(\frac{f_{4t}}{c^4} + \frac{f_{6t}}{c^6} + \frac{f_{8t}}{c^8} \right) \sin v + \left(\frac{i_{6t}}{c^6} + \frac{i_{8t}}{c^8} \right) \sin 2v + \left(\frac{h_{6t}}{c^6} + \frac{h_{8t}}{c^8} \right) \sin 3v + \frac{k_{8t}}{c^8} \sin 4v + \frac{j_{8t}}{c^8} \sin 5v, \quad (26)$$

$$\frac{2\pi}{\Phi} (\phi - \phi_0) = v + \left(\frac{f_{4\phi}}{c^4} + \frac{f_{6\phi}}{c^6} + \frac{f_{8\phi}}{c^8} \right) \sin 2v + \left(\frac{g_{4\phi}}{c^4} + \frac{g_{6\phi}}{c^6} + \frac{g_{8\phi}}{c^8} \right) \sin 3v + \left(\frac{i_{6\phi}}{c^6} + \frac{i_{8\phi}}{c^8} \right) \sin 4v + \left(\frac{h_{6\phi}}{c^6} + \frac{h_{8\phi}}{c^8} \right) \sin 5v + \frac{k_{8\phi}}{c^8} \sin 6v + \frac{j_{8\phi}}{c^8} \sin 7v, \quad (27)$$

where $v = 2 \arctan[\sqrt{(1 + e_\phi)/(1 - e_\phi)} \tan(u/2)]$. In what follows, we display the 4PN order expressions for the orbital elements a_r, n, Φ , and the post-Newtonian orbital functions that appear at 2PN, 3PN and 4PN orders in terms of the conserved quantities:

$$\begin{aligned} a_r = & \frac{1}{(-2E)} \left\{ 1 + \frac{(-2E)}{4c^2} (-7 + \eta) + \frac{(-2E)^2}{16c^4} \left[(1 + 10\eta + \eta^2) \right. \right. \\ & + \frac{1}{(-2Eh^2)} (-68 + 44\eta) \left. \right] + \frac{(-2E)^3}{192c^6} \left[3 - 9\eta - 6\eta^2 \right. \\ & + 3\eta^3 + \frac{1}{(-2Eh^2)} \left(864 + (-3\pi^2 - 2212)\eta + 432\eta^2 \right) \\ & + \frac{1}{(-2Eh^2)^2} \left(-6432 + (13488 - 240\pi^2)\eta - 768\eta^2 \right) \left. \right] \\ & + \frac{(-2E)^4}{3686400c^8} \left[14400 - 57600\eta + 28800\eta^2 - 158400\eta^3 + 14400\eta^4 \right. \\ & + \frac{1}{(-2Eh^2)} \left(-4147200 + (-38071488 + 1280250\pi^2)\eta \right. \\ & + (19038208 + 4030875\pi^2)\eta^2 + 4262400\eta^3 \left. \right) \\ & + \frac{1}{(-2Eh^2)^2} \left(316800000 + (-661398528 + 21132000\pi^2)\eta \right. \\ & + (363371776 - 26908200\pi^2)\eta^2 - 20160000\eta^3 \left. \right) \\ & + \frac{1}{(-2Eh^2)^3} \left(-1228492800 + (2644664832 - 59785200\pi^2)\eta \right. \end{aligned}$$

$$+ (-826707456 + 34613400 \pi^2) \eta^2 + 13824000 \eta^3 \Big) \Big] \Big\}, \quad (28a)$$

$$\begin{aligned} n = & (-2 E)^{3/2} \left\{ 1 + \frac{(-2 E)}{8 c^2} (-15 + \eta) + \frac{(-2 E)^2}{128 c^4} \left[555 + 30 \eta \right. \right. \\ & + 11 \eta^2 + \frac{192}{\sqrt{(-2 E h^2)}} (-5 + 2 \eta) \Big] + \frac{(-2 E)^3}{3072 c^6} \left[-29385 \right. \\ & - 4995 \eta - 315 \eta^2 + 135 \eta^3 - \frac{16}{(-2 E h^2)^{3/2}} \left(10080 + 123 \eta \pi^2 \right. \\ & - 13952 \eta + 1440 \eta^2 \Big) + \frac{5760}{\sqrt{(-2 E h^2)}} (17 - 9 \eta + 2 \eta^2) \Big] \\ & + \frac{(-2 E)^4}{1474560 c^8} \left[\frac{3317760 (-5 + 2 \eta)^2}{-2 E h^2} + \frac{138240}{\sqrt{(-2 E h^2)}} \right. \\ & \times (-1125 + 550 \eta - 175 \eta^2 + 38 \eta^3) + 135 \left(232881 \right. \\ & + 65300 \eta + 4070 \eta^2 - 460 \eta^3 + 241 \eta^4 \Big) \\ & - \frac{80}{(-2 E h^2)^{3/2}} \left(-5443200 + (10467328 - 150987 \pi^2) \eta \right. \\ & + (-3959808 + 32472 \pi^2) \eta^2 + 311040 \eta^3 \Big) \\ & + \frac{48}{(-2 E h^2)^{5/2}} \left(-17297280 + (37556864 - 771585 \pi^2) \eta \right. \\ & \left. \left. + (-13464960 + 236160 \pi^2) \eta^2 + 403200 \eta^3 \right) \right] \Big\}, \end{aligned} \quad (28b)$$

$$g_{4t} = \frac{3(-2 E)^2}{2} \left\{ \frac{5 - 2 \eta}{\sqrt{(-2 E h^2)}} \right\}, \quad (28c)$$

$$\begin{aligned} g_{6t} = & \frac{(-2 E)^3}{192} \left\{ \frac{1}{(-2 E h^2)^{3/2}} \left(10080 + 123 \eta \pi^2 - 13952 \eta \right. \right. \\ & + 1440 \eta^2 \Big) + \frac{1}{\sqrt{(-2 E h^2)}} (-3420 + 1980 \eta - 648 \eta^2) \Big\}, \end{aligned} \quad (28d)$$

$$\begin{aligned} g_{8t} = & -\frac{(-2 E)^4}{92160} \left\{ \frac{3}{(-2 E h^2)^{5/2}} \left(-17297280 + (37556864 \right. \right. \\ & - 771585 \pi^2) \eta + 1920 (-7013 + 123 \pi^2) \eta^2 + 403200 \eta^3 \Big) \\ & - \frac{5}{(-2 E h^2)^{3/2}} \left(-3628800 + (7835008 - 128847 \pi^2) \eta \right. \\ & + 36 (-98144 + 861 \pi^2) \eta^2 + 293760 \eta^3 \Big) + \frac{207360}{(-2 E h^2)} (5 - 2 \eta)^2 \\ & \left. \left. + \frac{1080}{\sqrt{(-2 E h^2)}} (-3375 + 1600 \eta - 755 \eta^2 + 246 \eta^3) \right\}, \end{aligned} \quad (28e)$$

$$f_{4t} = -\frac{1}{8} \frac{(-2 E)^2}{\sqrt{(-2 E h^2)}} \left\{ (4 + \eta) \eta \sqrt{(1 + 2 E h^2)} \right\}, \quad (28f)$$

$$\begin{aligned} f_{6t} = & \frac{(-2 E)^3}{192} \left\{ \frac{1}{(-2 E h^2)^{3/2}} \frac{1}{\sqrt{1 + 2 E h^2}} \left(1728 - 4148 \eta + 3 \eta \pi^2 \right. \right. \\ & + 600 \eta^2 + 33 \eta^3 \Big) + 3 \frac{\sqrt{(-2 E h^2)}}{\sqrt{(1 + 2 E h^2)}} \eta (-64 - 4 \eta + 23 \eta^2) \end{aligned}$$

$$\begin{aligned}
& + \frac{1}{\sqrt{(-2 E h^2)(1+2 E h^2)}} \left(-1728 + 4232 \eta - 3 \eta \pi^2 \right. \\
& \left. - 627 \eta^2 - 105 \eta^3 \right) \Big\}, \tag{28g}
\end{aligned}$$

$$\begin{aligned}
f_{8t} = & - \frac{(-2 E)^4}{14745600} \frac{(-2 E h^2)^{3/2}}{(1+2 E h^2)^{3/2}} \left\{ 7200 \eta (4672 + 912 \eta \right. \\
& - 303 \eta^2 + 902 \eta^3) + \frac{2764800}{\sqrt{(-2 E h^2)}} \eta (4 + \eta) (-5 + 2 \eta) \\
& + \frac{1}{(-2 E h^2)} \left(331776000 + 1350 (-919776 + 2377 \pi^2) \eta \right. \\
& + (568404992 + 2468925 \pi^2) \eta^2 - 94248000 \eta^3 - 16128000 \eta^4 \Big) \\
& - \frac{5529600}{(-2 E h^2)^{3/2}} \eta (4 + \eta) (-5 + 2 \eta) \\
& + \frac{1}{(-2 E h^2)^2} \left(-2226585600 + (10348301504 - 252478050 \pi^2) \eta \right. \\
& + 9 (-614377024 + 9064225 \pi^2) \eta^2 + 383328000 \eta^3 + 10411200 \eta^4 \Big) \\
& + \frac{2764800}{(-2 E h^2)^{5/2}} \eta (-20 + 3 \eta + 2 \eta^2) \\
& + \frac{1}{(-2 E h^2)^3} \left(3607142400 + 2 (-8729633504 + 247794225 \pi^2) \eta \right. \\
& + (9340505856 - 170534025 \pi^2) \eta^2 - 471441600 \eta^3 + 1152000 \eta^4 \Big) \\
& + \frac{1}{(-2 E h^2)^4} \left(-1712332800 + (8314359104 - 246319350 \pi^2) \eta \right. \\
& + (-4388287232 + 86487075 \pi^2) \eta^2 + 184226400 \eta^3 - 1944000 \eta^4 \Big) \Big\}, \tag{28h}
\end{aligned}$$

$$h_{6t} = \frac{(-2 E)^3}{32} \eta \left\{ \frac{(1+2 E h^2)}{(-2 E h^2)^{3/2}} (23 + 12 \eta + 6 \eta^2) \right\}, \tag{28i}$$

$$\begin{aligned}
h_{8t} = & \frac{(-2 E)^4}{921600} \left\{ - \frac{300}{\sqrt{-2 E h^2}} \eta \left(-8904 + 12207 \eta + 2356 \eta^2 + 864 \eta^3 \right) \right. \\
& + \frac{1}{(-2 E h^2)^{3/2}} \left(-1857600 + (10986256 - 1072425 \pi^2) \eta \right. \\
& + (-38708632 + 3152775 \pi^2) \eta^2 + 4891200 \eta^3 + 176400 \eta^4 \Big) \\
& + \frac{1}{(-2 E h^2)^{5/2}} \left(1857600 + (-12167056 + 1072425 \pi^2) \eta \right. \\
& + (43313932 - 3152775 \pi^2) \eta^2 - 3709200 \eta^3 + 126000 \eta^4 \Big) \Big\}, \tag{28j}
\end{aligned}$$

$$i_{6t} = \frac{13 (-2 E)^3}{192} \eta^3 \left(\frac{1+2 E h^2}{-2 E h^2} \right)^{3/2}, \tag{28k}$$

$$\begin{aligned}
i_{8t} = & \frac{(-2 E)^4}{14745600} \left(\frac{1+2 E h^2}{-2 E h^2} \right)^{1/2} \eta \left\{ -3600 \eta^2 (-839 + 526 \eta) \right. \\
& + \frac{1}{(-2 E h^2)} \left(6 (-9586592 + 405075 \pi^2) \right.
\end{aligned}$$

$$\begin{aligned}
& +5 \left(-21746432 + 2673315 \pi^2 \right) \eta + 23416800 \eta^2 + 1368000 \eta^3 \Big) \\
& + \frac{1}{(-2 E h^2)^2} \left(57519552 - 2430450 \pi^2 \right. \\
& \left. + (108732160 - 13366575 \pi^2) \eta - 23067600 \eta^2 + 900000 \eta^3 \right) \Big\}, \tag{28l}
\end{aligned}$$

$$k_{8t} = - \frac{(-2 E)^{3/2} \eta (150 \eta^3 + 2444 \eta^2 - 3303 \eta + 516) (1 + 2 E h^2)^2}{6144 h^5}, \tag{28m}$$

$$j_{8t} = - \frac{(-2 E)^{3/2} \eta^3 (66 \eta - 25) (1 + 2 E h^2)^{5/2}}{4096 h^5}, \tag{28n}$$

$$\begin{aligned}
\Phi = 2 \pi \Big\{ & 1 + \frac{3}{c^2 h^2} + \frac{(-2 E)^2}{4 c^4} \left[\frac{3}{(-2 E h^2)} (-5 + 2 \eta) \right. \\
& + \frac{15}{(-2 E h^2)^2} (7 - 2 \eta) \Big] + \frac{(-2 E)^3}{128 c^6} \left[\frac{24}{(-2 E h^2)} (5 - 5 \eta \right. \\
& + 4 \eta^2) - \frac{1}{(-2 E h^2)^2} (10080 - 13952 \eta + 123 \eta \pi^2 + 1440 \eta^2) \\
& + \frac{5}{(-2 E h^2)^3} (7392 - 8000 \eta + 123 \eta \pi^2 + 336 \eta^2) \Big] \\
& - \frac{(-2 E)^4}{73728 c^8} \frac{1}{(-2 E h^2)} \left[-6912 \eta^2 (-5 + 4 \eta) \right. \\
& + \frac{3}{(-2 E h^2)} \left(-1814400 + (5202688 - 106707 \pi^2) \eta \right. \\
& + 240 (-12944 + 123 \pi^2) \eta^2 + 276480 \eta^3 \Big) \\
& - \frac{6}{(-2 E h^2)^2} \left(-17297280 + (37556864 - 771585 \pi^2) \eta \right. \\
& + 1920 (-7013 + 123 \pi^2) \eta^2 + 403200 \eta^3 \Big) \\
& + \frac{7}{(-2 E h^2)^3} \left(-37065600 + (63502592 - 1275315 \pi^2) \eta \right. \\
& + 2400 (-6056 + 123 \pi^2) \eta^2 + 207360 \eta^3 \Big) \Big] \Big\}, \tag{28o}
\end{aligned}$$

$$f_{4\phi} = \frac{(-2 E)^2}{8} \frac{(1 + 2 E h^2)}{(-2 E h^2)^2} \eta (1 - 3 \eta), \tag{28p}$$

$$\begin{aligned}
f_{6\phi} = & \frac{(-2 E)^3}{256} \left\{ \frac{4 \eta}{(-2 E h^2)} (-11 - 40 \eta + 24 \eta^2) \right. \\
& + \frac{1}{(-2 E h^2)^2} \left(-256 + 1192 \eta - 49 \eta \pi^2 + 336 \eta^2 - 80 \eta^3 \right) \\
& + \frac{1}{(-2 E h^2)^3} \left(256 + 49 \eta \pi^2 - 1076 \eta - 384 \eta^2 - 40 \eta^3 \right) \Big\}, \tag{28q}
\end{aligned}$$

$$\begin{aligned}
f_{8\phi} = & \frac{(-2 E)^4}{7372800} \left\{ \frac{900 \eta}{(-2 E h^2)} \left(6844 - 13989 \eta - 1530 \eta^2 + 1888 \eta^3 \right) \right. \\
& + \frac{1}{(-2 E h^2)^2} \left(9273600 + 2 (-303923464 + 7907025 \pi^2) \eta \right. \\
& + (567130588 + 8219475 \pi^2) \eta^2 - 26411400 \eta^3 + 1180800 \eta^4 \Big)
\end{aligned}$$

$$\begin{aligned}
& -\frac{2}{(-2Eh^2)^3} \left(84844800 + 10(-149381636 + 4263405\pi^2)\eta \right. \\
& \left. -19(-67975466 + 173325\pi^2)\eta^2 - 54814500\eta^3 + 2980800\eta^4 \right) \\
& \frac{1}{(-2Eh^2)^4} \left(177004800 + (-2446310192 + 72629250\pi^2)\eta \right. \\
& \left. -15(-132716108 + 963535\pi^2)\eta^2 - 86679000\eta^3 + 1929600\eta^4 \right) \Big\}, \tag{28r}
\end{aligned}$$

$$g_{4\phi} = -\frac{3(-2E)^2}{32} \frac{\eta^2}{(-2Eh^2)^2} (1 + 2Eh^2)^{3/2}, \tag{28s}$$

$$\begin{aligned}
g_{6\phi} = & \frac{(-2E)^3}{768} \sqrt{(1 + 2Eh^2)} \left\{ -\frac{3}{(-2Eh^2)} \eta^2 (9 - 26\eta) \right. \\
& -\frac{1}{(-2Eh^2)^2} \eta (220 + 3\pi^2 + 312\eta + 150\eta^2) \\
& \left. + \frac{1}{(-2Eh^2)^3} \eta (220 + 3\pi^2 + 96\eta + 45\eta^2) \right\}, \tag{28t}
\end{aligned}$$

$$\begin{aligned}
g_{8\phi} = & \frac{(-2E)^4}{176947200} \frac{1}{\sqrt{(1 + 2Eh^2)}} \left\{ -10800\eta^2 (36 - 95\eta + 1226\eta^2) \right. \\
& + \frac{3\eta}{(-2Eh^2)} \left(-404533824 + 5453550\pi^2 \right. \\
& \left. + (731023360 + 381825\pi^2)\eta - 115070400\eta^2 - 9129600\eta^3 \right) \\
& + \frac{1}{(-2Eh^2)^2} \left(44236800 + 2(-6842155424 + 127907475\pi^2)\eta \right. \\
& \left. -87(-253902848 + 3210525\pi^2)\eta^2 \right. \\
& \left. -2262477600\eta^3 + 39096000\eta^4 \right) \\
& + \frac{1}{(-2Eh^2)^3} \left(-88473600 + (23556745280 - 464880750\pi^2)\eta \right. \\
& \left. + (-37649997312 + 561808575\pi^2)\eta^2 \right. \\
& \left. + 3436488000\eta^3 - 103766400\eta^4 \right) \\
& + \frac{1}{(-2Eh^2)^4} \left(44236800 + (-11086035904 + 225426450\pi^2)\eta \right. \\
& \left. + (17722415616 - 281347425\pi^2)\eta^2 \right. \\
& \left. -1527246000\eta^3 + 50133600\eta^4 \right) \Big\}, \tag{28u}
\end{aligned}$$

$$i_{6\phi} = \frac{(-2E)^3}{128} \frac{(1 + 2Eh^2)^2}{(-2Eh^2)^3} \eta (5 + 28\eta + 10\eta^2), \tag{28v}$$

$$\begin{aligned}
i_{8\phi} = & \frac{(-2E)^4}{14745600} \frac{\sqrt{(1 + 2Eh^2)}}{(-2Eh^2)^2} \left\{ -7200(440 - 1330\eta + 700\eta^2 + 173\eta^3) \right. \\
& + \frac{1}{(-2Eh^2)} \left(175308224 + 1767300\pi^2 \right. \\
& \left. + (-407514720 - 9062175\pi^2)\eta + 70257600\eta^2 - 1713600\eta^3 \right) \\
& \left. + \frac{1}{(-2Eh^2)^2} \left(-169548224 + 1767300\pi^2 \right. \right.
\end{aligned}$$

$$+ (412741920 - 9062175\pi^2) \eta - 58420800\eta^2 + 3535200\eta^3 \Big) \Big\}, \quad (28w)$$

$$h_{6\phi} = \frac{5(-2E)^3}{256} \frac{\eta^3}{(-2Eh^2)^3} (1 + 2Eh^2)^{5/2}, \quad (28x)$$

$$h_{8\phi} = \frac{(-2E)^4}{6553600} \frac{\eta}{(-2Eh^2)^2} (1 + 2Eh^2)^{3/2} \Big\{ 78000\eta^2 - 172000\eta^3 + \frac{1}{(-2Eh^2)} \Big(8273856 + 11250\pi^2 + (-24254464 - 579825\pi^2) \eta + 7604000\eta^2 - 238400\eta^3 \Big) + \frac{1}{(-2Eh^2)^2} \Big(-8273856 + 11250\pi^2 + (24254464 - 579825\pi^2) \eta - 6962000\eta^2 + 490400\eta^3 \Big) \Big\}, \quad (28y)$$

$$k_{8\phi} = - \frac{\eta(150\eta^3 + 4154\eta^2 - 5755\eta + 1476)(1 + 2Eh^2)^3}{24576h^8}, \quad (28z)$$

$$j_{8\phi} = - \frac{35(2\eta - 1)\eta^3(1 + 2Eh^2)^{7/2}}{16384h^8}. \quad (28aa)$$

Appendix C provides the explicit expressions for e_t and 4PN-order relations that connect e_r and e_ϕ to e_t . This is influenced by the GW phasing approach that usually employs the time eccentricity to characterize PN-accurate eccentric orbits. Borrowing from Ref. [42], we refer to as ‘phasing’, the task of specifying the time dependencies $r(t), \dot{r}(t), \phi(t)$ and $\dot{\phi}(t)$. In the limit of circular motion (*i.e.* $e_t = e_r = e_\phi = 0$), we display relations between some gauge invariant quantities

$$(-2E)|_{\text{circ}} = \frac{1}{h^2} + \frac{\eta + 9}{4c^2h^4} + \frac{\eta^2 - 7\eta + 81}{8c^4h^6} + \frac{15\eta^3 - 30\eta^2 + 246\pi^2\eta - 8833\eta + 11583}{192c^6h^8} + \frac{420\eta^4 - 360\eta^3 - 20(246\pi^2 - 8875)\eta^2 + (98715\pi^2 - 3959644)\eta + 3222180}{7680c^8h^{10}}, \quad (29a)$$

$$h|_{\text{circ}} = \frac{1}{c\sqrt{x}} \Big(1 + \frac{1}{6}(\eta + 9)x + \frac{1}{24}(\eta^2 - 57\eta + 81)x^2 + \frac{(7\eta^3 + 1674\eta^2 + 2214\pi^2\eta - 62001\eta + 10935)x^3}{1296} + \frac{(-220\eta^4 - 15480\eta^3 - 487080\pi^2\eta^2 + 12817260\eta^2 - 522855\pi^2\eta + 2666412\eta + 2755620)x^4}{124416} \Big), \quad (29b)$$

$$n|_{\text{circ}} = \frac{1}{h^3} + \frac{(\eta + 3)}{2c^2h^5} + \frac{3(\eta^2 + 5\eta + 9)}{8c^4h^7} + \frac{(30\eta^3 - 168\eta^2 + (970 + 123\pi^2)\eta - 486)}{96c^6h^9} + \frac{(2520\eta^4 - 3888\eta^3 + 24(1968\pi^2 - 74129)\eta^2 + (4753624 - 53571\pi^2)\eta - 2221992)}{9216c^8h^{11}}, \quad (29c)$$

$$\frac{\Phi}{2\pi}|_{\text{circ}} = 1 + \frac{3}{c^2h^2} + \frac{(45 - 12\eta)}{2c^4h^4} + \frac{96\eta^2 + 123\pi^2\eta - 6464\eta + 6480}{32c^6h^6} + \frac{-768(123\pi^2 - 4958)\eta^2 + (557301\pi^2 - 27133696)\eta + 18195840}{9216c^8h^8}, \quad (29d)$$

where $x = (\Phi n / (2\pi c^3))^{2/3}$. As mentioned earlier, we have verified that our $(-2E)|_{\text{circ}}$ and $(\Phi/(2\pi))|_{\text{circ}}$ are matched with the expression $E^{\text{loc,f,circ}}(j)$ from Eq. (8.26)

and $K^{\text{loc,f,circ}}(j)$ from Eq. (8.29) of Ref. [54], respectively. We also tried to verify the relation between x and h in the circular limit as given in Ref. [54]. Unfortunately, it

turned out to be rather difficult to do so as the local and nonlocal parts are not separated in Ref. [54].

Clearly, it is important to go through a consistency check in order to ensure the correctness of these lengthy expressions for the 4PN order orbital elements and functions. The plan is to adapt two consistency checks, detailed in Ref. [45]. This requires us to express PN-accurate expressions for \dot{r}^2 and $\dot{\phi}^2$, derived using the Hamiltonian equations of motion and given by Eqs. (8), in terms of E, h, η and $(1 - e_r \cos u)$ while using the fact that $r = a_r (1 - e_r \cos u)$. Note that the expressions for a_r and e_r^2 were obtained from the PN accurate roots s_- and s_+ , and therefore, do not involve any of our complicated integrals. In the first part of our check, we compare such an expression with the one that explicitly employed our parametric solution, namely $\dot{r}^2 = (dr/du \times du/dt)^2$. This expression for \dot{r}^2 is found to be in full agreement with our earlier \dot{r}^2 expression up to 4PN order after some elaborate simplifications. Thereafter, we performed a similar check on the angular part by computing $\dot{\phi}^2 = (d\phi/dv \times dv/du \times du/dt)^2$ in terms of E, h, η and $(1 - e_r \cos u)$. We have verified that such an expression is identical to our Hamiltonian equations of motion based $\dot{\phi}^2$ expression to 4PN order. Additionally, we have also performed the above two checks using \tilde{v} variable based parametric solution. These computations provided us with two powerful checks on our 4PN order generalized quasi-Keplerian parametrization.

C. Incorporating non-local in time 4PN Hamiltonian

Having dealt with the local-in-time component of the 4PN Hamiltonian in the previous subsection, we turn our attention to the non-local one. Our strategy will be to treat the 4PN tail effect as a perturbation to the basic Newtonian Kepler problem within the framework of the action-angle formalism. We will employ canonical (or classical) perturbation theory, a perturbation technique that is tailor-made for the action-angle framework [76], following the application this technique as was done in Ref. [68].

1. Action-angles of the Newtonian system

We start with a small review of the action-angle (De-launay) picture of the Newtonian system Ref. [68, 76–78]. We will consider the planar (two actions, two angles) version of the picture because the system is confined to a plane. The action-angle pairs $\{(\mathcal{L}, l), (\mathcal{G}, g)\}$ written in terms of more familiar quantities become [68]

$$\mathcal{L} = a^{1/2}, \quad \mathcal{G} = (a(1 - e^2))^{1/2}, \quad (30)$$

$$l = u - e \sin u, \quad g = \text{argument of periastron}, \quad (31)$$

where a and e are Newtonian versions of a_r and e_r ; u is as usual the eccentric anomaly. The Hamiltonian is a

function of only one of the actions

$$\mathcal{H}_N = -\frac{1}{2\mathcal{L}^2} \quad (32)$$

The rate of change of the first angle variable is

$$\frac{dl}{dt} = \frac{\partial \mathcal{H}_N}{\partial \mathcal{L}} = \frac{1}{\mathcal{L}^3} \equiv \Omega(\mathcal{L}), \quad (33)$$

whereas g does not change with time since $\partial \mathcal{H}_N / \partial \mathcal{G} = 0$.

2. The nonlocal-in-time 4PN tail Hamiltonian

To incorporate the effect of the nonlocal-in-time Hamiltonian $\mathcal{H}_{4\text{PN}}^{\text{nonlocal}}$ on the BBH dynamics, it suffices to consider it as a perturbation on the Newtonian dynamics. Then the reduced Hamiltonian of interest is [53]

$$\mathcal{H} = \frac{\hat{\mathbf{p}}^2}{2} - \frac{1}{r} + \mathcal{H}_{4\text{PN}}^{\text{nonlocal}}, \quad (34)$$

where

$$\mathcal{H}_{4\text{PN}}^{\text{nonlocal}} = -\frac{G^2}{5\eta c^8} I_{ij}^{(3)}(t') \text{Pf}_{2R/c} \int_{-\infty}^{+\infty} \frac{dw}{|w|} I_{ij}^{(3)}(t' + w). \quad (35)$$

In the above expression, $I_{ij}^{(3)}$ denotes the third derivative with respect to the coordinate time t' of the center-of-mass Newtonian quadrupole moment I_{ij} of the system (with r^i denoting the components of \mathbf{r})

$$I_{ij} \equiv (GM)^2 \mu \left(r^i r^j - \frac{1}{3} r^2 \delta^{ij} \right), \quad (36)$$

and $R \equiv |\mathbf{R}|$. Pf_T stands for the Hadamard partie finie which is defined as [53]

$$\text{Pf}_T \int_0^{+\infty} \frac{dw}{w} g(w) \equiv \int_0^T \frac{dw}{w} (g(w) - g(0)) + \int_T^{+\infty} \frac{dw}{w} g(w), \quad (37)$$

a quick application of which gives

$$\text{Pf}_T \int_0^{+\infty} \frac{dw}{w} \cos(\omega w) = -(\gamma_E + \ln(\omega T)), \quad (38)$$

with $\gamma_E = 0.577\dots$ being the Euler-Mascheroni constant. The two-sided integral in Eq. (35) needs to be converted into one-sided ones so as to make it amenable to the above definition of Pf_T .

Now focusing our attention on $\mathcal{H}_{4\text{PN}}^{\text{nonlocal}}$, to manipulate the integral in Eq. (35) we change the variable of differentiation from t' to l and decompose I_{ij} into Fourier components. We get (with $w' \equiv w/(GM)$)

$$\mathcal{H}_{4\text{PN}}^{\text{nonlocal}} = -\frac{G^2}{5\eta c^8} \left(\frac{\Omega}{GM}\right)^6 \sum_{p=-\infty}^{\infty} \frac{d^3(\mathcal{I}_{ij}(p)e^{ipl})}{dl^3} \text{Pf}_{2r/c} \int_{-\infty}^{+\infty} \frac{dw'}{|w'|} \sum_{q=-\infty}^{\infty} \frac{d^3(\mathcal{I}_{ij}(q)e^{iq(l+\Omega w')})}{dl^3}, \quad (39)$$

$$= \frac{G^2}{5\eta c^8} \left(\frac{\Omega}{GM}\right)^6 \sum_{p=-\infty}^{\infty} p^3 \mathcal{I}_{ij}(p) e^{ipl} \text{Pf}_{2r/c} \int_{-\infty}^{+\infty} \frac{dw'}{|w'|} \sum_{q=-\infty, q \neq 0}^{\infty} q^3 \mathcal{I}_{ij}(q) e^{iq(l+\Omega w')}, \quad (40)$$

$$= \frac{G^2}{5\eta c^8} \left(\frac{\Omega}{GM}\right)^6 \sum_{p,q=-\infty, q \neq 0}^{\infty} p^3 q^3 \mathcal{I}_{ij}(p) \mathcal{I}_{ij}(q) e^{i(p+q)l} \text{Pf}_{2r/c} \int_{-\infty}^{+\infty} \frac{dw'}{|w'|} e^{iq\Omega w'}, \quad (41)$$

$$= -\frac{2G^2}{5\eta c^8} \left(\frac{\Omega}{GM}\right)^6 \sum_{p,q=-\infty, q \neq 0}^{\infty} p^3 q^3 \mathcal{I}_{ij}(p) \mathcal{I}_{ij}(q) e^{i(p+q)l} (\gamma_E + \ln(|q|\Omega \times 2r/c)), \quad (42)$$

$$= -\frac{2G^2}{5\eta c^8} \left(\frac{\Omega}{GM}\right)^6 \left[\sum_{p,q=-\infty, q \neq 0}^{\infty} p^3 q^3 \mathcal{I}_{ij}(p) \mathcal{I}_{ij}(q) e^{i(p+q)l} (\gamma_E + \ln(|q|\Omega)) - \left(\frac{d^3 \mathcal{I}_{ij}}{dl^3}\right)^2 \ln(2r/c) \right]. \quad (43)$$

A few comments are needed to clarify the manipulations in the above lines. \mathcal{I}_{ij} 's are defined as per the following Fourier decomposition

$$I_{ij}(t') = \sum_{p=-\infty}^{\infty} \mathcal{I}_{ij}(p) e^{ipl}, \quad (44)$$

$$\mathcal{I}_{ij}(p) = \frac{1}{2\pi} \int_0^{2\pi} I_{ij}(t') e^{-ipl} dl. \quad (45)$$

These Fourier coefficients of the Newtonian multipole moments are available in terms of Bessel functions in the appendix of Ref. [79] in dimensionless form. In the above lines and the material below, the summation is over all integers from $-\infty$ to $+\infty$ except where it is explicitly mentioned that $q = 0$ be omitted. We have omitted $q = 0$ from the above summations because $\ln(0)$ is undefined. Also, with the variable of integration having changed from $w \rightarrow w'$, we also had to change the time-scale of the Pf operation from $2R/c \rightarrow 2r/c$. One may also notice another issue of the arguments inside the two \ln 's in Eq. (43) not being dimensionless, due to breaking the \ln in Eq. (42) into two \ln 's in the following line. This is no reason to worry since the final result in Eq. (52) combines back the two \ln 's into one with an argument which is indeed dimensionless. And finally, in Eq. (42), use has been made of the result in Eq. (38), and a similar result for sine being inside the integrand instead of cosine to evaluate the integral in terms of the logarithm.

Due to the definite integral having been performed above and the application of order-reduction (eliminating the derivatives of variables in the Hamiltonian with the equations of motion of a lower order [68]), we now have to deal only with the local dynamics². The 4PN tail Hamiltonian has been decomposed in this particular

way of Eq. (43) to render it amenable to the averaging procedure, to be carried out below.

3. 4PN tail effect as a perturbation to the Newtonian system

To deal with the 4PN tail Hamiltonian of Eq. (43), we employ the so called ‘‘Delaunay technique’’ of averaging the perturbation Hamiltonian which is discussed in Appendix E. The method dictates the following: take the perturbation part $\epsilon H_1(\phi_0, J_0)$ of the full Hamiltonian $H = H_0(J_0) + \epsilon H_1(\phi_0, J_0)$ and average it over ϕ_0 , thus yielding $\bar{H}_1(J_0)$. Then there exists a generating function $S(\phi_0, J)$ such that it gives new action-angles (J, ϕ) which are connected to the old ones via Eqs. (E3) and (E4), and the total Hamiltonian depends only on the new action J as $E(J) = E_0(J) + \epsilon E_1(J)$, where the functional dependence of E_0 and E_1 on J is the same as that of H_0 and \bar{H}_1 on J_0 . For our system in consideration, $H_1 = \mathcal{H}_{4\text{PN}}^{\text{nonlocal}}$ and $\phi_0 = l$. We now proceed to average H_1 over l .

The two additive terms in Eq. (43) will be averaged using different methods. This is so because they possess different structures and hence their averaging is tractable via different means. To average the first term of Eq. (43) (the one involving the summation), we note that the averaged value will be equal to the sum of all the terms in this double summation which correspond to $p + q = 0$. Hence, we substitute $q = -p$, thereby turning the double summation into a single summation over p and we choose to retain all the term with $|p| \lesssim 500$ terms in this

² See Refs. [80–82] for a background on order-reduction. The procedure of order-reducing the Hamiltonian leads to shifts in canon-

ical coordinates. Apart from the tail part [68], the instantaneous Hamiltonian of Eq. (6) is also order-reduced [82]. Since these shifts lead to amplitude and zero-average oscillatory phase corrections (rather than secular phase corrections), we ignore such shifts, as our IMR waveform is meant to be only leading order accurate in amplitude.

summation. This is so because we found by inspection that these many terms are enough for $e \lesssim 0.9$. We then try to come up with a certain Padé-like approximant for this series using a method that we now briefly sketch.

Using the Fourier coefficients of the Newtonian multipole moments as given in the appendix of Ref. [79], it can be shown that the summation in the first term of Eq. (43) (without the prefactor and $(\gamma_E + \ln(|q|\Omega))$ with $q = -p$ can be written as

$$\sum_{p,q=-\infty, q \neq 0}^{\infty} p^3 q^3 \mathcal{I}_{ij}(p) \mathcal{I}_{ij}(q) e^{i(p+q)l} \Big|_{q=-p} \quad (46)$$

$$= - \sum_{p=-\infty}^{\infty} p^6 |\mathcal{I}_{ij}(p)|^2 = -32\mu^2 (aGM)^4 \frac{1 + \frac{73e^2}{24} + \frac{37e^4}{96}}{(1-e^2)^{7/2}}.$$

We actually factored out $(1-e^2)^{-7/2}$ from the above sum before trying to evaluate it to preserve the formal structure in the limit of large angular momentum [83]³. Note that the above result appears to be exact in e and coincides with the “ $f(e)$ ” of Peters and Mathews [84]. Obtaining this nice exact in e expression became possible

due to factoring out $(1-e)^{-7/2}$ in the beginning and then series expanding the remnant.

Focusing our attention back to the summation in Eq. (43), we see that it can further be decomposed as (with $q = -p$)

$$- \sum_{p=-\infty}^{\infty} p^6 |\mathcal{I}_{ij}(p)|^2 [(\gamma_E + \ln \Omega) + \ln |p|]. \quad (47)$$

Since the first additive term in the above expression (in the parenthesis) has already been taken care of in Eq. (46), we now show how to deal with the second one (involving $\ln |p|$). Again, after factoring out $(1-e^2)^{-7/2}$, we first find the Padé approximation of this second term such that both the numerator and denominator are expanded up to $\mathcal{O}(e^{10})$. Then by hand, we add $p_{12}e^{12} + p_{14}e^{14}$ in the numerator, where p_{12} and p_{14} are to be determined by numerically matching (at high eccentricities like $e = 0.85, 0.90$) this new Padé-like ansatz with the evaluated value of the series where terms up to $|p| \lesssim 500$ have been retained. Tentatively, we have

$$- \sum_{p=-\infty}^{\infty} p^6 |\mathcal{I}_{ij}(p)|^2 \ln |p|$$

$$= -G^4 \mathcal{L}^8 M^6 \eta^2 \left[\frac{p_{14}e^{14} + p_{12}e^{12} - \frac{382996272e^{10}}{13601521} + \frac{579332351e^8}{4983158} - \frac{324710645e^6}{8433524} - \frac{758231515e^4}{3359177} + \frac{263415291e^2}{1639996} + \frac{286746937}{12927762}}{(1-e^2)^{7/2} \left(\frac{4447985e^{10}}{4076572203} + \frac{49804512e^8}{1158420851} - \frac{105413189e^6}{194334558} + \frac{103729937e^4}{57112735} - \frac{56374811e^2}{24380301} + 1 \right)} \right]. \quad (48)$$

We call the resulting approximant “Padé-like”, since it is a result of combining the methods of Padé approximation and numerical fitting. Such a procedure, combined with the idea of factoring out $(1-e^2)^{-7/2}$ gives us approximants which are valid up to higher e ’s than would have been possible with the standard Padé approximants. Interestingly, these approximants capture the eccentricity effects up to $e \lesssim 0.9$, despite the existence of Laplace limit of $e < 0.66\dots$ beyond which the series solution of Kepler equation in e diverges [62, 85, 86].

Finally, averaging the second term term of Eq. (43) (involving $\ln 2r/c$) over l in closed-form is possible, although lengthy. Using the order-reduced Newtonian equations

$$x = a(\cos u - e), \quad (49a)$$

$$y = a\sqrt{1-e^2} \sin u, \quad (49b)$$

$$z = 0 \quad (49c)$$

$$l = u - e \sin u, \quad (49d)$$

$$r = a(1 - e \cos u), \quad (49e)$$

$$I_{ij} = (GM)^2 \mu \left(r^i r^j - \frac{1}{3} r^2 \delta^{ij} \right), \quad (49f)$$

(with x, y, z being the components of \mathbf{r}) in the second term of Eq. (43), we arrive at

³ It can be checked that the average (over l) of the first term of the nonlocal Hamiltonian of Eq. (43) has the following structure in the $h \rightarrow \infty$ limit $\bar{H}_{1(A)} \sim (Eh^2)^2 h^{-7} \sum_{n=0}^{\infty} a_n \alpha^n$, with $\alpha = (Eh^2)^{-1}$. This, along with $e^2 = 1 + 2Eh^2$, lets us see that

$\bar{H}_{1(A)}$ has the form $\bar{H}_{1(A)} \sim F(e)/h^7 = F(e) (2E/(e^2 - 1))^{7/2}$. This motivated us to first factor out $(1-e^2)^{-7/2}$ from the Bessel series whose Padé-like approximant is sought.

$$\frac{1}{2\pi a^4 G^4 M^4 \mu^2} \int_0^{2\pi} \left(\frac{d^3 I_{ij}}{dl^3} \right)^2 \ln(2r/c) dl = \frac{2}{3\pi} \int_0^{2\pi} \frac{(24 - 23e^2 - e^2 \cos 2u) \left(\ln \left[\frac{2a(1-e \cos u)}{c} \right] \right)}{(1 - e \cos u)^5} du \quad (50)$$

$$= \frac{12(37e^4 + 292e^2 + 96) \ln \left[\frac{4a(1-e^2)(1-\sqrt{1-e^2})}{c e^2} \right] - (255e^4 + 3792e^2 + 2408)}{36(1-e^2)^{7/2}} + \frac{(673e^2 + 602)}{9(1-e^2)^3}. \quad (51)$$

Finally, Eqs. (46), (48) and (50) culminate in the expression of order-reduced averaged 4PN tail Hamiltonian

$$\begin{aligned} \bar{\mathcal{H}}_{4\text{PN}}^{\text{nonlocal}} &= \frac{2\eta}{5c^8 \mathcal{L}^{10}} \left[\frac{12(37e^4 + 292e^2 + 96) \ln \left[\frac{4(1-e^2)(1-\sqrt{1-e^2}) \exp(\gamma_E)}{\mathcal{L} c e^2} \right] - (255e^4 + 3792e^2 + 2408)}{36(1-e^2)^{7/2}} + \frac{(673e^2 + 602)}{9(1-e^2)^3} \right. \\ &\quad \left. + \mathcal{H}_{\text{Padé}} \right], \end{aligned} \quad (52)$$

where

$$\mathcal{H}_{\text{Padé}} = \frac{\frac{14262437e^{14}}{328008227} - \frac{6775509e^{12}}{248174614} - \frac{382996272e^{10}}{13601521} + \frac{579332351e^8}{4983158} - \frac{324710645e^6}{8433524} - \frac{758231515e^4}{3359177} + \frac{263415291e^2}{1639996} + \frac{286746937}{12927762}}{(1-e^2)^{7/2} \left(\frac{4447985e^{10}}{4076572203} + \frac{49804512e^8}{1158420851} - \frac{105413189e^6}{194334558} + \frac{103729937e^4}{57112735} - \frac{56374811e^2}{24380301} + 1 \right)}, \quad (53)$$

is the Padé-like approximant that we constructed above. Eliminating e using $e = \sqrt{1 - \mathcal{G}^2/\mathcal{L}^2}$ expresses this averaged Hamiltonian in terms of only the actions.

Now, in the action-angles formalism, one can compute the “frequencies” corresponding to all the angle variables by partially differentiating the Hamiltonian with respect to the corresponding action variables. Application of this to our system in consideration yields the 4PN tail correction to the frequencies n and kn (where n denotes the mean motion and k is the periastron advance parameter) [60]. After partially differentiating with respect to \mathcal{L} and \mathcal{G} , we write the results in terms of \mathcal{L} and e . For illustration, we give their small e expanded expressions

$$n_{\text{tail}} \equiv \frac{\partial \bar{\mathcal{H}}_{4\text{PN}}^{\text{nonlocal}}(\mathcal{G}, \mathcal{L})}{\partial \mathcal{L}} \quad (54)$$

$$\begin{aligned} &= \frac{19289894530752349825264\eta}{323061509079949009095\mathcal{L}^{11}c^8} + \frac{592\eta \left(\ln \left(\frac{1}{\mathcal{L}c} \right) + \gamma_E + \ln(2) \right)}{15\mathcal{L}^{11}c^8} \\ &+ \frac{e^2\eta \left(-184 \ln \left(\frac{1}{\mathcal{L}c} \right) - 184\gamma_E + \frac{176764157117697232864351125327585955400510029}{604435714840557267408843920105441163950610} - 184 \ln(2) \right)}{5\mathcal{L}^{11}c^8} + \mathcal{O}(e^4), \end{aligned} \quad (55)$$

$$(kn)_{\text{tail}} \equiv \frac{\partial \bar{\mathcal{H}}_{4\text{PN}}^{\text{nonlocal}}(\mathcal{G}, \mathcal{L})}{\partial \mathcal{G}}, \quad (56)$$

$$\begin{aligned} k_{\text{tail}} &= -\frac{74831546379478710201598\eta}{323061509079949009095\mathcal{L}^8c^8} + \frac{352\eta}{5\mathcal{L}^8c^8} - \frac{2512\eta \left(\ln \left(\frac{1}{\mathcal{L}c} \right) + \gamma_E + \ln(2) \right)}{15\mathcal{L}^8c^8} \\ &+ \frac{e^2\eta \left(-\frac{5164100568419311748345089878114388585281349219}{201478571613519089136281306701813721316870} - 13264 \ln \left(\frac{1}{\mathcal{L}c} \right) - 13264\gamma_E + 10196 - 13264 \ln(2) \right)}{15\mathcal{L}^8c^8} + \mathcal{O}(e^4). \end{aligned} \quad (57)$$

Note that $k = \Delta\Phi/2\pi$, where $\Delta\Phi$ is the angle of periastron advance in the radial period (periastron to periastron) P , which means that $k = \Phi/(2\pi) - 1$. This means that among the earlier presented set of equations for the 4PN local-in-time quasi-Keplerian parameterization (QKP), it is Eqs. (28b) and (28o) which should include the effects encoded in Eqs. (54) and (56), but

they do not since Eqs. (28b) and (28o) are meant to include only the local-in-time contributions only. We have checked that Eqs. (54) and (56) agree with the results of Ref. [54] in the circular limit.

Also, note that the argument of \ln in Eqs. (50) and (52) becomes undefined at $e = 0$ although its $e \rightarrow 0$ limit is well defined. Therefore, in our MATHEMATICA package,

we chose to replace this argument of \ln by its Taylor expansion so that it is valid in the range $0 \leq e \lesssim 0.85$.

To bring all the pieces together, let us have a bird's eye view of the situation. We are trying to include the effect of 4PN tail Hamiltonian as a perturbation to the Newtonian one in the action-angles framework. The effect entails

1. the action-angles being perturbed as per Eqs. (E2), (E3) and (E4)
2. the functional dependence of the Hamiltonian on the actions being perturbed as per Eqs. (E5), (E7) and Eq. (52)

At this point, we invoke the “semi-perturbation” scheme detailed in Appendix F, whereby we don't use the information contained in Eqs. (E2), (E3) and (E4), but rather only make use of the information in Eqs. (E5), (E7). This way we don't need the oscillatory corrections to the action-angles and the generating function. All one needs to do is to average the perturbation Hamiltonian and find the perturbed frequencies, as has already been done in Eqs. (54) and (56) above.

Now we discuss how to merge the results of Eqs. (54) and (56) into the QKP Eqs. (28) if one wants to. Since we have chosen not to perturb the actions, there won't be any corrections to the eccentricity and semi-major axis due to the tail effects (see Eqs. (30)). This means that in the RHSs of Eqs. (54) and (56), after evaluating the partial derivatives, we can replace \mathcal{L} and \mathcal{G} with a and e using Eqs. (30) and then make the substitutions $(e, a) \rightarrow ((1 + 2Eh^2)^{1/2}, -1/(2E))$ to write n_{tail} and k_{tail} in terms of E and h . Then with the earlier derived equation $k = \Phi/(2\pi) - 1$, n_{tail} and k_{tail} can both be incorporated as the 4PN tail effects into the quasi-Keplerian solution (specifically Eqs. (28b) and (28o)) for the 4PN local Hamiltonian presented in the previous subsection. We do not take it because we have reserved Eqs. (28) for local-in-time effects only. Note that in accordance with our decision to adopt the semi-perturbation scheme, the 4PN tail corrections do not enter in the expressions for any other quantity except n and Φ (or k), as far as the 4PN conservative quasi-Keplerian solution is concerned.

Strictly speaking, we have not worked out the full 4PN dynamics since we have ignored the corrections to the action-angles (linear in ϵ terms on the RHSs of Eqs. (E3) and (E4)) due to the tail effects. Adopting the semi-perturbation scheme rather than full perturbation scheme simplifies the calculations and the ignored 4PN zero-average, oscillatory corrections to action-angles (due to tail effects) are less important than the 4PN secular tail effects for GW data analysis purposes. An alert reader may be able to point out that we have included the oscillatory terms in the Keplerian type solution for the 4PN local Hamiltonian (the ones with sinusoidal functions of integer multiples of v in Eq. (26)), despite dropping the oscillatory correction terms to action-angles (as per the semi-perturbation scheme) resulting

from the 4PN tail effect. One may insist that all the oscillatory terms should be discarded. One could do so. We decided to include these oscillatory terms for the local Hamiltonian in Eq. (26) just to be in line with the tradition of including all the terms, be it oscillatory or secular, while giving the QKP solution of a BBH for various PN accurate local conservative Hamiltonians as has been done in Refs. [44, 45, 59].

We finally mention beforehand that both Eqs. (54) and (56) have a bearing on Eq. (71b) which gives the mean motion n , so that when it comes to the IMR waveform construction, of all the equations in Sec. III, only Eq. (71b) incorporates the 4PN tail effect as per our choice of adopting the semi-perturbation strategy to include the tail effects. The accompanying MATHEMATICA notebook contains the relevant expressions for n (both local and nonlocal). We now move on to apply the above parametric solution to construct a time-domain eccentric IMR waveform, influenced by Ref. [28].

III. AN IMPROVED TIME-DOMAIN ECCENTRIC IMR WAVEFORM

The present section details our effort to incorporate 4PN order Keplerian type parametric solution into a MATHEMATICA package, namely `EccentricIMR`, available as an open source software [56], in an accurate and efficient manner. This package implements an eccentric IMR model, detailed in Ref. [28], where an eccentric PN-accurate inspiral model was combined with a quasi-circular merger waveform. Detailed interpolation using several non-eccentric and non-spinning NR waveforms in the neighborhood of their merger phase ensured that the analytic quasi-circular merger waveform of Ref. [28] is accurate for non-spinning BH binaries with mass ratio $q \equiv m_1/m_2$ between 1 and 4 and for arbitrary ϕ_0 (the initial phase of the waveform). The IMR model of Ref. [28] combines the post-Newtonian inspiral waveform, adapted from Ref. [87], and their above described quasi-circular merger model (CMM) to obtain a time-domain eccentric IMR waveform. This involves ‘blending’ of the above two models in a transition region where neither PN approximation is valid nor the binary can be assumed to have circularized.

It was noted in Ref. [28] that incorporating higher order PN corrections should improve the performance of the early inspiral phase. In fact, Ref. [28] invoked 3PN order conservative and 2PN order reactive contributions to the BBH dynamics for describing the inspiral part of their IMR $h(t)$. The present effort improves the treatment of the conservative part in the `EccentricIMR` package with the help of our 4PN order Keplerian type parametric solution while adapting PN-accurate results from Refs. [51, 88] to incorporate effects of 3PN-accurate GW emission. Moreover, we provide computationally efficient version of the x -model, employed in `EccentricIMR`, by adapting the GW phasing approach of Refs. [42, 43] dur-

ing the modeling of the eccentric inspiral phase. These changes are incorporated into the MATHEMATICA package accompanying Ref. [28] and we treat their circular merger model as a black box [56]. The resulting package is available at Ref. [57, 58]. In what follows, we present our approach to improve various aspects of the x -model. In this section we will employ t to denote the ADM coordinate time for the sake of convenience (unlike the previous section). A derivative with respect to the ADM time will be represented by an overdot.

A. 4PN conservative and 3PN radiative phasing

We begin by listing the usual expression for the quadrupolar order (or restricted) complex gravitational waveform for compact binaries in non-circular orbits [41, 42, 49, 87]

$$h_{\text{sig}} = h_+ - ih_\times \quad (58a)$$

$$h_+ = -\frac{GM\eta}{c^4 D} \left\{ (\cos^2 \theta + 1) \left[\left(\frac{GM}{R} - \dot{R}^2 + R^2 \dot{\phi}^2 \right) \cos 2\phi' + 2R\dot{\phi}\dot{R} \sin 2\phi' \right] + \left(\frac{GM}{R} - \dot{R}^2 - R^2 \dot{\phi}^2 \right) \sin^2 \theta \right\}, \quad (58b)$$

$$h_\times = -\frac{2GM\eta}{c^4 D} \cos \theta \left\{ \left(\frac{GM}{R} - \dot{R}^2 + R^2 \dot{\phi}^2 \right) \sin 2\phi' - 2R\dot{\phi}\dot{R} \cos 2\phi' \right\}, \quad (58c)$$

where $\phi' \equiv \phi - \varphi$ and θ and φ are the spherical polar angles that specify the observer in a frame centered around the source which is a distance D away from the detector. Recall that R and ϕ serve to specify the relative separation vector \mathbf{R} between the two BHs whereas $r \equiv R/(GM)$. Also, we have $\dot{r} \equiv dr/dt$ and $\dot{\phi} \equiv d\phi/dt$. The NR relevant spin-weight -2 , $\ell = 2$, $m = 2$ spherical harmonic mode of $h(t)$ reads

$$h^{22} = \int -{}_2Y_2^{2*}(\theta, \varphi) h_{\text{sig}}(\theta, \varphi) d\Omega$$

$$= -\frac{4GM\eta e^{-2i\phi}}{c^4 D} \sqrt{\frac{\pi}{5}} \left(\frac{GM}{R} + (\dot{\phi}R + i\dot{R})^2 \right), \quad (59)$$

where the spherical harmonic ${}_2Y_2^2(\theta, \varphi) = \frac{1}{2}e^{2i\varphi}\sqrt{5/\pi}\cos^4(\theta/2)$. In what follows, we describe our improved x -model to obtain $h^{22}(t)$ for non-spinning BH binaries inspiralling along relativistic eccentric orbits in a computationally accurate and efficient manner.

We adapt, as mentioned earlier, the GW phasing approach of Refs. [42, 43] to model eccentric inspiral of BH binaries to describe the temporal evolution of dynamical variables that appear in the above $h^{22}(R(t), \dot{R}(t), \phi(t), \dot{\phi}(t))$ expression. This approach imposes numerically the effects of GW emission on the conservative dynamics of eccentric binaries by incorporating changes in orbital configurations that occur at the

orbital, periapsis advance and gravitational radiation reaction time scales. In the GW phasing approach, the conservative BBH dynamics is described using our Keplerian type parametric solution and we first focus on describing parametrically the temporal evolution of r, \dot{r} and $\dot{\phi}$, whereas ϕ will be dealt with later. We begin by expressing the 4PN-accurate expressions for these variables as

$$r(-2E, h, u) = a_r(-2E, h) \times \left(1 - e_r(-2E, h) \times \cos u \right), \quad (60)$$

$$\dot{r}(-2E, h, u) = \frac{dr}{du} \times \frac{du}{dt}, \quad (61)$$

$$\dot{\phi}(-2E, h, u) = \frac{d\phi}{dv} \times \frac{dv}{du} \times \frac{du}{dt}. \quad (62)$$

where

$$\frac{du}{dt} = \frac{du}{dl} \frac{dl}{dt} = \frac{du}{dl} \frac{n}{GM}. \quad (63)$$

Recall that t in this section stands for the ADM time, whereas it stood for the scaled ADM time in Sec. II. Employing the 4PN solution given in Eqs. (25)-(27), we can see that the resulting 4PN order expressions of r, \dot{r} and $\dot{\phi}$ will be functions of $(-2E), h, e_r, e_t, e_\phi, u$ and η . Conventionally in the x -model, we rather write these expressions in terms of ω, e_t and u . This is achieved with the help of the following steps.

In the first step, we define a 4PN order ω from our 4PN order expressions for n and $k = \Delta\Phi/2\pi$ as $\omega \equiv n \times (1+k)$. It is now possible to invert 4PN order ω expression in a PN-accurate manner to express $(-2E)$ in terms of ω and h . In the next step, we invert 4PN order e_t expression (given by the first of Eqs. (C1)) to get an intermediate 4PN order expression for h in terms of e_t and $(-2E)$. Then use the above obtained expression of $(-2E)$ (in terms of ω and h) to express h in terms of e_t and ω up to 4PN order in a post-Newtonian perturbative way. Using this expression of $h(e_t, \omega)$ in the above expression of $(-2E)$ finally gives us $(-2E)$ in terms of e_t and ω . The resulting relations for $(-2E)$ and h (in terms of e_t and ω) allow us to express e_r and e_ϕ in terms of ω, e_t to 4PN order with the help of Eqs. (C1). All these relations in conjunction with Eqs. (60)-(62) lead to 4PN order parametric expressions for r, \dot{r} and $\dot{\phi}$ in terms of ω, e_t, u . We provide the expressions of E and h in terms of $x \equiv (GM\omega/c^3)^{2/3}$ and e_t in Appendix D.

An additional requirement of the GW phasing approach is to split the orbital phase into two parts such that (with $\lambda(t_0) = 0$)

$$\phi(t) = \lambda(t) + W(u(l), (-2E), h), \quad (64a)$$

$$\lambda(t) = (1+k)n(t-t_0) \equiv \omega(t-t_0), \quad (64b)$$

as done in Ref. [42]. Note that Eqs. (64) are for conservative dynamics only and need to be modified by the application of the method of variation of arbitrary constants (as done in Ref. [42]) to include the radiation reaction

effects⁴. This will be done later in Eqs. (71). The above equations ensure that the secular evolution of the orbital phase depends linearly on time which makes it easier to track the evolution of the argument of periapsis while the W part provides the periodic variations, present in the ϕ evolution due to its dependence on l . Additionally, we need to express the above 4PN order expression for W in terms of ω, e_t and u which we write symbolically as

$$W = (v - u) + e_t \sin u + W^{1\text{PN}} x + W^{2\text{PN}} x^2 + W^{3\text{PN}} x^3 + W^{4\text{PN}} x^4. \quad (65)$$

For the ease of implementation, it is helpful to use the following 4PN order expression of Ref. [43]

$$v - u = 2 \arctan \left(\frac{\beta_\phi \sin u}{1 - \beta_\phi \cos u} \right). \quad (66)$$

Our parametric solution allows us to obtain the following

$$\frac{\dot{R}}{c} = \frac{\sqrt{x} e_t \sin u}{1 - e_t \cos u} \left\{ 1 + \dot{R}^{1\text{PN}}(\eta, e_t) x + \dot{R}^{2\text{PN}}(\eta, e_t, u) x^2 + \dot{R}^{3\text{PN}}(\eta, e_t, u) x^3 + \dot{R}^{4\text{PN}}(\eta, e_t, u) x^4 \right\}, \quad (68a)$$

$$\dot{\phi} = \frac{x^{3/2} c^3 \sqrt{1 - e_t^2}}{GM(1 - e_t \cos u)^2} \left\{ 1 + \dot{\phi}^{1\text{PN}}(\eta, e_t, u) x + \dot{\phi}^{2\text{PN}}(\eta, e_t, u) x^2 + \dot{\phi}^{3\text{PN}}(\eta, e_t, u) x^3 + \dot{\phi}^{4\text{PN}}(\eta, e_t, u) x^4 \right\}, \quad (68b)$$

$$R = \frac{GM(1 - e_t \cos u)}{c^2 x} \left\{ 1 + R^{1\text{PN}}(\eta, e_t, u) x + R^{2\text{PN}}(\eta, e_t, u) x^2 + R^{3\text{PN}}(\eta, e_t, u) x^3 + R^{4\text{PN}}(\eta, e_t, u) x^4 \right\}, \quad (68c)$$

$$\phi = \lambda + W, \quad (68d)$$

$$\lambda(t) = \omega(t - t_0), \quad (68e)$$

$$W = (v - u) + e_t \sin u + W^{1\text{PN}}(\eta, e_t, u) x + W^{2\text{PN}}(\eta, e_t, u) x^2 + W^{3\text{PN}}(\eta, e_t, u) x^3 + W^{4\text{PN}}(\eta, e_t, u) x^4, \quad (68f)$$

where we employ the 4PN-accurate expression for $(v - u)$ given symbolically by Eq. (66). It should be noted that the above equations provide analytically 4PN order conservative dynamics of BH binaries in terms of u and we require to numerically solve our 4PN order Kepler equation after re-writing it in terms of x and e_t to obtain $u(l(t))$. Our full system however, is not conservative and as we will soon see that inclusion of the radiation reaction effects will modify some of the above equations. For the purpose of illustration, we list the 1PN contributions that appear in Eqs. (68) as

$$\dot{R}^{1\text{PN}}(\eta, e_t) = \frac{-7\eta + e_t^2(-6 + 7\eta)}{6(1 - e_t^2)}, \quad (69a)$$

$$\dot{\phi}^{1\text{PN}}(\eta, e_t, u) = \frac{(-1 + \chi + e_t^2)(-4 + \eta)}{\chi(1 - e_t^2)}, \quad (69b)$$

4PN order expression for β_ϕ in terms of e_t, x, u as

$$\beta_\phi = \frac{1 - \sqrt{1 - e_t^2}}{e_t} + \beta_\phi^{1\text{PN}} x + \beta_\phi^{2\text{PN}} x^2 + \beta_\phi^{3\text{PN}} x^3 + \beta_\phi^{4\text{PN}} x^4. \quad (67)$$

The explicit and lengthy expressions for these 4PN order quantities are listed in the accompanying MATHEMATICA notebook [57, 58].

We now collect relevant expressions that describe the temporal evolution of a precessing eccentric orbit whose conservative (without radiation reaction) orbital dynamics is specified by the 4PN order Hamiltonian, given by Eq. (8.41) of Ref. [52]. These equations may be symbolically written as

$$R^{1\text{PN}}(\eta, e_t, u) = \frac{1}{6\chi(1 - e_t^2)} (-24 + 9\eta + \chi(18 - 7\eta) + e_t^2[24 - 9\eta + \chi(-6 + 7\eta)]), \quad (69c)$$

$$W^{1\text{PN}}(\eta, e_t, u) = 3 \frac{e_t \sin u + (v - u)_{1\text{PN}}}{1 - e_t^2},$$

$$\beta_\phi^{1\text{PN}}(\eta, e_t) = \frac{-4 + \eta + e_t^2(8 - 2\eta) + (4 - \eta)\sqrt{1 - e_t^2}}{e_t \sqrt{1 - e_t^2}}, \quad (69d)$$

where χ stands for $1 - e_t \cos u$.

We now impose the effects of GW emission and explain how we provide the full temporal evolution for a BBH, characterized by m_1 and m_2 and specified by initial values of (x, e_t, λ, l) . Clearly, we require to specify how these variables vary in time and Ref. [42] demonstrated that ω (or x) and e_t evolve due to gravitational radiation reaction effects. It turns out that the secular variations of ω and e_t arise by employing the orbital (binding) energy and angular momentum balance arguments [90]. This requires PN accurate expressions of ω

⁴ See Box. 3.3 of Ref. [89] for a pedagogical treatment of the method of variation of arbitrary constants.

and e_t in terms of $(-2E)$ and h and PN-accurate expressions for the orbit-averaged far-zone energy and angular momentum fluxes associated with non-spinning compact

binaries in PN-accurate eccentric orbits [49, 91]. We employ the following 3PN-accurate expressions for \dot{x} and \dot{e}_t , extractable from Ref. [51], and displayed symbolically as

$$\dot{x} = \frac{c^3 x^5 \eta}{GM} \left\{ \frac{192 + 584e_t^2 + 74e_t^4}{15(1 - e_t^2)^{7/2}} + \dot{x}^{1\text{PN}}(\eta, e_t) x + \dot{x}^{1.5\text{PN}}(\eta, e_t) x^{3/2} + \dot{x}^{2\text{PN}}(\eta, e_t) x^2 + \dot{x}^{2.5\text{PN}}(\eta, e_t) x^{2.5} + \dot{x}^{3\text{PN}}(\eta, e_t) x^3 \right\}, \quad (70a)$$

$$\dot{e}_t = -\frac{c^3 x^4 \eta e_t}{GM} \left\{ \frac{304 + 121e_t^2}{15(1 - e_t^2)^{5/2}} + \dot{e}_t^{1\text{PN}}(\eta, e_t) x + \dot{e}_t^{1.5\text{PN}}(\eta, e_t) x^{3/2} + \dot{e}_t^{2\text{PN}}(\eta, e_t) x^2 + \dot{e}_t^{2.5\text{PN}}(\eta, e_t) x^{2.5} + \dot{e}_t^{3\text{PN}}(\eta, e_t) x^3 \right\}. \quad (70b)$$

The explicit expressions for various PN contributions are available in Refs. [51, 88]. We would like to point out that the contributions appearing at the 1.5PN, 2.5PN and 3PN orders contain certain hereditary contributions while the Newtonian, 1PN and 2PN terms are purely instantaneous. Additionally, the 1.5PN and 2.5PN contributions in the above equations are purely hereditary and the relative 3PN terms contain both instantaneous and hereditary parts. The hereditary parts are expressed in terms of certain ‘eccentricity enhancement functions’ (such as the ones given in Eqs. 6.22 of [51]). We employed accurate Padé approximants for these enhancement functions and ensured that they are consistent with analytic fits to these functions up to at least $e_t = 0.85$, as detailed in Ref. [88].

We now provide a prescription for the secular evolution λ and l as we specify the orbital configuration of our eccentric BH binary by specifying the initial values of (x, e_t, λ, l) . Eqs. (26) and (68e) which imply constant time derivatives of l and λ , are valid only when the radiation reaction is ignored. Under the radiation reaction, the differential equations that specify the secular evolution of λ and l can be considered to be extensions of our 4PN order Keplerian type parametric solution and are given by

$$\frac{d\lambda}{dt} = \omega \equiv \frac{x^{3/2} c^3}{GM}, \quad (71a)$$

$$\frac{dl}{dt} = n = \frac{x^{3/2} c^3}{GM} \left\{ 1 + l^{1\text{PN}}(e_t) x + l^{2\text{PN}}(\eta, e_t) x^2 + l^{3\text{PN}}(\eta, e_t) x^3 + l^{4\text{PN}}(\eta, e_t, \ln x) x^4 \right\} \quad (71b)$$

Promoting Eqs. (64) to Eqs. (71) to incorporate radiation-reaction effects is basically an application of the method of variation of arbitrary constants [42, 89]. Both the 4PN local and nonlocal-in-time contributions can be found in the accompanying MATHEMATICA notebook [57, 58]. Note that Eq. (71b) arises from our 4PN order expression for n , given by Eq. (28b), and requires 4PN order expressions for $(-2E)$ and 3PN order expression for h in terms of ω and e_t . Plus, as per our choice of ignoring the oscillatory 4PN tail corrections to action-angles (as per the semi-perturbation scheme) as detailed in IIC3, Eq. (71b) is the only equation in this Sec. III which incorporates the 4PN tail effects via Eqs. (54) and (56), as far as the IMR waveform construction is concerned. Also, we are only imposing secular variations to the four variables whose initial values we employ to specify the BBH configurations. It is fairly straightforward to include quasi-periodic variations to these variables that occur at 2.5PN and 3.5PN orders, detailed in Ref. [43]. We now give the 1PN contributions to Eqs. (70) and (71) for illustration

$$\dot{x}^{1\text{PN}}(\eta, e_t) = \frac{-11888 - 14784\eta + e_t^2(87720 - 159600\eta) + e_t^4(171038 - 141708\eta) + e_t^6(11717 - 8288\eta)}{420(1 - e_t^2)^{9/2}}, \quad (72)$$

$$\dot{e}_t^{1\text{PN}}(\eta, e_t) = -\frac{67608 + 228704\eta + e_t^2(-718008 + 651252\eta) + e_t^4(-125361 + 93184\eta)}{2520(1 - e_t^2)^{7/2}}, \quad (73)$$

$$l^{1\text{PN}}(e_t) = -\frac{3}{1 - e_t^2}. \quad (74)$$

The last ingredient, required to obtain temporal evolu-

tion for the dynamical variables $(r, \dot{r}, \dot{\phi}, \phi = \lambda + W)$, is an

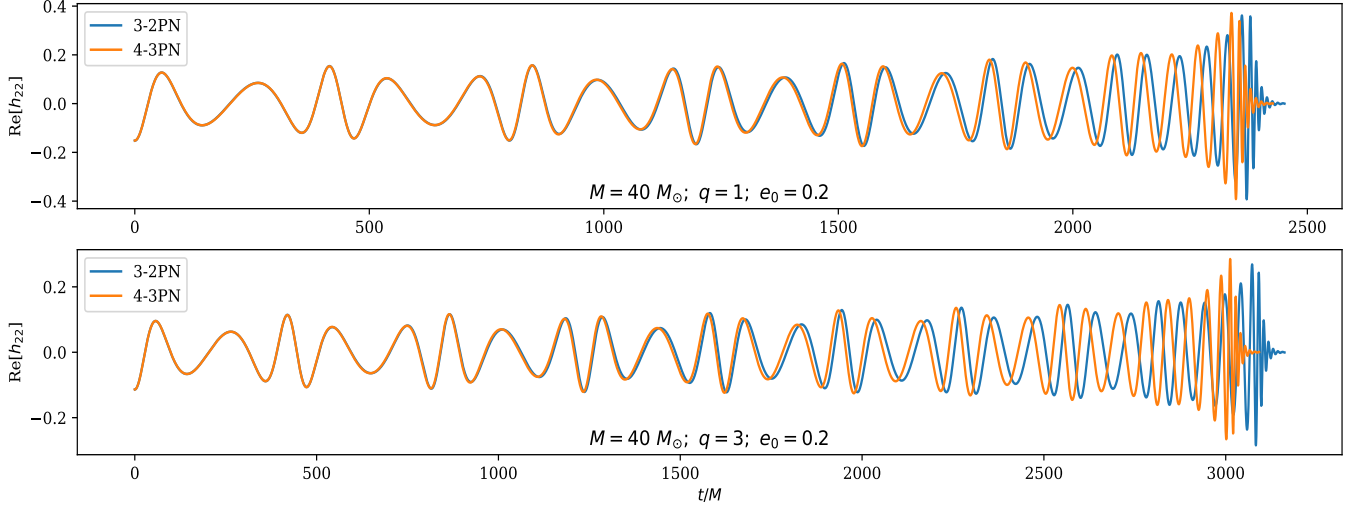


FIG. 1. Plots of GW strains that originate from our approach (4PN-3PN) against the 3PN-2PN IMR family of Ref. [28] for BH binaries with $q = 1$ (top) and $q = 3$ (bottom). Both plots begin at $F_{\text{orb}} = 15\text{Hz}$ and we observe significant de-phasing towards the later part of the inspiral. This may be attributed to the use of 2PN order equations to describe the inspiral dynamics in Ref. [28]. “ $n\text{PN}-m\text{PN}$ ” label stands for a waveform which includes $n(m)\text{PN}$ conservative (reactive) dynamics. $e_0 \equiv e_t(F_{\text{orb}} = 15\text{Hz})$ and $G = c = 1$ has been assumed for these plots.

accurate and efficient way of solving our 4PN order Kepler equation, given by Eq. (24), which we symbolically write as $l = \mathcal{L}(u, x, e_t)$. We employ Mikkola’s method [92] to numerically solve the 4PN order Kepler equation. Since Mikkola’s method was originally built and optimized to handle the classical Kepler equation (with no PN corrections), the process of solving the 4PN order Kepler equation using this method requires the numerical inversion to be done in a PN iterative manner as detailed in Ref. [93]. The need to bypass this numerical iteration procedure led us to introduce a new ‘auxiliary eccentric anomaly’ \hat{u} such that our 4PN order Kepler equation takes the same form as the Newtonian one when written

in terms of \hat{u}

$$\mathcal{L}(u, x, e_t) = \hat{u} - e_t \sin \hat{u}, \quad (75)$$

and therefore we can obtain \hat{u} values essentially by employing Mikkola’s method just once on Eq. (75). Thereafter, we evaluate u from the PN accurate relation $u = u(\hat{u}, x, e_t)$ by demanding that the following equality holds

$$l = \hat{u} - e_t \cos \hat{u} = u - e_t \cos u + \mathcal{O}(x^2), \quad (76)$$

where the RHS of the last equality includes corrections all the way up to 4PN as in Eq. (24). The straightforward way to do so would be to start with an ansatz $u = \sum C_i(\hat{u})x^i$ and plug it into the RHS of the second equality of Eq. (76) and evaluate the undetermined $C_i(\hat{u})$ as functions of \hat{u} . For illustration, we present u in terms of \hat{u} up to 2PN order as

$$u = \hat{u} + x^2 \left\{ \frac{e_t \eta (4 + \eta) \sin \hat{u}}{8(1 - e_t \cos \hat{u})^2} + \frac{3(5 - 2\eta)}{\sqrt{1 - e_t^2}(1 - e_t \cos \hat{u})} \arctan \left(\frac{(\sqrt{1 - e_t^2} - 1) \sin \hat{u}}{(\sqrt{1 - e_t^2} - 1) \cos \hat{u} + e_t} \right) \right\} + \mathcal{O}(x^3), \quad (77)$$

whereas the 4PN-accurate version of the above equation is provided in the accompanying MATHEMATICA notebook `Lengthy_Expressions.nb` [57, 58]. We have verified that the relative difference between numerical values of u and \hat{u} around late inspiral for a handful of cases is

$\sim 0.0001\% - 0.01\%$ with the lower and upper bounds corresponding to cases with $q \sim 1$ and 3 respectively.

We now sketch our procedure to generate temporally evolving eccentric inspiral $h^{22}(t)$ in a computationally efficient way. The following steps are required

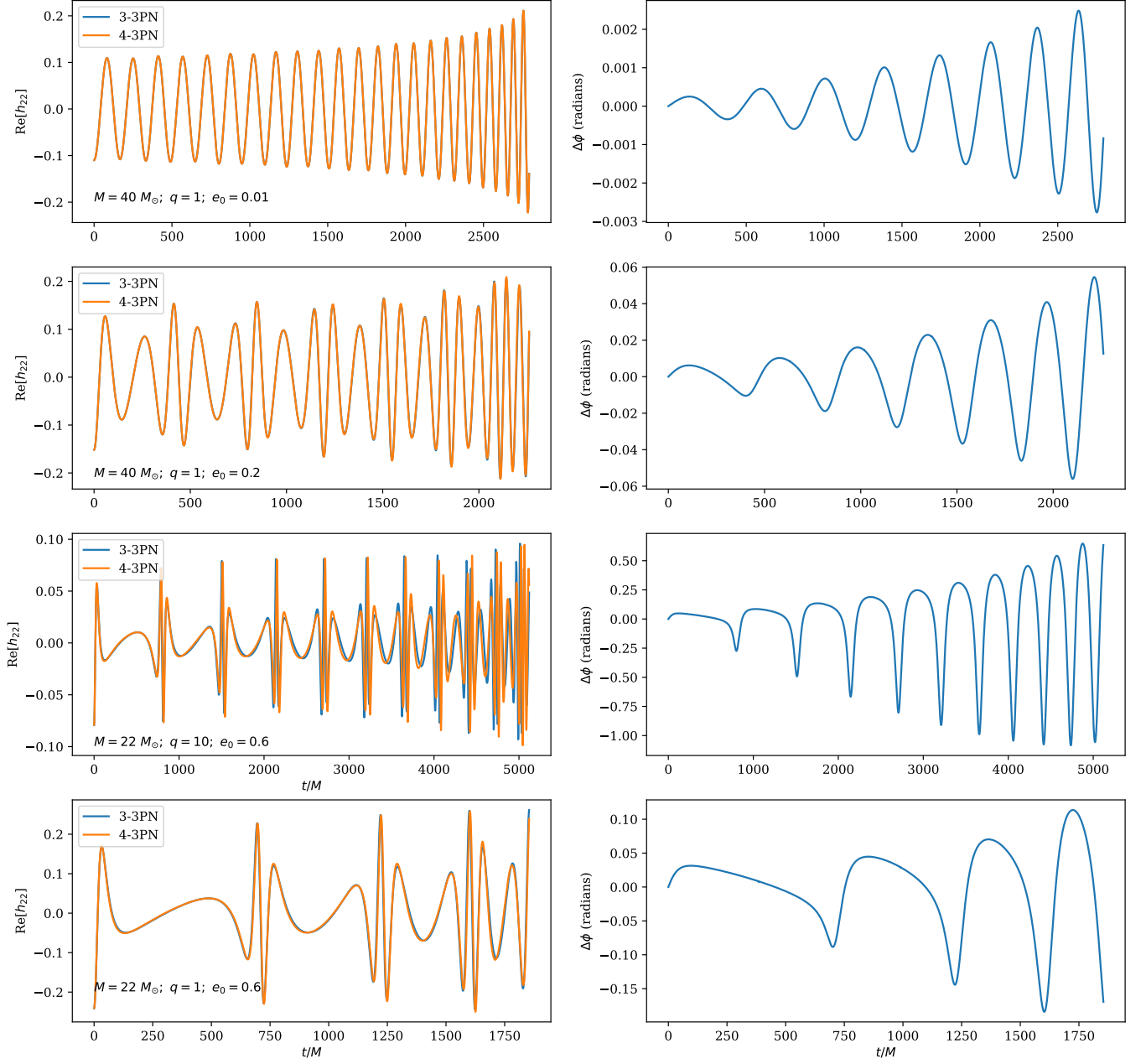


FIG. 2. We overlay plots of inspiral GW strains associated with the (4PN-3PN) and (3PN-3PN) inspiral families in the left panel. These plots are from $F_{\text{orb}} = 15\text{Hz}$ to $x = 1/6$ while varying values of the initial eccentricity and the mass ratio. The associated differences in the accumulated orbital phases between these two inspiral families are plotted in the right panel. The 4PN conservative contributions make noticeable differences for the moderately high and large mass ratio BH binaries. Similar to Fig. 1, “ $n\text{PN}-m\text{PN}$ ” label stands for a waveform which includes $n(m)\text{PN}$ conservative (reactive) dynamics. $e_0 \equiv e_t(F_{\text{orb}} = 15\text{Hz})$ and $G = c = 1$ has been assumed for these plots.

1. Specify an eccentric BH binary configuration by providing values for $\{x, e_t, \lambda, l\}$ at an initial epoch t_0 along with values of fixed parameters like m_1, m_2 and D .
2. With the help of our numerical solution to 4PN order Kepler equation via Eq. (75) and Eqs. (68) for R, \dot{R}, ϕ and $\dot{\phi}$, we evaluate Eq. (59) and obtain

the value of h^{22} at t_0 .

3. Thereafter, solve the coupled differential equations for x, e_t, λ and l to obtain their values at $t_0 + \Delta t$. Find $R, \dot{R}, \phi, \dot{\phi}$ and h^{22} at $t_0 + \Delta t$ using the same steps as before and so on.

This gives the quadrupolar order waveform h^{22} associated with our eccentric and non-spinning BH binary that

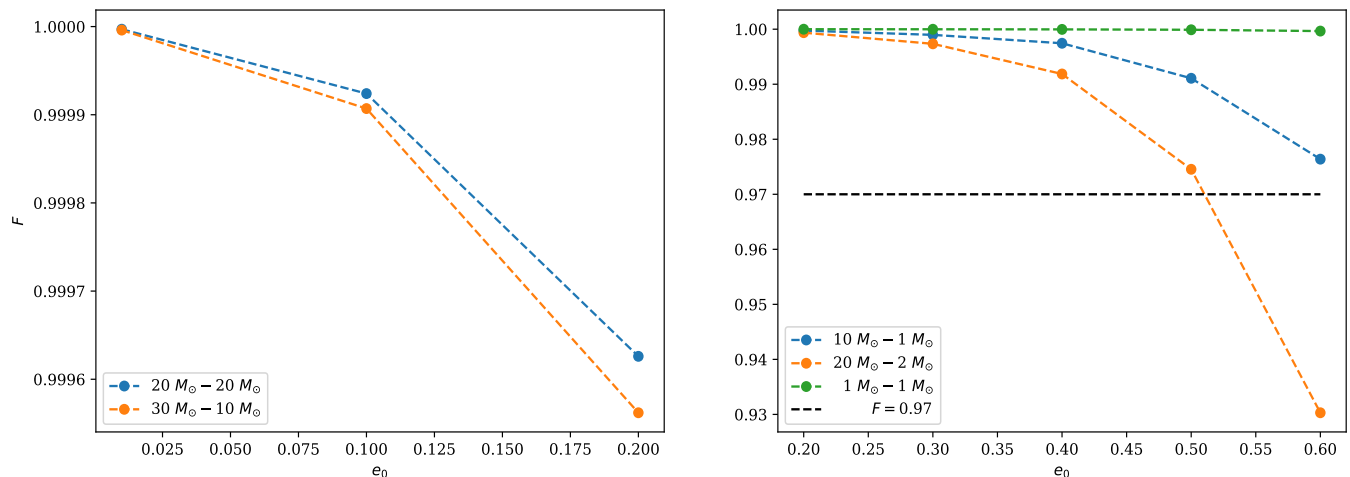


FIG. 3. Faithfulness plots between 4PN-3PN and 3PN-3PN eccentric IMR waveforms (left panel) and the associated inspiral only waveforms (right panel) for various initial eccentricities at $F_{\text{orb}} = 15\text{Hz}$ and mass ratios with $e_0 \equiv e_t(F_{\text{orb}} = 15\text{Hz})$. The inspiral waveforms of the right panel end at $x = 1/6$. Small values of e_0 and q ($q \equiv m_1/m_2$) are employed in the left panel to ensure the validity of our IMR waveforms. The inclusion of 4PN contributions do not affect the faithfulness estimates significantly. The right panel plots show that 4PN order effects are relevant for BBHs with higher e_0 and q . This is consistent with the de-phasing plots of Fig. 2. As noted earlier, the “ n PN- m PN” label stands for a waveform which includes $n(m)$ PN conservative (reactive) dynamics.

inspirals due to the effect of 3PN-accurate GW emission along 4PN order orbits.

A few comments are required to contrast our approach with the x -model of Ref. [28]. A close inspection reveals that our differential equations for x, e_t, λ and l do not contain any orbital time scale variations. However, the numerical treatment of $\dot{\phi}$ equation in the x -model of Ref. [28] ensures that the secular and periodic variations are intertwined in their approach, especially while dealing with the orbital phase evolution. The reason behind this contrast is that we have closed-form solutions for the orbital time-scale dynamics (in the form of 4PN generalized quasi-Keplerian parameterization) and hence numerical integration can happen on radiation-reaction time scale. Additionally, we use Mikkola method to solve our PN Kepler equation without needing to iterate as in Ref. [93] because of writing the PN Kepler equation in terms of a new variable $\hat{u}(u)$. These features make our computation routine efficient, apart from being accurate (3PN and 4PN accurate in reactive and conservative dynamics, respectively). It should be noted that we have not incorporated the GW emission induced orbital time scale variations to x, e_t, λ and l , as detailed in Refs. [42, 43], although this is fairly straightforward to do so using our prescription. However, it will be rather difficult to include such periodic contributions in the x -model of Ref. [28] due to their use of PN-accurate $\dot{\phi}(x, e_t, u)$ expression. In what follows, we explain briefly how we attach our eccentric inspiral h^{22} to the circular merger h^{22} model of Ref. [28] while treating their approach as a black box.

B. Stitching the circular merger-ringdown waveform to the eccentric inspiral waveform

As mentioned earlier, we exclusively follow Ref. [28] as a black box when it comes to stitching the merger-ringdown waveform to our inspiral waveform and it involves the following steps. First, we mark four special time instants: $t_{\text{ref}}, t_{\text{blend}}, t_{\text{circ}}$ and t_{peak} such that $t_{\text{ref}} < t_{\text{blend}} < t_{\text{circ}} < t_{\text{peak}}$. The first two instants correspond to epochs when $x = 0.11$ and 0.12 , respectively. Further, the instant t_{circ} is the time after which the binary can be treated as circular and t_{peak} is the time at which the dominant $\ell = 2, m = 2$ mode of the GW strain h_{22} reaches the maximum value in magnitude.

Importantly, Ref. [28] demonstrated the circularization of BBHs with $q < 3$ and initial eccentricity $e_t \lesssim 0.2$ (measured when $x \sim 0.07$) for $t > t_{\text{peak}} - 30M$. This implies that $t_{\text{circ}} = t_{\text{peak}} - 30M$. It allowed Ref. [28] to propose the use of their circular merger model (CMM) for $t > t_{\text{circ}}$. For its construction, three circular, non-spinning BBH waveforms from the Simulating eXtreme Spacetimes catalog [94] with $q = 1, 2$ and 4 were used and an interpolating function for the amplitude and frequency was constructed for all q values in the range $1 < q < 4$.

We employ our earlier described PN-accurate eccentric waveform in the interval $t < t_{\text{blend}}$ by specifying the eccentric BBH with its PN parameters (x, e_t, ϕ, l) ⁵ at a certain initial epoch. We employ the CMM for $t > t_{\text{circ}}$.

⁵ Switching from (x, e_t, λ, l) to (x, e_t, ϕ, l) is easy since $\phi = \lambda + W(u(l))$

This leaves only the ‘blending region’ to deal with, which is the interval $t_{\text{blend}} < t < t_{\text{circ}}$. Using 23 NR simulations, a fitting function for $\Delta t \equiv t_{\text{peak}} - t_{\text{ref}}$ was arrived at (see Eq. (9) of Ref. [28]) with $q, e_t(x = 0.11)$ and $l(x = 0.11)$ as its arguments. This Δt fit is crucial to model the waveform in the blending region as we soon see below in Eqs. (78).

Let us mention that there was a certain “NR-PN” fitting done in Ref. [87] which made it possible to assign PN parameters (x and e) to the 23 NR simulations in Table I of Ref. [28]; the top row of the table displays those PN parameters. Assignment of these parameters was crucial to performing the above mentioned Δt fit and by extension, constructing the IMR waveform of Ref. [28]. As expected, this NR-PN fitting is sensitive to the PN model used and becomes less so if the fit is performed earlier during the inspiral phase, as is evident in Figs. 4 and 5 of Ref. [87]. This is so because the PN parameter is smaller during earlier stages of inspiral. Since Ref. [87] explicitly mentions that the authors chose the earliest possible fitting interval to extract “a unique set of PN parameters”, we don’t feel the need to redo these NR-PN fits and thereby the Δt fit. Hence we don’t perform them and stick with Eq. (9) of Ref. [28] for our IMR waveform.

Now we discuss how to deal with the blending region. The waveform is written as $h_{\text{sig}} = Ae^{i\phi_w}$ with $\omega_w \equiv \dot{\phi}_w$. The subscript ‘ w ’ stand for ‘wave’ and serves to distinguish ϕ_w and ω_w from the orbital phase ϕ and frequency ω . The IMR waveform in the blending region is then given by Eqs. (10)-(17) of Ref. [28] which we reproduce almost exactly below (with the superscripts ‘PN’ and ‘circ’ standing for the PN waveform model and the CMM)⁶

$$t_{\text{peak}} = t_{\text{ref}} + \Delta t, \quad (78a)$$

$$t_{\text{circ}} = t_{\text{peak}} - 30M, \quad (78b)$$

$$\alpha(t) = \mathcal{T}(t; t_{\text{blend}}, t_{\text{circ}}), \quad (78c)$$

$$h_{\text{sig}}(t) = A(t)e^{i\phi_w(t)}, \quad (78d)$$

$$A(t) = (1 - \alpha(t))A^{\text{PN}} + \alpha(t)A^{\text{circ}}(t - t_{\text{peak}}), \quad (78e)$$

$$\omega_w(t) = (1 - \alpha(t))\omega_w^{\text{PN}} + \alpha(t)\omega_w^{\text{circ}}(t - t_{\text{peak}}), \quad (78f)$$

$$\phi_w(t) = \int^t \omega_w(t')dt'. \quad (78g)$$

$$\mathcal{T}(t, t_1, t_2) = \begin{cases} 0 & t \leq t_1, \\ \left[\exp\left(\frac{t_2 - t_1}{t - t_1} + \frac{t_2 - t_1}{t - t_2}\right) + 1 \right]^{-1} & t_1 < t < t_2, \\ 1 & t \geq t_2. \end{cases} \quad (79)$$

A few remarks in regard to the above equations are in order. $A^{\text{PN}}, \omega_w^{\text{PN}}, A^{\text{circ}}$ and ω_w^{circ} refer to the values of the amplitude and frequency (time derivative of the phase) of the PN and the CMM waveforms, respectively. The

function $\mathcal{T}(t, t_1, t_2)$ is a smooth function which goes from 0 to 1 between t_1 to t_2 and essentially does the job of ‘blending’ the PN waveform with the CMM waveform. The argument of A^{circ} and ω_w^{circ} in the above equations is $(t - t_{\text{peak}})$ because the CMM is time-shifted such that the peak occurs at $t = 0$.

We are now in a position to plot the waveforms got from our extension of the eccentric IMR family of Ref. [28] which we term as the 4-3PN (4PN conservative, 3PN reactive) IMR waveform in contrast to the 3-2PN (3PN conservative, 2PN reactive) family of Ref. [28]. In Fig. 1, we provide a visual contrast between these two IMR families for two mass ratios, namely $q = 1$ and 3. Clearly, some dephasing is evident near the late inspiral and it may be attributed to the use of 3PN-accurate effects of GW emission in our approach. Let us mention that we have added some missing terms in the expression of \dot{x} in the MATHEMATICA package accompanying Ref. [28] prior to plotting. Further, we have gauge-transformed the eccentricity parameter before making the above comparison because the work of Ref. [28] was done in the harmonic gauge. We now move on to explore preliminary data analysis implications of our time-domain IMR waveforms.

C. Preliminary data analysis implications

It will be interesting to explore the de-phasing and possible data analysis implications of our updated eccentric IMR waveform family in comparison with what is available in the literature. A cursory look of the Fig. 1 reveals that the effect of neglecting 3PN contributions to the GW emission can be substantial and we infer that this is mainly due to the late inspiral stage de-phasing of 4-3PN IMR waveform in contrast to the 3-2PN family. Therefore, we here restrict our attention to explore the implications of our 4PN order contributions to the conservative dynamics while keeping the radiation reactions effects fixed at the 3PN order. Further, we restrict our attention to the inspiral domain only. The plots in Fig. 2 provide visual comparisons between the members of the eccentric 4-3PN and 3-3PN inspiral waveform families and the associated orbital phase differences for 3 different initial values of orbital eccentricity. The plotted waveforms on the left panels of the first two rows are visually indistinguishable and their differences in the accumulated orbital phases are less than a fraction of a radian. However, the plots in the bottom row suggests that the effects of 4PN contributions to the conservative dynamics can shift the location of periastron passages in the moderately high initial eccentricity scenario as is evident from the differences in the peaks of these two waveform families. Additionally, the accumulated orbital phase difference can be roughly a radian for such eccentric binaries. Therefore, it is reasonable to expect that 4PN order contributions to the conservative orbital dynamics should be relevant for high eccentric black hole

⁶ Eqs. (78e) and (78f) are different from Eqs. (14) and (15) of Ref. [28] because there are typos in the latter set of equations.

binaries.

We now move on to probe a preliminary GW data analysis implications of our 4PN order corrections to the orbital dynamics by computing certain “faithfulness” estimates between the members of the above two inspiral families. The faithfulness between two GW signals $h_1(t)$ and $h_2(t)$ is defined as the following integral, maximized over the time and phase of coalescence t_c and ϕ_c such that [28, 95, 96]

$$F(h_1, h_2) \equiv \max_{t_c, \phi_c} \frac{(h_1(t_c, \phi_c), h_2)}{\sqrt{(h_1, h_1)(h_2, h_2)}}, \quad (80)$$

and the above inner product between two waveforms (h_1, h_2) being defined as

$$(h_1, h_2) \equiv 4 \Re \int_{f_{\min}}^{f_{\max}} \frac{\tilde{h}_1^*(f) \tilde{h}_2(f)}{S_h(f)} df, \quad (81)$$

where $\tilde{h}_i(f)$ stands for the Fourier transform of $h_i(t)$ and $S_h(f)$ is the noise power spectral density of the aLIGO detector. For the present analysis, we employed the zero-detuned, high-power noise configuration of aLIGO [97]. The faithfulness plots of Fig. 3 are for non-spinning compact binaries of different mass ratios. The faithfulness values are above the traditional 0.97 value for equal mass binaries which suggest that 3-3PN inspiral templates are ‘faithful’ to the expected 4-3PN inspiral GW signals [96]. Additionally, the above commonly accepted lower bound ensures the recovery of 90% of the hidden signals in the noisy data [98, 99]. However, the 3-3PN inspiral templates need not be ‘faithful’ to their 4-3PN counterparts for moderately eccentric and unequal mass compact binaries as evident from the plots in the right panel of Fig. 3. Therefore, it should be interesting to pursue computations to incorporate the effects of 4PN hereditary contributions to the conservative dynamics and model the resulting inspiral templates.

A true measure of validity of our 4-3PN IMR waveform can be had from comparisons with the corresponding NR simulations which we do not perform this paper. However it’s reasonable to expect our IMR waveform to be valid across a slightly larger parameter range than that for the waveform of Ref. [28] although we have not checked it. As far as the Ref. [28] is concerned, the faithfulness F (defined in Eq. (80)) between their IMR waveform and the NR counterparts > 0.97 for systems with $M \leq 85M_\odot$, $e_{t(7)} \leq 0.08$, $q \leq 3$ and $M \geq 70M_\odot$, $e_{t(7)} \lesssim 0.05$, $q \leq 3$ with $e_{t(7)}$ here standing for the eccentricity at ~ 7 cycles before the merger. This faithfulness was computed in Ref. [28] with the detector configuration of the first observing run (O1) of advanced LIGO with f_{\min} (lower frequency limit in Eq. (80)) being 30 Hz.

It should be obvious that the validity range in eccentricity of our inspiral prescription (based on PN equations) should be much larger than that for the entire IMR waveform. This is so because stitching the inspiral part

with the CMM part severely restricts the validity range of the IMR waveform in eccentricity as the CMM assumes that the BBH has circularized towards the merger. We therefore also present a derived package which outputs the waveform by only using the PN equations of motion [57, 58] and is valid for much higher e_t ’s. Recall that most of our PN equations are exact in e_t , except for the Padé approximants, all of which do reasonably well up to $e_t \lesssim 0.85$. Of course, this PN package can be trusted for the inspiral part only.

IV. SUMMARY AND NEXT STEPS

We incorporated the dynamics entailed by the 4PN-accurate Hamiltonian for non-spinning compact binaries, available in Ref. [52]. This was done using Keplerian type solution for the local part of the Hamiltonian and canonical perturbation theory for the non-local part. We ignored certain zero-average, oscillatory terms from our solution arising due to 4PN tail effects. Additionally, we provided consistency checks with existing results and detailed checks on the correctness of our lengthy results. Thereafter, we employed our results to obtain an eccentric IMR family by adapting what is done in Ref. [28]. This included providing an accurate and efficient implementation of GW phasing approach of Ref. [42] to model the inspiral part of eccentric IMR family. A preliminary and quick study revealed that the conservative 4PN order contributions should be relevant for BH binaries with high mass ratios and moderately high initial eccentricities.

We modify the publicly available MATHEMATICA package [56] of Ref. [28] to obtain our updated eccentric IMR family using our 4PN-order parametric solution [57, 58]. We also present a derived package which makes use of only the PN equations of motion to produce the waveforms and hence can be trusted only for the inspiral part. Since this second package does not use the circular-merger-model, it should be valid for a much higher range of e_t ($e_t \lesssim 0.85$) than our former package.

There are a number of extensions that should be pursued in the near future to provide a ready-to-use time domain eccentric IMR templates. Naturally, such a waveform family should be able to model eccentric mergers that should allow us to model BH binaries with moderately high initial eccentricities of $e_t \sim 0.5$. A very recent effort that developed a method to reconstruct eccentric merger waveforms from its circular counterparts, detailed in Ref. [40], should be helpful for such an effort. It will be interesting to stitch what is done in Ref. [40] to our inspiral approximant and probe its validity with the full NR based eccentric IMR waveforms for various initial eccentricities and mass ratios. It will be also desirable to include the spin effects to our inspiral part as these effects are now fully computed to the next-to-leading order [100, 101]. However, it will be desirable to develop Keplerian type parametric solution associated with these

next-to-leading order effects by extending what is pursued in Ref. [88]. Additionally, efforts should be pursued to extend our solution for non-spinning binaries to higher PN orders since the action and Hamiltonian computations of compact binaries have recently been pushed to 6PN [102–104]. Very recent efforts suggest that it should be possible to include 4PN order contributions to the GW emission in the coming years [105, 106]. However, this will require us to provide our improved Keplerian type parametric solution to 4PN order in the modified harmonic gauge with the help of Ref. [75]. We plan to complete 4PN-accurate GW phasing for eccentric binaries with such inputs while incorporating the currently missing radiation reaction induced periodic terms in orbital elements that appear at 2.5, 3.5PN and 4PN orders [42, 43].

ACKNOWLEDGEMENTS

We are grateful to Piotr Jaranowski, Gerhard Schäfer and Donato Bini for their encouragements and illuminative suggestions. We appreciate the detailed construc-

tive feedback from the anonymous referee. We also thank Thibault Damour, Leo Stein, Jan Steinhoff, Antoni Ramos Buades, Sumeet Kulkarni, Anuradha Gupta and Justin Vines for helpful discussions and comments. G.C is supported by the European Research Council (ERC) Consolidator Grant “Precision Gravity: From the LHC to LISA” provided by the ERC under the European Union’s H2020 research and innovation programme, grant agreement No. 817791. A.G. acknowledges support of the Department of Atomic Energy, Government of India, under Project Identification No. RTI 4002. HML was supported by the National Research Foundation of Korea grant number NRF-2021R1A2C2012473 from Ministry of Science and ICT, Korea.

Appendix A: Obtaining factorized PN-accurate expressions for dt/ds and $d\phi/ds$

We provide steps that are required to obtain Eqs. (13) and (16) from PN-accurate expressions for $\dot{r}^2 = \dot{s}^2/s^4$ and $d\phi/ds = \dot{\phi}/\dot{s}$ while restricting our attention to the 1PN order. The 1PN-accurate expression for \dot{r}^2 reads

$$\dot{r}^2 \equiv \frac{1}{s^4} \left(\frac{ds}{dt} \right)^2 = \left(2E + \frac{3E^2}{c^2}(-1 + 3\eta) \right) + \left(2 + \frac{2E}{c^2}(-6 + 7\eta) \right) s + \left(-h^2 + \frac{1}{c^2} \left[5(-2 + \eta) + 2h^2 E(1 - 3\eta) \right] \right) s^2 + \frac{h^2}{c^2} (8 - 3\eta)^2 s^3. \quad (A1)$$

We may symbolically write $\dot{r}^2 \equiv \dot{s}^2/s^4$ expression as $a_0 + a_1 s + a_2 s^2 + a_3 s^3$. $a_0 + a_1 s + a_2 s^2 + a_3 s^3 = 0$ has 3 roots but only two real roots s_- and s_+ exist at the Newtonian order and therefore are of interest to us. These two roots, expressed in terms of h , E and η , have already been given in Eq. (10). It is possible to factorize in the following form

$$\dot{r}^2 \equiv \frac{1}{s^4} \left(\frac{ds}{dt} \right)^2 = (s_- \times s) \times (s - s_+) \left(\frac{h^2(-8 + 3\eta)}{c^2} s + h^2 + \frac{1}{c^2} [-6 + \eta + 2h^2 E(-1 + 3\eta)] \right) + \mathcal{O}\left(\frac{1}{c^4}\right). \quad (A2)$$

It is now straightforward to write Eq.(A1) as

$$\begin{aligned} \frac{dt}{ds} &= \pm \frac{1}{s^2} \frac{1}{\sqrt{a_0 + a_1 s + a_2 s^2 + a_3 s^3}}, \\ &= \pm \frac{1}{s^2} \frac{1}{\sqrt{(s_- - s)(s - s_+)}} \left\{ \frac{1}{h} + \frac{-\eta + h^2(2 - 6\eta)E + 6}{2c^2 h^3} + \frac{8 - 3\eta}{2c^2 h^3} s + \mathcal{O}(1/c^4) \right\}, \\ &= \pm \frac{1}{s^2} \frac{A_0 + A_1 s}{\sqrt{(s_- - s)(s - s_+)}}. \end{aligned} \quad (A3)$$

It is now straightforward to extend the above computation to obtain to 4PN order

$$\frac{dt}{ds} = \frac{A_0 + A_1 s + A_2 s^2 + A_3 s^3 + A_4 s^4 + A_5 s^5 + A_6 s^6 + A_7 s^7}{\sqrt{(s_- - s)(s - s_+) s^2}}. \quad (A4)$$

This allows to write Eq. (13) for $(t - t_0)$ at 4PN order.

In a similar fashion, we may start from 4PN order expression for $\dot{\phi}$, namely $\dot{\phi} = b_2 s^2 + b_3 s^3 + b_4 s^4 + b_5 s^5 +$

$b_6 s^6 + b_7 s^7 + b_8 s^8 + b_9 s^9$, where again each of these coefficients are expressed in terms of h , E and η , and extract a suitable expression for $d\phi/ds$. Restricting our attention

to 1PN order, we find

$$b_2 = h - \frac{h E (1 + 3\eta)}{c^2}, \quad (\text{A5a})$$

$$b_3 = \frac{2 h (-2 + \eta)}{c^2}, \quad (\text{A5b})$$

while all other coefficients have no contributions at 1PN order. Using Eq.(A3),

$$\begin{aligned} \frac{d\phi}{ds} &= \frac{d\phi}{dt} \times \frac{dt}{ds} \\ &= \pm \frac{b_2 + b_3 s}{\sqrt{(s_- - s)(s - s_+)}} \left\{ \frac{1}{h} + \frac{-\eta + h^2(2 - 6\eta) E + 6}{2 c^2 h^3} + \frac{8 - 3\eta}{2 c^2 h^3} s \right\} + \mathcal{O}\left(\frac{1}{c^4}\right), \\ &= \pm \frac{B_0 + B_1 s}{\sqrt{(s_- - s)(s - s_+)}} + \mathcal{O}\left(\frac{1}{c^4}\right). \end{aligned} \quad (\text{A6})$$

This procedure may be extended to 4PN order and this leads to

$$\frac{d\phi}{ds} = \pm \frac{B_0 + B_1 s + B_2 s^2 + B_3 s^3 + B_4 s^4 + B_5 s^5 + B_6 s^6 + B_7 s^7}{\sqrt{(s_- - s)(s - s_+)}}. \quad (\text{A7})$$

This helps us obtain the parametric solution for the angular part.

Appendix B: Evaluating the temporal and angular integrals

Here we sketch the steps required to obtain Eqs. (15) and (19) from their integral forms, namely Eqs. (13) and (18). The plan is to provide details of the 1PN computations as their PN extensions are fairly straightforward although computationally demanding. We begin by inspecting the 1PN-accurate version of Eq. (13) which may be written as

$$t - t_0 = \int_s^{s_-} \frac{A_0 + A_1 \bar{s}}{\sqrt{(s_- - \bar{s})(\bar{s} - s_+)} \bar{s}^2} d\bar{s}, \quad (\text{B1})$$

A direct integration, if possible, should lead to an expression in terms of E, h, s_-, s_+ and s . Therefore, certain additional relations are required to obtain Eq. (15) that employs the auxiliary true anomaly like variable. It is obvious that we need to tackle integrals like

$$\int_s^{s_-} \frac{ds}{\sqrt{(s_- - s)(s - s_+)}} f(s) \quad (\text{B2})$$

where $s = 1/(a_r(1 - e_r \cos u))$ and $ds = du s^2 a_r e_r \sin u$. This leads to

$$\int_0^u \frac{du \sqrt{1 - e_r^2}}{a_r (1 - e_r \sin u)} f(u),$$

where $f(u) = f(s(u))$. The structures of the temporal and angular integrals suggest that we require to tackle

integrals of the form

$$I(u, n) = \int_0^u \frac{d\bar{u}}{(1 - e_r \cos \bar{u})^n}, \quad (\text{B3})$$

where n is an integer. We may introduce an angular variable $\tilde{\nu}(u) \equiv \sqrt{1 - e_r^2} I(u, 1) = 2 \arctan(\sqrt{(1 + e_r)/(1 - e_r)} \tan \frac{u}{2})$. It turns out that $d\tilde{\nu}/du = \sqrt{1 - e_r^2} f(u)$ where $f(u) \equiv 1/(1 - e_r \cos u)$ such that

$$f(u) = \frac{1 + e_r \cos(\tilde{\nu}(u))}{1 - e_r^2}. \quad (\text{B4})$$

The above relation is influenced by the relation that connects eccentric and true anomalies of the Keplerian parametrization. We now introduce a functional $G^{(n)}[\tilde{\nu}]$ such that $I(u, n) = G^{(n)}[\tilde{\nu}]$ and we differentiate it with respect to u to get

$$\frac{d}{du} I(u, n) = f(u)^n, \quad (\text{B5})$$

$$\frac{d}{du} G^{(n)}[\tilde{\nu}] = \frac{\delta G^{(n)}}{\delta \tilde{\nu}} \frac{d\tilde{\nu}}{du} = \sqrt{1 - e_r^2} f(u) \frac{\delta G^{(n)}}{\delta \tilde{\nu}}.$$

We now equate the above two expressions to obtain

$$\frac{\delta G^{(n)}}{\delta \tilde{\nu}} = \frac{f^{n-1}(u)}{\sqrt{1 - e_r^2}} = \frac{1}{(1 - e_r^2)^{n-\frac{1}{2}}} (1 + e_r \cos(\tilde{\nu}))^{n-1}. \quad (\text{B6})$$

The above equation allows us to write integrals like $I(u, n)$ in terms of simple trigonometric integrations like $\int \cos(n\tilde{\nu}) d\tilde{\nu}$.

With these inputs, we may tackle the above 1PN accurate temporal integral

$$t - t_0 = \int_s^{s_-} \frac{A_0 + A_1 \bar{s}}{\sqrt{(s_- - \bar{s})(\bar{s} - s_+)} \bar{s}^2} d\bar{s}, \quad (\text{B7})$$

$$= \sqrt{1 - e_r^2} \int_0^u d\bar{u} \left(\frac{A_0}{\bar{s}} + A_1 \right) \quad (\text{B8})$$

$$= \sqrt{1 - e_r^2} (A_0 a_r (u - e_r \sin u) + A_1 u) \quad (\text{B9})$$

$$\equiv \tilde{A}_0 u + \tilde{A}_1 \sin u. \quad (\text{B10})$$

Similar arguments allow us to tackle the 1PN-accurate orbital phase integral and it gives

$$\phi - \phi_0 = \int_s^{s_-} \frac{B_0 + B_1 \bar{s}}{\sqrt{(s_- - \bar{s})(\bar{s} - s_+)}} , \quad (\text{B11})$$

$$= \sqrt{1 - e_r^2} \int_0^u d\bar{u} (B_0 \bar{s} + B_1 \bar{s}^2), \quad (\text{B12})$$

$$= B_0 \tilde{\nu} + \frac{B_1}{(1 - e_r^2)} \int d\tilde{\nu} (1 + e_r \cos(\tilde{\nu})), \quad (\text{B13})$$

$$= B_0 \tilde{\nu} + \frac{B_1}{(1 - e_r^2)} (\tilde{\nu} + e_r \sin(\tilde{\nu})) \quad (\text{B14})$$

It is not very difficult to figure out that the above ex-

pressions lead to 1PN versions of Eqs. (15) and (19).

Finally, we note that additional relations like

$$s = \frac{1}{a_r (1 - e_r \cos(u))} = \frac{1 + e_r \cos \tilde{\nu}}{a(1 - e_r^2)}, \quad (\text{B15a})$$

$$u = \arccos \left(\frac{s_- + s_+}{s_- - s_+} - 2 \frac{s_- \times s_+}{(s_- - s_+)s} \right), \quad (\text{B15b})$$

$$\tilde{\nu} = \arccos \left(\frac{2s}{s_- - s_+} - \frac{s_- + s_+}{s_- - s_+} \right). \quad (\text{B15c})$$

are required to obtain 4PN order Kepler Equation and they are also heavily employed to obtain the parametric solution to the angular integral at higher PN orders.

Appendix C: Explicit 4PN order expressions for e_t and its connection with e_r and e_ϕ

We display below 4PN order expressions for the radial, time and angular eccentricities in ADM-like gauge

$$\begin{aligned} e_t^2 = & 1 + 2 E h^2 + \frac{(-2 E)}{4 c^2} \left\{ -8 + 8 \eta - (-17 + 7 \eta) (-2 E h^2) \right\} \\ & + \frac{(-2 E)^2}{8 c^4} \left\{ 8 + 4 \eta + 20 \eta^2 - (-2 E h^2) (112 - 47 \eta + 16 \eta^2) \right. \\ & - 24 \sqrt{(-2 E h^2)} (-5 + 2 \eta) + \frac{4}{(-2 E h^2)} (17 - 11 \eta) \\ & \left. - \frac{24}{\sqrt{(-2 E h^2)}} (5 - 2 \eta) \right\} \\ & + \frac{(-2 E)^3}{192 c^6} \left\{ 24 (-2 + 5 \eta) (-23 + 10 \eta + 4 \eta^2) - 15 \left(-528 \right. \right. \\ & + 200 \eta - 77 \eta^2 + 24 \eta^3 \left. \right) (-2 E h^2) - 72 (265 - 193 \eta \\ & + 46 \eta^2) \sqrt{(-2 E h^2)} - \frac{2}{(-2 E h^2)} \left(6732 + 117 \eta \pi^2 - 12508 \eta \right. \\ & + 2004 \eta^2 \left. \right) + \frac{2}{\sqrt{(-2 E h^2)}} \left(16380 - 19964 \eta + 123 \eta \pi^2 \right. \\ & + 3240 \eta^2 \left. \right) - \frac{2}{(-2 E h^2)^{3/2}} \left(10080 + 123 \eta \pi^2 - 13952 \eta \right. \\ & + 1440 \eta^2 \left. \right) + \frac{96}{(-2 E h^2)^2} \left(134 - 281 \eta + 5 \eta \pi^2 + 16 \eta^2 \right) \left. \right\} \\ & + \frac{(-2 E)^4}{460800 c^8} \left\{ 3600 (-25500 + 25804 \eta - 7267 \eta^2 + 1236 \eta^3 \right. \\ & + 280 \eta^4) - 28800 (1828 - 563 \eta + 237 \eta^2 - 84 \eta^3 \\ & + 25 \eta^4) (-2 E h^2) - 10800 (-18795 + 15344 \eta - 6303 \eta^2 \\ & + 1262 \eta^3) \sqrt{(-2 E h^2)} + \frac{50}{\sqrt{(-2 E h^2)}} \left(-9265320 \right. \\ & + (16589440 - 179031 \pi^2) \eta + 12 (-620854 + 4305 \pi^2) \eta^2 \\ & \left. + 851472 \eta^3 \right) + \frac{1}{(-2 E h^2)} \left(215107200 + 6 (-58544128 \right. \end{aligned}$$

$$\begin{aligned}
& +595725\pi^2)\eta + (159273712 - 4409175\pi^2)\eta^2 - 19425600\eta^3) \\
& - \frac{20}{(-2Eh^2)^{3/2}} \left(-36918720 + (84382336 - 1538535\pi^2)\eta \right. \\
& + 30(-1188608 + 16359\pi^2)\eta^2 + 2030400\eta^3) + \\
& + \frac{1}{(-2Eh^2)^2} \left(-324777600 + (765039936 - 16500150\pi^2)\eta \right. \\
& + (-348347776 + 13645725\pi^2)\eta^2 + 15062400\eta^3) \\
& + \frac{30}{(-2Eh^2)^{5/2}} \left(-17297280 + (37556864 - 771585\pi^2)\eta \right. \\
& + 1920(-7013 + 123\pi^2)\eta^2 + 403200\eta^3) \\
& - \frac{6}{(-2Eh^2)^3} \left(-51187200 - 6(-18365728 + 415175\pi^2)\eta \right. \\
& \left. + (-34446144 + 1442225\pi^2)\eta^2 + 576000\eta^3) \right\}. \tag{C1a}
\end{aligned}$$

The three eccentricities e_r, e_t and e_ϕ , which differ from each other at PN orders, are related by

$$\begin{aligned}
\frac{e_r}{e_t} = 1 & + \frac{(-2E)}{c^2} \left(4 - \frac{3\eta}{2} \right) + \frac{(-2E)}{8c^4h^2} \left(h^2(-2E)(6\eta^2 - 63\eta + 56) + 12h\sqrt{(-2E)}(5 - 2\eta) - 22\eta + 34 \right) \\
& + \frac{(-2E)}{192h^4} \left(-12h^4(-2E)^2(2\eta^3 - 98\eta^2 + 299\eta - 192) + 36h^3(-2E)^{3/2}(6\eta^2 - 69\eta + 65) \right. \\
& + h^2(-2E)(492\eta^2 + (3\pi^2 - 2252)\eta + 3828) \\
& + h\sqrt{(-2E)}(1440\eta^2 + (123\pi^2 - 13952)\eta + 10080) + 48(16\eta^2 + (5\pi^2 - 281)\eta + 134) \Big) \\
& - \frac{(-2E)}{3686400c^8h^6} \left(14400h^6(-2E)^3(603\eta^3 - 5474\eta^2 + 10176\eta - 5248) \right. \\
& + 43200h^5(-2E)^{5/2}(6\eta^3 - 779\eta^2 + 2632\eta - 1775) + h^4(-2E)^2(1152000\eta^3 + (4131675\pi^2 - 8360192)\eta^2 \\
& + 18(3594784 + 52725\pi^2)\eta - 175104000) \\
& - 200h^3(-2E)^{3/2}(86400\eta^3 + 324(41\pi^2 - 2528)\eta^2 + (410752 - 81615\pi^2)\eta + 829440) \\
& + 8h^2(-2E)(705600\eta^3 - (25311328 + 2355525\pi^2)\eta^2 + (141245184 - 670500\pi^2)\eta - 57484800) \\
& + 120h\sqrt{(-2E)}(403200\eta^3 + 1920(123\pi^2 - 7013)\eta^2 + (37556864 - 771585\pi^2)\eta - 17297280) + 24(576000\eta^3 \\
& \left. + (1442225\pi^2 - 34446144)\eta^2 - 6(415175\pi^2 - 18365728)\eta - 51187200) \right), \tag{C2}
\end{aligned}$$

$$\begin{aligned}
\frac{e_\phi}{e_t} = 1 & - \frac{(-2E)}{c^2}(\eta - 4) + \frac{(-2E)}{32c^4h^2} \left(h^2(-2E)(11\eta^2 - 168\eta + 224) - 48h\sqrt{(-2E)}(2\eta - 5) - 15\eta^2 - 144\eta + 272 \right) \\
& - \frac{(-2E)}{768c^6h^4} \left(6h^4(-2E)^2(3\eta^3 - 370\eta^2 + 1488\eta - 1536) \right. \\
& + 144h^3(-2E)^{3/2}(2\eta^2 + 49\eta - 65) + h^2(-2E)(-90\eta^3 + 918\eta^2 \\
& + (7420 + 3\pi^2)\eta - 30624) - 4h\sqrt{(-2E)}(1440\eta^2 + (123\pi^2 - 13952)\eta + 10080) \\
& \left. - 3(-70\eta^3 + 2416\eta^2 + (1005\pi^2 - 47452)\eta + 19200) \right) + \frac{(-2E)}{29491200c^8h^6} \left(1800h^6(-2E)^3(62\eta^4 - 11607\eta^3 \right. \\
& + 150368\eta^2 - 381952\eta + 335872) - 345600h^5(-2E)^{5/2}(46\eta^3 - 287\eta^2 + 1712\eta - 1775) + h^4(-2E)^2(586800\eta^4 \\
& - 27495000\eta^3 + (445236992 + 2929725\pi^2)\eta^2 + 1350(1481\pi^2 - 291040)\eta + 2801664000)
\end{aligned}$$

$$\begin{aligned}
& + 1600h^3(-2E)^{3/2}(181440\eta^3 + 12(1599\pi^2 - 121400)\eta^2 \\
& + (417664 - 81615\pi^2)\eta + 1416960) - 12h^2(-2E)(207300\eta^4 - 46247250\eta^3 + (930614528 + 892025\pi^2)\eta^2 \\
& + (454556608 + 23726550\pi^2)\eta - 750336000) - 960h\sqrt{(-2E)}(403200\eta^3 + 1920(123\pi^2 - 7013)\eta^2 \\
& + (37556864 - 771585\pi^2)\eta - 17297280) - 2300400\eta^4 - 889504200\eta^3 + (38875770624 - 584054625\pi^2)\eta^2 \\
& + 10(223387845\pi^2 - 8201607776)\eta + 23705395200 \Big). \tag{C3}
\end{aligned}$$

Appendix D: Energy and angular momentum in terms of x and e_t

$$\begin{aligned}
E = & \frac{-xc^2}{2} \left(1 + \left(\frac{5}{4} - 2\zeta^2 - \frac{\eta}{12} \right) x + \left(\frac{5}{8} + 5\zeta + \frac{7\zeta^2}{2} - \frac{25\zeta^4}{2} + \left(-\frac{5}{8} - 2\zeta - 4\zeta^2 + 9\zeta^4 \right) \eta - \frac{\eta^2}{24} \right) x^2 \right. \\
& + \left(-\frac{185}{192} + \frac{5\zeta}{2} + \frac{9\zeta^2}{2} + 30\zeta^3 + \frac{207\zeta^4}{4} - 30\zeta^5 - \frac{205\zeta^6}{3} \right. \\
& + \left(-\frac{75}{64} + \frac{23\zeta}{6} + \frac{2\zeta^2}{3} + 12\zeta^5 + \zeta^6 \left(\frac{613}{3} - \frac{205\pi^2}{64} \right) + \zeta^3 \left(-\frac{463}{9} + \frac{41\pi^2}{96} \right) \right. \\
& + \zeta^4 \left(-\frac{1301}{12} + \frac{41\pi^2}{64} \right) \eta + \left(-\frac{25}{288} - \frac{10\zeta}{3} - \frac{40\zeta^2}{9} + 7\zeta^3 + 36\zeta^4 - \frac{147\zeta^6}{4} \right) \eta^2 - \frac{35\eta^3}{5184} \Big) x^3 \\
& + \left(-\frac{931}{384} - \frac{85\zeta}{8} + \frac{155\zeta^2}{48} - \frac{435\zeta^3}{8} - \frac{559\zeta^4}{32} + \frac{3693\zeta^5}{8} + \frac{18551\zeta^6}{48} - 495\zeta^7 - \frac{29035\zeta^8}{96} \right. \\
& + \left(\frac{245}{1152} + \frac{67\zeta}{6} + \frac{47\zeta^2}{12} + \zeta^8 \left(\frac{847091}{432} - \frac{1964855\pi^2}{36864} \right) + \zeta^3 \left(\frac{14363}{54} - \frac{43441\pi^2}{9216} \right) + \zeta^4 \left(\frac{19793}{72} - \frac{53281\pi^2}{12288} \right) \right. \\
& + \zeta^7 \left(\frac{2114}{3} - \frac{41\pi^2}{16} \right) + \zeta^5 \left(-\frac{124841}{120} + \frac{16709\pi^2}{1024} \right) + \zeta^6 \left(-\frac{318437}{144} + \frac{334715\pi^2}{6144} \right) \Big) \eta \\
& + \left(\frac{245}{1152} - \frac{37\zeta}{18} - \frac{8\zeta^2}{3} - 150\zeta^7 + \frac{\zeta^6(2023688 - 35547\pi^2)}{1152} + \frac{1}{96}\zeta^5(47668 - 615\pi^2) \right. \\
& + \zeta^4 \left(-\frac{22025}{72} + \frac{533\pi^2}{192} \right) + \frac{\zeta^3(-370768 + 3567\pi^2)}{1728} + \frac{5\zeta^8(-396856 + 8733\pi^2)}{1152} \Big) \eta^2 \\
& + \left. \left(\frac{175}{5184} - \frac{28\zeta}{9} - \frac{280\zeta^2}{81} + \frac{82\zeta^3}{3} + 80\zeta^4 - \frac{107\zeta^5}{4} - \frac{431\zeta^6}{2} + \frac{1133\zeta^8}{8} \right) \eta^3 + \frac{77\eta^4}{31104} \right) x^4 \Big), \tag{D1}
\end{aligned}$$

$$\begin{aligned}
h = & \frac{1}{c\sqrt{x}} \left(\frac{1}{\zeta} + \left(\frac{3}{2\zeta} + \left(-\frac{5}{6\zeta} + \zeta \right) \eta \right) x + \left(5 + \frac{11}{8\zeta} - 8\zeta - \frac{15\zeta^2}{2} + \frac{25\zeta^3}{2} \right. \right. \\
& + \left(-2 - \frac{73}{24\zeta} + \frac{83\zeta}{12} + 3\zeta^2 - \frac{29\zeta^3}{4} \right) \eta + \left(\frac{5}{24\zeta} + \frac{\zeta}{3} - \frac{\zeta^3}{2} \right) \eta^2 \Big) x^2 \\
& + \left(5 + \frac{13}{48\zeta} + \frac{39\zeta}{4} + \frac{95\zeta^2}{4} - 97\zeta^3 - 30\zeta^4 + \frac{290\zeta^5}{3} + \left(-\frac{14}{3} - \frac{283}{48\zeta} - \frac{71\zeta}{48} \right. \right. \\
& + \frac{1}{384}\zeta^3(58808 - 357\pi^2) + \zeta^4 \left(\frac{236}{3} - \frac{41\pi^2}{64} \right) + \zeta^2 \left(-\frac{2023}{36} + \frac{41\pi^2}{96} \right) + \zeta^5 \left(-\frac{2537}{12} + \frac{365\pi^2}{128} \right) \Big) \eta \\
& + \left(-\frac{1}{3} + \frac{71}{36\zeta} + \frac{223\zeta}{36} + 12\zeta^2 - \frac{241\zeta^3}{6} - \frac{27\zeta^4}{2} + \frac{281\zeta^5}{8} \right) \eta^2 \\
& + \left(\frac{25}{1296\zeta} + \frac{17\zeta}{72} - \frac{3\zeta^3}{4} + \frac{\zeta^5}{2} \right) \eta^3 \Big) x^3 + \left(-\frac{35}{8} - \frac{173}{128\zeta} + \frac{93\zeta}{8} - \frac{315\zeta^2}{16} + \frac{21487\zeta^3}{64} \right. \\
& - \frac{709\zeta^4}{16} - \frac{15235\zeta^5}{16} + \frac{1581\zeta^6}{16} + \frac{38265\zeta^7}{64} + \left(-\frac{39}{4} - \frac{6991}{1152\zeta} - \frac{2179\zeta}{192} + \zeta^5 \left(\frac{42531499}{14400} - \frac{684125\pi^2}{12288} \right) \right.
\end{aligned}$$

$$\begin{aligned}
& + \zeta^6 \left(\frac{155773}{240} - \frac{47503\pi^2}{2048} \right) + \zeta^2 \left(\frac{5344}{27} - \frac{41473\pi^2}{9216} \right) + \zeta^3 \left(-\frac{4869481}{7200} + \frac{165109\pi^2}{24576} \right) + \zeta^4 \left(-\frac{23789}{30} + \frac{47461\pi^2}{2048} \right) \\
& + \zeta^7 \left(-\frac{24652879}{10800} + \frac{3632879\pi^2}{73728} \right) \eta + \left(-\frac{5}{36} + \frac{2963}{384\zeta} + \frac{11393\zeta}{2304} + \frac{\zeta^3(407299312 - 6357975\pi^2)}{921600} \right) \\
& + \zeta^7 \left(\frac{11872813}{7200} - \frac{74123\pi^2}{2048} \right) + \zeta^4 \left(\frac{23909}{36} - \frac{3649\pi^2}{384} \right) + \zeta^6 \left(-\frac{28367}{48} + \frac{41\pi^2}{4} \right) + \zeta^5 \left(-\frac{2319157}{1200} + \frac{454727\pi^2}{12288} \right) \\
& + \frac{1}{432} \zeta^2 \left(-60904 + 615\pi^2 \right) \eta^2 + \left(\frac{8}{9} - \frac{217}{576\zeta} + \frac{10687\zeta}{1728} + \frac{45\zeta^2}{2} - \frac{56027\zeta^3}{576} - \frac{309\zeta^4}{4} + \frac{22117\zeta^5}{96} \right. \\
& \left. + \frac{441\zeta^6}{8} - \frac{2245\zeta^7}{16} \right) \eta^3 + \left(-\frac{175}{31104\zeta} + \frac{35\zeta}{324} - \frac{13\zeta^3}{16} + \frac{4\zeta^5}{3} - \frac{5\zeta^7}{8} \right) \eta^4 \Big) x^4 \Big), \tag{D2}
\end{aligned}$$

where $\zeta \equiv 1/\sqrt{1 - e_t^2}$.

Appendix E: Canonical perturbation theory

Focusing our attention on an integrable and one degree of freedom⁷ system for now, we have the total Hamiltonian (unperturbed plus the perturbation) written as

$$H(\phi_0, J_0) = H_0(J_0) + \epsilon H_1(\phi_0, J_0), \tag{E1}$$

where (ϕ_0, J_0) are the action-angles of the unperturbed system. If the perturbed system is also integrable in the perturbative sense, then there exists a canonical transformation to the new action-angles $(\phi_0, J_0) \leftrightarrow (\phi, J)$ such that $E(J)$ is the total Hamiltonian in terms of the new action J : $E(J) = H(\phi_0, J_0)$. With a type-2 generator $S(\phi_0, J)$ of the form

$$S(\phi_0, J) = \phi_0 J + \epsilon S_1(\phi_0, J) + \mathcal{O}(\epsilon^2), \tag{E2}$$

we have

$$J_0 = \frac{\partial S}{\partial \phi_0} = J + \epsilon \frac{\partial S_1}{\partial \phi_0} + \mathcal{O}(\epsilon^2), \tag{E3}$$

$$\phi = \frac{\partial S}{\partial J} = \phi_0 + \epsilon \frac{\partial S_1}{\partial J} + \mathcal{O}(\epsilon^2). \tag{E4}$$

One of the main results of the canonical perturbation theory is that the leading and the linear in ϵ order contributions to $E(J) = E_0(J) + \epsilon E_1(J) + \mathcal{O}(\epsilon^2)$ read

$$E_0(J) = H_0(J) \tag{E5}$$

$$E_1(J) = H_1(\phi_0, J) + \frac{\partial H_0}{\partial J} \frac{\partial S_1}{\partial \phi_0}. \tag{E6}$$

It is implied here that $H_0(J)$ and $H_1(\phi_0, J)$ have the same functional dependence on J as $H_0(J_0)$ and $H_1(\phi_0, J_0)$

⁷ One degree of freedom implies one position and one conjugate momentum variable. Integrability is equivalent to the existence of action-angle variables [76].

have on J_0 . We have borrowed the above concept and presentation largely from Sec. 6.3 of Ref. [76]; the reader is referred to it for more details, including how to obtain S_1 . Evaluation of S_1 is required to get the perturbed action-angles from the unperturbed ones.

As explained in Ref. [68], it is easy to see from Eq. (E6) that a term of the form $A(J) \cos n\phi_0$ in H_1 (with n being a non-zero integer) can be eliminated by a term $-A(J) \sin n\phi_0/(n\Omega)$ in S_1 where $\Omega(J) \equiv \partial H_0(J)/\partial J$. And since all the sine terms in H_1 can also be eliminated similarly, all there is left to deal with is the non-oscillatory part of H_1 possessing a non-zero average over ϕ_0 . Hence, we can write

$$E_1(J) = \overline{H}_1, \tag{E7}$$

where \overline{H}_1 denotes the average of $H_1(\phi_0, J)$ over ϕ_0 .

Actually, this technique of averaging the perturbation is basically the von Zeipel-Brouwer technique applied to the Kepler problem (also known as the Delaunay technique). The von Zeipel-Brouwer technique is one of the many *degenerate* perturbation techniques [78], which differs from the non-degenerate one [76] in one crucial aspect that the averaging is not performed over all the angles (as in non-degenerate perturbation theory) but rather only a subset of them. This variation of the non-degenerate method can cure the problem of vanishing denominators which occurs when one tries to apply non-degenerate perturbation method to a degenerate system, such as the Newtonian Kepler system.

Appendix F: The “semi-perturbation” scheme: neglecting oscillatory corrections to action-angles

The main results of canonical perturbation theory are mainly contained in Eqs. (E3), (E4), (E5), (E6), and (E7), along with an equation for S_1 , which we don’t present. But often it is not necessary to retain all the information contained in these equations. We will elucidate this with a 1 DOF example of a simple harmonic oscillator (SHO).

With (q, p) being the pair of canonical variables (q in this appendix does not stand for the mass ratio), the full

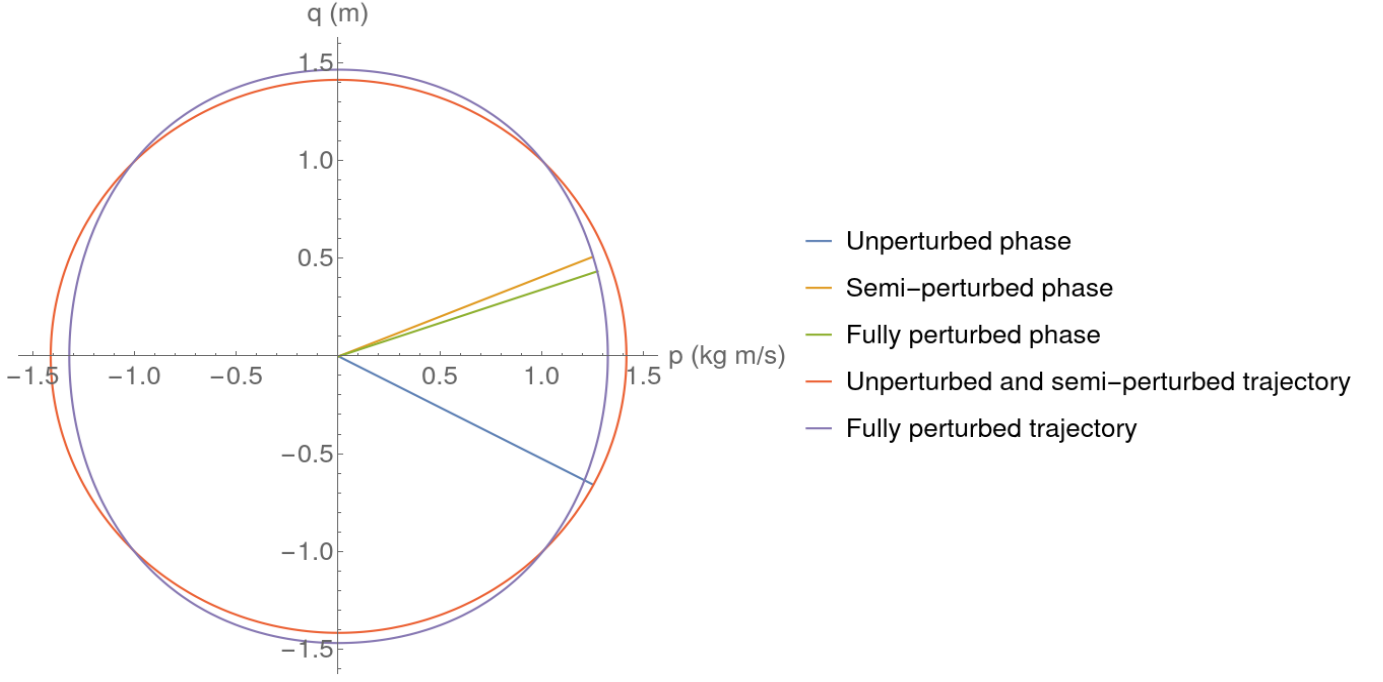


FIG. 4. The unperturbed, semi-perturbed and fully perturbed trajectories of a harmonic oscillator with the perturbation being a quartic function of the position coordinate q . The unperturbed and semi-perturbed cases have the same trajectory which is an “averaged” version of the fully perturbed trajectory. In all three cases, we start from an initial phase of 0 radians which corresponds to being on the positive p -axis. The three rays show the phase at $t = 5.8$ s (arbitrarily chosen). There is a large secular dephasing in the unperturbed case with respect to the other two cases. The semi-perturbed and the fully perturbed cases have small zero-average, oscillatory dephasing between them. There exists no secular difference between the phase-space trajectories for these two cases.

Hamiltonian of the perturbed SHO is

$$H = \frac{p^2}{2m} + \frac{1}{2}m\omega_0^2 q^2 + \frac{1}{4}\epsilon m q^4 \equiv H_0 + \epsilon H_1, \quad (\text{F1})$$

where $\omega_0 = \sqrt{k/m}$ with k and m being the spring constant and the mass of the oscillator respectively. ϵ is a small perturbation parameter. This is the subject of Worked Example 6.5 of Ref. [76]. We will simply use the results obtained there without showing the entire derivation. (q, p) as a function of unperturbed action-angles (J_0, ϕ_0) is

$$\begin{aligned} q &= \sqrt{\frac{2J_0}{m\omega_0}} \sin \phi_0, \\ p &= \sqrt{2J_0 m \omega_0} \cos \phi_0, \end{aligned} \quad (\text{F2})$$

whereas Eqs. (E3) and (E4) connect the unperturbed action-angles with the perturbed ones as (with $\mu = 1/m\omega_0^2$)

$$\begin{aligned} J_0 &= J + \epsilon \frac{\mu J^2}{8\omega_0} (4 \cos 2\phi - \cos 4\phi) + \mathcal{O}(\epsilon^2), \\ \phi_0 &= \phi - \epsilon \frac{\mu J}{4\omega_0} (2 \sin^2 \phi + 3) \sin \phi \cos \phi + \mathcal{O}(\epsilon^2). \end{aligned} \quad (\text{F3})$$

Note that Eqs. (F3) look a little different than the ones in the Worked Example 6.5 of Ref. [76] because we have

swapped $\phi \leftrightarrow \phi_0$ in linear in ϵ term. This is justified since it makes a difference at the $\mathcal{O}(\epsilon^2)$ absolute order. Finally, Eqs. (E5) and (E6) give the perturbed Hamiltonian and the perturbed frequency as

$$\begin{aligned} E(J) &= \omega_0 J + \epsilon \frac{3\mu}{8} J^2 + \mathcal{O}(\epsilon^2), \\ \omega = \frac{\partial E}{\partial J} &= \omega_0 + \epsilon \frac{3\mu}{4} J + \mathcal{O}(\epsilon^2). \end{aligned} \quad (\text{F4})$$

We now try to describe this system at three varying levels of complication: (i) unperturbed (least accurate) (ii) fully perturbed (most accurate) (iii) semi-perturbed (slightly less accurate than the “fully perturbed” scheme).

1. Unperturbed: The equations of motion (EOMs) are Eqs. (F2) with $\phi_0 = \omega_0 t$ and a given fixed value of J_0 . The unperturbed action J_0 stays constant during evolution.

2. Fully perturbed: The EOMs are Eqs. (F2), (F3) and (F4) with $\phi = \omega t$ with J (rather than J_0) staying constant.

3. Semi-perturbed: The EOMs are

$$\begin{aligned} q &= q(J_0, \phi_0)|_{(J_0, \phi_0) \rightarrow (J, \phi)} = \sqrt{\frac{2J}{m\omega_0}} \sin \phi, \\ p &= p(J_0, \phi_0)|_{(J_0, \phi_0) \rightarrow (J, \phi)} = \sqrt{2Jm\omega_0} \cos \phi, \end{aligned} \quad (\text{F5})$$

again with $\phi = \omega t$. In other words, in the semi-perturbed scheme, (q, p) are taken to have the same dependence on (J, ϕ) as they have on (J_0, ϕ_0) . Along with this, we also have Eqs. (F4). Thus, in the semi-perturbed scheme, the oscillatory corrections to action-angles and the generating function S (Eqs. (E3), (E4) and (E2)) don't need to be computed and hence can be ignored. This leads to significant simplifications when compared to the fully perturbed case without much loss of information, as we will see below. An example of these zero-average oscillatory corrections are the sinusoidal terms in Eqs. F3.

To see what concrete effects the three above schemes bring about, we plot the respective trajectories in the phase space for all the three cases in Fig. 4, for the following numerical values: $k = 1 \text{ N/m}$, $m = 1 \text{ kg}$, $J = J_0 = 1 \text{ kg m}^2/\text{s}$, $\epsilon = 0.2$. The closed contours denote the trajectories and the three rays denote the phase swept ($\arctan(m\omega_0 q/p)$) for all the above three cases from $t = 0$ to $t = 5.8 \text{ s}$ (an arbitrarily chosen numerical value). Since $\phi_0(t = 0) = \phi(t = 0) = 0$, at $t = 0$ we start from the points where the closed trajectories of Fig. 4 intersect the positive p -axis for all the above three cases. At the final time $t = 5.8 \text{ s}$, in the fully perturbed and semi-perturbed cases, we have swept a little over a full revolution whereas in the unperturbed case, we have a significant phase lag compared with the other two. The full effect of the perturbation ϵH_1 (corresponding to the “fully perturbed” case above) is that the perturbed trajectory starts to deform around the unperturbed one and there is a dephasing which increases with time. The dephasing is due to

the frequency correction term (linear in ϵ) in Eq. (F4). In addition, note that the unperturbed trajectory (labeled by $J_0 = J_N$) is the “averaged version” of the fully perturbed trajectory (labeled by $J = J_N$), with J_N standing for some numerical value of the action.

Now let's come to the semi-perturbed case. The semi-perturbed approximation gives us the same trajectory as the unperturbed one (see Fig. 4), but with a phase (yellow ray) that differs from the fully perturbed phase (green ray) in an oscillatory fashion, rather than secular. This means that we get the averaged version of the fully perturbed trajectory and a small amount of oscillatory dephasing with respect to the fully perturbed one, which does not grow in time and whose time-average is zero. The upshot is that instead of capturing the full perturbation effect, we can settle with the semi-perturbed case which has got no secular differences (either in phase or amplitude) with respect to the fully perturbed case. This way we don't need to compute S . Similar approaches have been adopted in some textbooks (Sec. 12.3 and 12.4 of Ref. [77]). Even from the GW data analysis point of view, it is the secular effects that matter much more than the oscillatory ones because the method of matched filter employed in the analysis builds up signal-to-noise ratio by following the phase of the two waveforms to be matched in a coherent manner [107–109].

It is important to note that to model the system using the semi-perturbed scheme, one needs to be given the numerical values of (J, ϕ) at some initial time; initial values of (q, p) or (J_0, ϕ_0) won't do. On the other hand, initial numerical values of (q, p) or (J_0, ϕ_0) are required to model the system as per the unperturbed and the fully-perturbed schemes. All this is not a cause for concern because the 4-3PN IMR MATHEMATICA package [57, 58] provided with this paper requires the user to input the PN parameter x and eccentricity which are ultimately related to the perturbed actions of the BBH system.

-
- [1] B. Abbott *et al.* (LIGO Scientific, Virgo), GWTC-1: A Gravitational-Wave Transient Catalog of Compact Binary Mergers Observed by LIGO and Virgo during the First and Second Observing Runs, *Phys. Rev. X* **9**, 031040 (2019), arXiv:1811.12907 [astro-ph.HE].
 - [2] R. Abbott *et al.* (LIGO Scientific, Virgo), GWTC-2: Compact Binary Coalescences Observed by LIGO and Virgo During the First Half of the Third Observing Run, (2020), arXiv:2010.14527 [gr-qc].
 - [3] B. Abbott *et al.* (LIGO Scientific, Virgo), GW170817: Observation of Gravitational Waves from a Binary Neutron Star Inspiral, *Phys. Rev. Lett.* **119**, 161101 (2017), arXiv:1710.05832 [gr-qc].
 - [4] R. Poggiani, LIGO Scientific Collaboration, and Virgo Collaboration, Multi-messenger Observations of a Binary Neutron Star Merger, in *Multifrequency Behaviour of High Energy Cosmic Sources - XIII. 3-8 June 2019. Palermo* (2019) p. 19.
 - [5] T. Venumadhav, B. Zackay, J. Roulet, L. Dai, and M. Zaldarriaga, New binary black hole mergers in the second observing run of Advanced LIGO and Advanced Virgo, *Phys. Rev. D* **101**, 083030 (2020), arXiv:1904.07214 [astro-ph.HE].
 - [6] R. Abbott *et al.* (LIGO Scientific, Virgo), Population Properties of Compact Objects from the Second LIGO-Virgo Gravitational-Wave Transient Catalog, (2020), arXiv:2010.14533 [astro-ph.HE].
 - [7] B. Abbott *et al.*, A gravitational-wave standard siren measurement of the Hubble constant, *Nature* **551**, 85 (2017), arXiv:1710.05835 [astro-ph.CO].
 - [8] R. Abbott *et al.* (LIGO Scientific, Virgo), Tests of General Relativity with Binary Black Holes from the second LIGO-Virgo Gravitational-Wave Transient Catalog, (2020), arXiv:2010.14529 [gr-qc].
 - [9] J. Aasi *et al.* (LIGO Scientific), Advanced LIGO, *Class. Quant. Grav.* **32**, 074001 (2015), arXiv:1411.4547 [gr-qc].
 - [10] F. Acernese *et al.* (VIRGO), Advanced Virgo: a second-

- generation interferometric gravitational wave detector, *Class. Quant. Grav.* **32**, 024001 (2015), arXiv:1408.3978 [gr-qc].
- [11] T. Akutsu *et al.* (KAGRA), KAGRA: 2.5 Generation Interferometric Gravitational Wave Detector, *Nature Astron.* **3**, 35 (2019), arXiv:1811.08079 [gr-qc].
- [12] M. Mapelli, Astrophysics of stellar black holes, *Proc. Int. Sch. Phys. Fermi* **200**, 87 (2020), arXiv:1809.09130 [astro-ph.HE].
- [13] I. Mandel and A. Farmer, Merging stellar-mass binary black holes, arXiv e-prints, arXiv:1806.05820 (2018), arXiv:1806.05820 [astro-ph.HE].
- [14] K. A. Postnov and L. R. Yungelson, The Evolution of Compact Binary Star Systems, *Living Reviews in Relativity* **9**, 6 (2006), arXiv:astro-ph/0701059 [astro-ph].
- [15] M. U. Kruckow, T. M. Tauris, N. Langer, M. Kramer, and R. G. Izzard, Progenitors of gravitational wave mergers: binary evolution with the stellar grid-based code COMBINE, *MNRAS* **481**, 1908 (2018), arXiv:1801.05433 [astro-ph.SR].
- [16] I. Kowalska, T. Bulik, K. Belczynski, M. Dominik, and D. Gondek-Rosinska, The eccentricity distribution of compact binaries, *Astron. Astrophys.* **527**, A70 (2011), arXiv:1010.0511 [astro-ph.CO].
- [17] G. Fragione and O. Bromberg, Eccentric binary black hole mergers in globular clusters hosting intermediate-mass black holes, *MNRAS* **488**, 4370 (2019), arXiv:1903.09659 [astro-ph.GA].
- [18] J. Samsing, Eccentric Black Hole Mergers Forming in Globular Clusters, *Phys. Rev. D* **97**, 103014 (2018), arXiv:1711.07452 [astro-ph.HE].
- [19] J. Kumamoto, M. S. Fujii, and A. Tanikawa, Merger rate density of binary black holes formed in open clusters, *MNRAS* **495**, 4268 (2020), arXiv:2001.10690 [astro-ph.HE].
- [20] R. M. O’Leary, B. Kocsis, and A. Loeb, Gravitational waves from scattering of stellar-mass black holes in galactic nuclei, *Mon. Not. Roy. Astron. Soc.* **395**, 2127 (2009), arXiv:0807.2638 [astro-ph].
- [21] W. M. Farr, S. Stevenson, M. C. Miller, I. Mandel, B. Farr, and A. Vecchio, Distinguishing spin-aligned and isotropic black hole populations with gravitational waves, *Nature* **548**, 426 (2017), arXiv:1706.01385 [astro-ph.HE].
- [22] M. A. Sedda, M. Mapelli, M. Spera, M. Benacquista, and N. Giacobbo, Fingerprints of binary black hole formation channels encoded in the mass and spin of merger remnants, *Astrophys. J.* **894**, 133 (2020), arXiv:2003.07409 [astro-ph.GA].
- [23] D. Park, C. Kim, H. M. Lee, Y.-B. Bae, and K. Belczynski, Black hole binaries dynamically formed in globular clusters, *MNRAS* **469**, 4665 (2017), arXiv:1703.01568 [astro-ph.HE].
- [24] J. Hong and H. M. Lee, Black hole binaries in galactic nuclei and gravitational wave sources, *MNRAS* **448**, 754 (2015), arXiv:1501.02717 [astro-ph.GA].
- [25] C. L. Rodriguez, P. Amaro-Seoane, S. Chatterjee, K. Kremer, F. A. Rasio, J. Samsing, C. S. Ye, and M. Zevin, Post-Newtonian dynamics in dense star clusters: Formation, masses, and merger rates of highly-eccentric black hole binaries, *Phys. Rev. D* **98**, 123005 (2018), arXiv:1811.04926 [astro-ph.HE].
- [26] I. M. Romero-Shaw, P. D. Lasky, and E. Thrane, Searching for eccentricity: signatures of dynamical formation in the first gravitational-wave transient catalogue of LIGO and Virgo, *MNRAS* **490**, 5210 (2019), arXiv:1909.05466 [astro-ph.HE].
- [27] L. Gondán and B. Kocsis, High Eccentricities and High Masses Characterize Gravitational-wave Captures in Galactic Nuclei as Seen by Earth-based Detectors, arXiv e-prints, arXiv:2011.02507 (2020), arXiv:2011.02507 [astro-ph.HE].
- [28] I. Hinder, L. E. Kidder, and H. P. Pfeiffer, Eccentric binary black hole inspiral-merger-ringdown gravitational waveform model from numerical relativity and post-Newtonian theory, *Phys. Rev. D* **98**, 044015 (2018), arXiv:1709.02007 [gr-qc].
- [29] E. A. Huerta, C. J. Moore, P. Kumar, D. George, A. J. K. Chua, R. Haas, E. Wessel, D. Johnson, D. Glennon, A. Rebei, A. M. Holgado, J. R. Gair, and H. P. Pfeiffer, Eccentric, nonspinning, inspiral, Gaussian-process merger approximant for the detection and characterization of eccentric binary black hole mergers, *Phys. Rev. D* **97**, 024031 (2018), arXiv:1711.06276 [gr-qc].
- [30] T. Hinderer and S. Babak, Foundations of an effective-one-body model for coalescing binaries on eccentric orbits, *Phys. Rev. D* **96**, 104048 (2017), arXiv:1707.08426 [gr-qc].
- [31] Z. Cao and W.-B. Han, Waveform model for an eccentric binary black hole based on the effective-one-body-numerical-relativity formalism, *Phys. Rev. D* **96**, 044028 (2017), arXiv:1708.00166 [gr-qc].
- [32] D. Chiamello and A. Nagar, Faithful analytical effective-one-body waveform model for spin-aligned, moderately eccentric, coalescing black hole binaries, *Phys. Rev. D* **101**, 101501 (2020), arXiv:2001.11736 [gr-qc].
- [33] S. Tiwari, A. Gopakumar, M. Haney, and P. Hemantakumar, Ready-to-use Fourier domain templates for compact binaries inspiraling along moderately eccentric orbits, *Phys. Rev. D* **99**, 124008 (2019), arXiv:1905.07956 [gr-qc].
- [34] A. Ramos-Buades, S. Tiwari, M. Haney, and S. Husa, Impact of eccentricity on the gravitational-wave searches for binary black holes: High mass case, *Phys. Rev. D* **102**, 043005 (2020), arXiv:2005.14016 [gr-qc].
- [35] A. Nagar, A. Bonino, and P. Rettengo, All in one: effective one body multipolar waveform model for spin-aligned, quasi-circular, eccentric, hyperbolic black hole binaries, arXiv e-prints, arXiv:2101.08624 (2021), arXiv:2101.08624 [gr-qc].
- [36] I. M. Romero-Shaw, N. Farrow, S. Stevenson, E. Thrane, and X.-J. Zhu, On the origin of GW190425, *MNRAS* **496**, L64 (2020), arXiv:2001.06492 [astro-ph.HE].
- [37] I. Romero-Shaw, P. D. Lasky, E. Thrane, and J. Calderón Bustillo, GW190521: Orbital Eccentricity and Signatures of Dynamical Formation in a Binary Black Hole Merger Signal, *ApJ* **903**, L5 (2020), arXiv:2009.04771 [astro-ph.HE].
- [38] E. A. Huerta, P. Kumar, S. T. McWilliams, R. O’Shaughnessy, and N. Yunes, Accurate and efficient waveforms for compact binaries on eccentric orbits, *Phys. Rev. D* **90**, 084016 (2014), arXiv:1408.3406 [gr-qc].
- [39] B. Moore, M. Favata, K. G. Arun, and C. K. Mishra,

- Gravitational-wave phasing for low-eccentricity inspiralling compact binaries to 3PN order, *Phys. Rev. D* **93**, 124061 (2016), arXiv:1605.00304 [gr-qc].
- [40] Y. Setyawati and F. Ohme, Adding eccentricity to quasi-circular binary-black-hole waveform models, arXiv e-prints, arXiv:2101.11033 (2021), arXiv:2101.11033 [gr-qc].
- [41] E. A. Huerta *et al.*, Complete waveform model for compact binaries on eccentric orbits, *Phys. Rev. D* **95**, 024038 (2017), arXiv:1609.05933 [gr-qc].
- [42] T. Damour, A. Gopakumar, and B. R. Iyer, Phasing of gravitational waves from inspiralling eccentric binaries, *Phys. Rev. D* **70**, 064028 (2004), gr-qc/0404128.
- [43] C. Königsdörffer and A. Gopakumar, Phasing of gravitational waves from inspiralling eccentric binaries at the third-and-a-half post-Newtonian order, *Phys. Rev. D* **73**, 124012 (2006), gr-qc/0603056.
- [44] G. Schäfer and N. Wex, Second post-Newtonian motion of compact binaries, *Physics Letters A* **174**, 196 (1993).
- [45] R.-M. Memmesheimer, A. Gopakumar, and G. Schäfer, Third post-Newtonian accurate generalized quasi-Keplerian parametrization for compact binaries in eccentric orbits, *Phys. Rev. D* **70**, 104011 (2004), gr-qc/0407049.
- [46] G. Schäfer and P. Jaranowski, Hamiltonian formulation of general relativity and post-Newtonian dynamics of compact binaries, *Living Reviews in Relativity* **21**, 7 (2018), arXiv:1805.07240 [gr-qc].
- [47] L. Blanchet, Gravitational Radiation from Post-Newtonian Sources and Inspiralling Compact Binaries, *Living Reviews in Relativity* **17**, 2 (2014), arXiv:1310.1528 [gr-qc].
- [48] L. Blanchet and G. Schafer, Higher order gravitational radiation losses in binary systems., *MNRAS* **239**, 845 (1989).
- [49] W. Junker and G. Schaefer, Binary systems - Higher order gravitational radiation damping and wave emission, *MNRAS* **254**, 146 (1992).
- [50] A. Gopakumar and B. R. Iyer, Gravitational waves from inspiraling compact binaries: Angular momentum flux, evolution of the orbital elements, and the waveform to the second post-Newtonian order, *Phys. Rev. D* **56**, 7708 (1997), arXiv:gr-qc/9710075 [gr-qc].
- [51] K. G. Arun, L. Blanchet, B. R. Iyer, and S. Sinha, Third post-Newtonian angular momentum flux and the secular evolution of orbital elements for inspiralling compact binaries in quasi-elliptical orbits, *Phys. Rev. D* **80**, 124018 (2009), arXiv:0908.3854 [gr-qc].
- [52] P. Jaranowski and G. Schäfer, Derivation of local-in-time fourth post-Newtonian ADM Hamiltonian for spinless compact binaries, *Phys. Rev. D* **92**, 124043 (2015), arXiv:1508.01016 [gr-qc].
- [53] T. Damour, P. Jaranowski, and G. Schäfer, Nonlocal-in-time action for the fourth post-Newtonian conservative dynamics of two-body systems, *Phys. Rev. D* **89**, 064058 (2014), arXiv:1401.4548 [gr-qc].
- [54] D. Bini, T. Damour, and A. Geralico, Sixth post-Newtonian nonlocal-in-time dynamics of binary systems, *Phys. Rev. D* **102**, 084047 (2020), arXiv:2007.11239 [gr-qc].
- [55] J. Blümlein, A. Maier, P. Marquard, and G. Schäfer, Fourth post-Newtonian Hamiltonian dynamics of two-body systems from an effective field theory approach, *Nuclear Physics B* **955**, 115041 (2020), arXiv:2003.01692 [gr-qc].
- [56] <https://github.com/ianhinder/EccentricIMR> (2017).
- [57] <https://github.com/sashwattanay/EccentricIMR> (2021).
- [58] See Supplemental Material at [URL will be inserted by publisher] for the MATHEMATICA packages, notebook and pdf files that produce the gravitational waveforms (IMR and inspiral) and contain various lengthy expressions.
- [59] T. Damour and N. Deruelle, General relativistic celestial mechanics of binary systems. I. The post-Newtonian motion., *Ann. Inst. Henri Poincaré Phys. Théor.*, Vol. 43, No. 1, p. 107 - 132 **43**, 107 (1985).
- [60] T. Damour and G. Schafer, Higher-order relativistic periastron advances and binary pulsars., *Nuovo Cimento B Serie* **101**, 127 (1988).
- [61] S. A. Klioner, Basic Celestial Mechanics, arXiv e-prints, arXiv:1609.00915 (2016), arXiv:1609.00915 [astro-ph.IM].
- [62] P. Colwell, *Solving Kepler's Equation Over Three Centuries* (Willmann-Bell, 1993).
- [63] Y. Boetzel, A. Susobhanan, A. Gopakumar, A. Klein, and P. Jetzer, Solving post-Newtonian accurate Kepler equation, *Phys. Rev. D* **96**, 044011 (2017), arXiv:1707.02088 [gr-qc].
- [64] G. Cho, A. Gopakumar, M. Haney, and H. M. Lee, Gravitational waves from compact binaries in post-Newtonian accurate hyperbolic orbits, *Phys. Rev. D* **98**, 024039 (2018), arXiv:1807.02380 [gr-qc].
- [65] T. Damour and N. Deruelle, General relativistic celestial mechanics of binary systems. II. The post-Newtonian timing formula., *Ann. Inst. Henri Poincaré Phys. Théor* **44**, 263 (1986).
- [66] T. Damour and J. H. Taylor, Strong-field tests of relativistic gravity and binary pulsars, *Phys. Rev. D* **45**, 1840 (1992).
- [67] A. Susobhanan, A. Gopakumar, G. Hobbs, and S. R. Taylor, Pulsar timing array signals induced by black hole binaries in relativistic eccentric orbits, *Phys. Rev. D* **101**, 043022 (2020), arXiv:2002.03285 [gr-qc].
- [68] T. Damour, P. Jaranowski, and G. Schäfer, Fourth post-Newtonian effective one-body dynamics, *Phys. Rev. D* **91**, 084024 (2015), arXiv:1502.07245 [gr-qc].
- [69] C. R. Galley, A. K. Leibovich, R. A. Porto, and A. Ross, Tail effect in gravitational radiation reaction: Time nonlocality and renormalization group evolution, *Phys. Rev. D* **93**, 124010 (2016), arXiv:1511.07379 [gr-qc].
- [70] T. Damour, P. Jaranowski, and G. Schäfer, Dimensional regularization of the gravitational interaction of point masses, *Physics Letters B* **513**, 147 (2001), arXiv:gr-qc/0105038 [gr-qc].
- [71] P. Jaranowski and G. Schäfer, Towards the fourth post-Newtonian Hamiltonian for two-point-mass systems, *Phys. Rev. D* **86**, 061503 (2012), arXiv:1207.5448 [gr-qc].
- [72] P. Jaranowski and G. Schäfer, Dimensional regularization of local singularities in the fourth post-Newtonian two-point-mass Hamiltonian, *Phys. Rev. D* **87**, 081503 (2013), arXiv:1303.3225 [gr-qc].
- [73] S. Foffa, R. A. Porto, I. Rothstein, and R. Sturani, Conservative dynamics of binary systems to fourth post-

- Newtonian order in the EFT approach. II. Renormalized Lagrangian, *Phys. Rev. D* **100**, 024048 (2019), arXiv:1903.05118.
- [74] S. Foffa and R. Sturani, Conservative dynamics of binary systems to fourth post-Newtonian order in the EFT approach. I. Regularized Lagrangian, *Phys. Rev. D* **100**, 024047 (2019), arXiv:1903.05113.
- [75] T. Marchand, L. Bernard, L. Blanchet, and G. Faye, Ambiguity-free completion of the equations of motion of compact binary systems at the fourth post-Newtonian order, *Phys. Rev. D* **97**, 044023 (2018), arXiv:1707.09289 [gr-qc].
- [76] J. José and E. Saletan, *Classical Dynamics: A Contemporary Approach* (Cambridge University Press, 1998).
- [77] H. Goldstein, C. Poole, and J. Safko, *Classical Mechanics* (Addison Wesley, 2002).
- [78] S. Ferraz-Mello, *Canonical Perturbation Theories: Degenerate Systems and Resonance*, Astrophysics and Space Science Library (Springer New York, 2007).
- [79] K. G. Arun, L. Blanchet, B. R. Iyer, and M. S. S. Qusailah, Tail effects in the third post-Newtonian gravitational wave energy flux of compact binaries in quasi-elliptical orbits, *Phys. Rev. D* **77**, 064034 (2008), arXiv:0711.0250 [gr-qc].
- [80] T. Damour and G. Schaefer, Redefinition of position variables and the reduction of higher order Lagrangians, *J. Math. Phys.* **32**, 127 (1991).
- [81] T. Damour, P. Jaranowski, and G. Schäfer, Conservative dynamics of two-body systems at the fourth post-Newtonian approximation of general relativity, *Phys. Rev. D* **93**, 084014 (2016), arXiv:1601.01283 [gr-qc].
- [82] T. Damour, P. Jaranowski, and G. Schaefer, Dynamical invariants for general relativistic two-body systems at the third postNewtonian approximation, *Phys. Rev. D* **62**, 044024 (2000), arXiv:gr-qc/9912092.
- [83] C. Dlapa, G. Kälin, Z. Liu, and R. A. Porto, Dynamics of Binary Systems to Fourth Post-Minkowskian Order from the Effective Field Theory Approach, arXiv e-prints, arXiv:2106.08276 (2021), arXiv:2106.08276 [hep-th].
- [84] P. C. Peters and J. Mathews, Gravitational Radiation from Point Masses in a Keplerian Orbit, *Physical Review* **131**, 435 (1963).
- [85] F. Moulton, *An Introduction to Celestial Mechanics*, Dover books in astronomy (Dover Publications, 1970).
- [86] S. Finch and G. Rota, *Mathematical Constants*, Encyclopedia of Mathematics and its Applications (Cambridge University Press, 2003).
- [87] I. Hinder, F. Herrmann, P. Laguna, and D. Shoemaker, Comparisons of eccentric binary black hole simulations with post-Newtonian models, *Phys. Rev. D* **82**, 024033 (2010), arXiv:0806.1037 [gr-qc].
- [88] A. Klein, Y. Boetzel, A. Gopakumar, P. Jetzer, and L. de Vittori, Fourier domain gravitational waveforms for precessing eccentric binaries, *Phys. Rev. D* **98**, 104043 (2018), arXiv:1801.08542 [gr-qc].
- [89] E. Poisson and C. Will, *Gravity: Newtonian, Post-Newtonian, Relativistic* (Cambridge University Press, 2014).
- [90] L. Blanchet and G. Schaefer, Higher order gravitational radiation losses in binary systems., *MNRAS* **239**, 845 (1989).
- [91] A. Gopakumar and B. R. Iyer, Gravitational waves from inspiraling compact binaries: Angular momentum flux, evolution of the orbital elements, and the waveform to the second post-Newtonian order, *Phys. Rev. D* **56**, 7708 (1997), gr-qc/9710075.
- [92] S. Mikkola, A cubic approximation for Kepler's equation, *Celestial Mechanics* **40**, 329 (1987).
- [93] S. Tanay, M. Haney, and A. Gopakumar, Frequency and time-domain inspiral templates for comparable mass compact binaries in eccentric orbits, *Phys. Rev. D* **93**, 064031 (2016), arXiv:1602.03081 [gr-qc].
- [94] A. H. Mroue *et al.*, Catalog of 174 Binary Black Hole Simulations for Gravitational Wave Astronomy, *Phys. Rev. Lett.* **111**, 241104 (2013), arXiv:1304.6077 [gr-qc].
- [95] S. Tanay, A. Klein, E. Berti, and A. Nishizawa, Convergence of Fourier-domain templates for inspiraling eccentric compact binaries, *Phys. Rev. D* **100**, 064006 (2019), arXiv:1905.08811 [gr-qc].
- [96] T. Damour, B. R. Iyer, and B. S. Sathyaprakash, Frequency domain P approximant filters for time truncated inspiral gravitational wave signals from compact binaries, *Phys. Rev. D* **62**, 084036 (2000), arXiv:gr-qc/0001023.
- [97] https://dcc.ligo.org/public/0002/T0900288/003/ZERO_DET_high_P.txt/.
- [98] T. A. Apostolatos, Search templates for gravitational waves from precessing, inspiraling binaries, *Phys. Rev. D* **52**, 605 (1995).
- [99] B. J. Owen and B. S. Sathyaprakash, Matched filtering of gravitational waves from inspiraling compact binaries: Computational cost and template placement, *Phys. Rev. D* **60**, 022002 (1999), arXiv:gr-qc/9808076 [gr-qc].
- [100] L. Blanchet, A. Buonanno, and G. Faye, Higher-order spin effects in the dynamics of compact binaries. II. Radiation field, *Phys. Rev. D* **74**, 104034 (2006), arXiv:gr-qc/0605140 [gr-qc].
- [101] G. Cho, B. Pardo, and R. A. Porto, Gravitational radiation from inspiraling compact objects: Spin-spin effects completed at the next-to-leading post-Newtonian order, *Phys. Rev. D* **104**, 024037 (2021), arXiv:2103.14612 [gr-qc].
- [102] D. Bini, T. Damour, and A. Geralico, Novel Approach to Binary Dynamics: Application to the Fifth Post-Newtonian Level, *Phys. Rev. Lett.* **123**, 231104 (2019), arXiv:1909.02375 [gr-qc].
- [103] D. Bini, T. Damour, and A. Geralico, Binary dynamics at the fifth and fifth-and-a-half post-Newtonian orders, *Phys. Rev. D* **102**, 024062 (2020), arXiv:2003.11891 [gr-qc].
- [104] D. Bini, T. Damour, and A. Geralico, Sixth post-Newtonian local-in-time dynamics of binary systems, *Phys. Rev. D* **102**, 024061 (2020), arXiv:2004.05407 [gr-qc].
- [105] F. Larrouitrou, Q. Henry, L. Blanchet, and G. Faye, The Quadrupole Moment of Compact Binaries to the Fourth post-Newtonian Order: I. Non-Locality in Time and Infra-Red Divergencies, arXiv e-prints, arXiv:2110.02240 (2021), arXiv:2110.02240 [gr-qc].
- [106] F. Larrouitrou, L. Blanchet, Q. Henry, and G. Faye, The Quadrupole Moment of Compact Binaries to the Fourth post-Newtonian Order: II. Dimensional Regularization and Renormalization, arXiv e-prints, arXiv:2110.02243 (2021), arXiv:2110.02243 [gr-qc].
- [107] M. Maggiore, *Gravitational Waves: Volume 1: Theory and Experiments*, Gravitational Waves (OUP Oxford,

- 2008).
- [108] J. Creighton and W. Anderson, *Gravitational-Wave Physics and Astronomy: An Introduction to Theory, Experiment and Data Analysis*, Wiley Series in Cosmology (Wiley, 2012).
- [109] B. S. Sathyaprakash and B. F. Schutz, Physics, Astrophysics and Cosmology with Gravitational Waves, Living Rev. Rel. **12**, 2 (2009), arXiv:0903.0338 [gr-qc].